University of Wisconsin Milwaukee
UWM Digital Commons

Theses and Dissertations

August 2020

Design and Analysis of Fully-Electronic Magnet-Free Non-Reciprocal Metamaterial

Swadesh Poddar
University of Wisconsin-Milwaukee

Follow this and additional works at: https://dc.uwm.edu/etd

 Part of the Electrical and Electronics Commons, and the Electromagnetics and Photonics Commons

Recommended Citation

Poddar, Swadesh, "Design and Analysis of Fully-Electronic Magnet-Free Non-Reciprocal Metamaterial" (2020). *Theses and Dissertations*. 2578.
https://dc.uwm.edu/etd/2578

This Thesis is brought to you for free and open access by UWM Digital Commons. It has been accepted for inclusion in Theses and Dissertations by an authorized administrator of UWM Digital Commons. For more information, please contact open-access@uwm.edu.

DESIGN AND ANALYSIS OF FULLY-ELECTRONIC MAGNET-FREE NON-RECIPROCAL METAMATERIAL

by

Swadesh Poddar

A Thesis Submitted in

Partial Fulfillment of the

Requirements for the Degree of

Master of Science

in Engineering

at

The University of Wisconsin-Milwaukee

August 2020

ABSTRACT

DESIGN AND ANALYSIS OF FULLY-ELECTRONIC MAGNET-FREE NON-RECIPROCAL METAMATERIAL

by

Swadesh Poddar

The University of Wisconsin-Milwaukee, 2020

Under the Supervision of Professor George Hanson

Reciprocity is a fundamental and very important characteristics of the vast majority of electronic devices, and requires that signals travel in both forward and reverse directions in the same manner. Similarly, electromagnetic non-reciprocity or one way wave propagation, implies that the field created by a source at an observation point is not the same when source and observation points are interchanged. Non-reciprocal devices such as isolators, circulators, phase shifters, polarizers, switches, tunable resonators, tunable filters, and gyrators enable new applications from radio frequencies to optical frequencies. However, non-reciprocity has been implemented in the past using ferrites in the presence of an external permanent magnetic bias in devices (isolators, circulators, and gyrators) which make the device bulky, expensive, and incompatible with semiconductor technology. Therefore, in recent years, scientists have investigated various approaches to implement artificial non-reciprocity.

The aim of this research is to design and analyze fully electronic, magnet-free, non-

reciprocal (gyrotropic) devices. When a material, in the presence of a static magnet, exhibits different refractive indices for left and right handed elliptically/circularly polarized waves, it is called a gyrotropic material.

The implementation of non-reciprocity requires time reversal symmetry breaking and can be realized with odd vector quantities that are odd (antisymmetric) under time reversal. Examples include magnetic fields, current, momentum, and orbital angular momentum. Travelling-wave resonant ring particles loaded by unidirectional components exhibit gyromagnetic properties by mimicking similar electron spin precession of a ferrite material in presence of magnetic bias. This artificial design offers numerous advantages in comparison with conventional approaches, such as smaller size, lower weight, lower cost, and flexible compatibility with semiconductor devices. This has been shown that two major properties of a magnet free, non-reciprocal devices, Faraday and Kerr rotation can be controlled by varying electric biasing conditions.

Finally, this thesis presents several concepts, optimization approaches, and measurement environments, which have been investigated and developed during this MS program. These concepts and approaches include metamaterial design, implementing non-reciprocity in multi-layer configurations, and design consideration of practical devices.

© Copyright by Swadesh Poddar, 2020

All Rights Reserved

To my beloved parents.....

TABLE OF CONTENTS

LIST OF FIGURES

LIST OF TABLES

ACKNOWLEDGEMENTS

As the conclusion of my M.Sc. study, I would like to express my sincere appreciation to my supervisor Dr. George Hanson for his generous acceptance of me as a member of his research group. He convincingly mentored and encouraged me to be more goal oriented and focused towards the right direction even when the road got tough. Without his continuous guidance, the aim of this research project would not have been materialized. I always feel very privileged to be a part of one of the excellent research groups in electromagnetic theory and working with very cooperative team members.

Besides, I would like to acknowledge Dr. Marius Schmidt and Dr. Chiu-Tai Law, for having accepted to examine this thesis, their valuable comments, time, and presence to my thesis defense. I would also like to thank all lab members notably Behnaam, Alex, and Samane for their continuous support and guidance. Furthermore, I would like to mention Dr. Tanvir Hasan from Jessore University, Bangladesh and Mr. Salahuddin Tariq from JMA wireless for their continuous help and suggestions. Besides, it is my pleasure to mention Mr. Jack Malluege from Ansys for his generous access to the Ansys learning hub from where I got guidance and training from simulation experts. For their precious help, my gratitude is extended to Mr. David Mclanahan for his technical support, Mrs. Elisabeth A Warras for her administrative work, and Mr. Dusko V. Jofisovoski for his IT support. Lastly, I would like to express my gratitude to all my friends in Milwaukee with whom I spent very good times.

Last but not least, I would like to thank my parents and my sister, Dipika Poddar, who always supports and believes in me. I would like to express my profound gratitude to my source of happiness, my wife, Dr. Aditi Roy, for her endless love, encouragement, and

inspiration throughout this journey.

Finally, I would like to thank you as the reader of my research work, which I hope will be useful to you.

Chapter 1

Introduction

1.1 Definition and Basic Concepts

"From a long view of the history of mankind - seen from, say, ten thousand years from now - there can be little doubt that the most significant event of the 19th century will be judged as Maxwell's discovery of the laws of electrodynamics. The American Civil War will pale into provincial insignificance in comparison with this important scientific event of the same decade" Richard P. Feynman.[1]

From the beginning of mankind, humans have always tried to learn and replicate from nature, which is the gradual development of science. In a more simplified form, science is the knowledge of the world of nature. Since the emergence of Homo sapiens, in order to survive as a species, humans have had to recognize and learn many patterns. The way the sun and the moon periodically repeat their movements or periodicity in butterfly wings or reflection of light are classic examples. Therefore, nature was always a learning toolbox, and humans, over time, learned, developed, and explored in various fields of sciences.

Physics, the science of nature, in which wave-matter interaction is a very important phenomenon paves the foundation of many innovative branches, where it guides numerous,

significant, and sophisticated applications. Based on the concept of classical electromagnetism, which stands on Maxwell's equations, wave-matter interactions can be subdivided into two broad categories: reciprocal and non-reciprocal.

When signals travel in both forward and reverse directions in the same manner, the system can be called reciprocal. Most of our daily life applications such as antenna, electrical circuits, and components are based on reciprocity. However, reciprocity imposes severe restrictions on device operation. Components that violate reciprocity, by breaking time reversal symmetry, such as gyrators, isolators, and circulators, are very important in many advanced applications because of their novel application oriented features, are called non-reciprocal.[2] In 1845, Michael Faraday discovered the first physical relationship between light and magnetism. He demonstrated that a magnetic field in the direction of propagation of a light beam in a transparent medium produces the effects of circular birefringence, which is now known as the Faraday rotation, or the Faraday effect.[3] Since WWII, non-reciprocal devices have obtained popularity, however, exclusively based on permanent magnetic bias which made the practical implementation voluminous and expensive. Besides, non-reciprocal materials embedded with permanent magnets are difficult to integrate with fabricating modern devices. Therefore, creating non-reciprocal components without the use of a static magnet has attracted many researchers, and recently been re-investigated due to enormous advancements in semiconductor technology.[2,4] As a result, the concept of magnet-free non-reciprocity has opened vast areas of research including but not limited to military applications, leaky wave antennas, isolators, and circulators.[5]

1.1.1 Maxwell's Equations

The propagation and excitation of electromagnetic waves are governed mathematically by Maxwell's equations. The differential forms of Maxwell's equations are represented as Fara-

day's law of induction,

$$\nabla \times \mathbf{E} = -\frac{\partial \mathbf{B}}{\partial t}, \tag{1.1}$$

generalized Ampere's law,

$$\nabla \times \mathbf{H} = \frac{\partial \mathbf{D}}{\partial t} + \mathbf{J}, \tag{1.2}$$

Gauss's law for the magnetic field,

$$\nabla \cdot \mathbf{B} = 0, \tag{1.3}$$

and Gauss's law for the electric field,

$$\nabla \cdot \mathbf{D} = \rho, \tag{1.4}$$

where, E = electric field intensity (vector), volts/meter, $(\frac{V}{m})$,

H = magnetic field intensity (vector), amperes/meter, $(\frac{A}{m})$,

D = electric flux density (vector), coulombs/meter^2, $(\frac{C}{m^2})$,

B = magnetic flux intensity (vector), webers/meter^2, $(\frac{Wb}{m^2})$,

J = electric current density (vector), amperes/meter^2, $(\frac{A}{m^2})$,

ρ = electric charge density (scalar), coulombs/meter^3, $(\frac{C}{m^3})$.

The law of conservation of electric charge or the continuity equation can be represented as

$$\nabla \cdot \mathbf{J} = -\frac{\partial \rho}{\partial t}. \tag{1.5}$$

Maxwell's equations in frequency domain must be supplemented by relations which describe the behaviour of the medium under the influence of the field. These relations are known as constitutive relations and in vacuum are represented as[6]

$$\mathbf{D} = \varepsilon_0 \mathbf{E}, \tag{1.6}$$

$$\mathbf{B} = \mu_0 \mathbf{H}. \tag{1.7}$$

where $\varepsilon_0 = 8.854{*}10^{-12}$ F/m and $\mu_0 = 4\pi{*}10^{-7}$ H/m. A medium is said to be isotropic if electric and magnetic properties is represented as

$$\mathbf{D} = \varepsilon_0 \varepsilon \mathbf{E}, \tag{1.8}$$

$$\mathbf{B} = \mu_0 \mu \mathbf{H}, \tag{1.9}$$

where dielectric constant, ε and permeability, μ are scalars. For anisotropic media, the electric and magnetic properties is represented as

$$\mathbf{D} = \varepsilon_0 \overrightarrow{\varepsilon} \cdot \mathbf{E}, \tag{1.10}$$

$$\mathbf{B} = \mu_0 \overrightarrow{\mu} \cdot \mathbf{H}, \tag{1.11}$$

where $\overrightarrow{\varepsilon}$ and $\overrightarrow{\mu}$ are respectively the permitivity and permeability tensors which will be discussed in following sections.

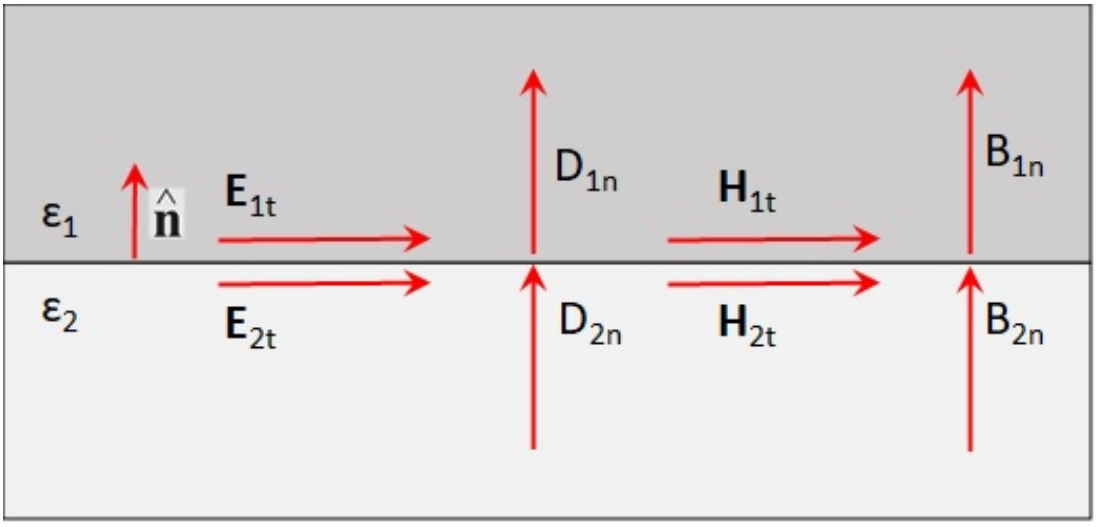

Figure 1-1: Field directions at boundary.

In order to continue the solution of Maxwell's equations from one region to another so that the resulting solution is unique and valid everywhere, we need boundary conditions to

impose on the field vectors at the interface,

$$\mathbf{E_{1t}} - \mathbf{E_{2t}} = 0, \tag{1.12}$$

$$\mathbf{H_{1t}} - \mathbf{H_{2t}} = \mathbf{J_s} \times \widehat{\mathbf{n}}, \tag{1.13}$$

$$\mathbf{D_{1n}} - \mathbf{D_{2n}} = \rho_s, \tag{1.14}$$

$$\mathbf{B_{1n}} - \mathbf{B_{2n}} = 0, \tag{1.15}$$

where subscript t and n dictates the corresponding tangential and normal components at the interface and $\widehat{\mathbf{n}}$ is the unit vector normal to the boundary, pointing from medium 2 to medium 1. Besides, ρ_s and J_s are any external surface charge and surface current densities on the boundary surface. Figure 1-1 depicts the field directions at a boundary.

1.1.2 Polarization

The polarization of a radiated wave is defined as "that property of a radiated electromagnetic wave describing the time-varying direction and relative magnitude of the electric field vector; specifically, the figure traced as a function of time by the extremity of the vector at a fixed location in space, and the sense in which it is traced, as observed along the direction of propagation".[7] In simple words, polarization is the direction of the time-varying real-valued field vector where electric fields are required to be observed along the propagation direction. Figure 1-2 depicts typical trace of a forward moving wave as a function of time.

A forward propagating wave can be represented mathematically as

$$\mathbf{E}(z,t) = (\widehat{\mathbf{x}}A_+ + \widehat{\mathbf{y}}B_+)e^{j\omega t - jkz}. \tag{1.16}$$

More precisely, polarization is the direction of the time-varying real-valued electric field $\mathbf{E}$(z,t) = Re[$\mathbf{E}$(z,t)]. At any fixed point z, the field vector $\mathbf{E}$(z,t) may be along a fixed

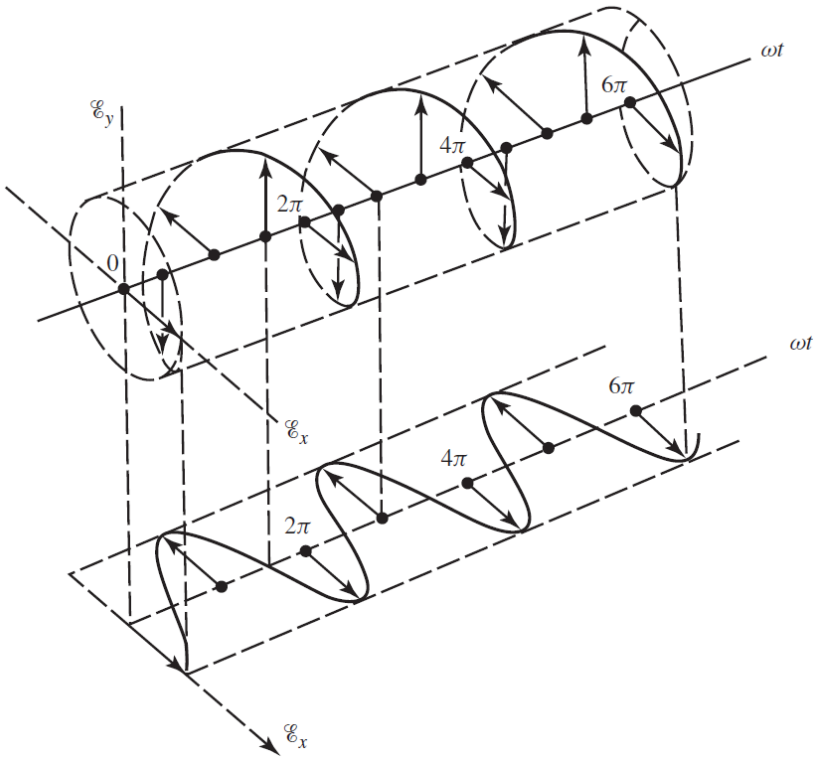

Figure 1-2: Rotation of plane electromagnetic wave at z=0.[7]

linear direction or it may be rotating as a function of time, t, tracing a circle or an ellipse.[8] The polarization properties of the plane wave are determined by the relative phase and magnitudes of the complex-valued constants A_+ and B_+, where $A_+ = Ae^{j\phi_a}$ and $B_+ = Be^{j\phi_b}$ (A and B are real-valued). Taking the time dependence of the field and following some trigonometric rules,

$$\mathbf{E}(z,t) = \frac{E_x^2}{A^2} + \frac{E_y^2}{B^2} - 2cos\phi\frac{E_xE_y}{AB} = sin^2\phi \tag{1.17}$$

where ϕ is the relative phase angle and defined as $\phi = \phi_a$ - ϕ_b. Polarization may be classified into three categories: linear, circular, and elliptical. From the above equation this is understood that we can obtain different polarizations by changing only three quantities i.e. A, B, and ϕ. Figure 1-3 is the graphical representation of various polarizations of an electric field as a function of time.

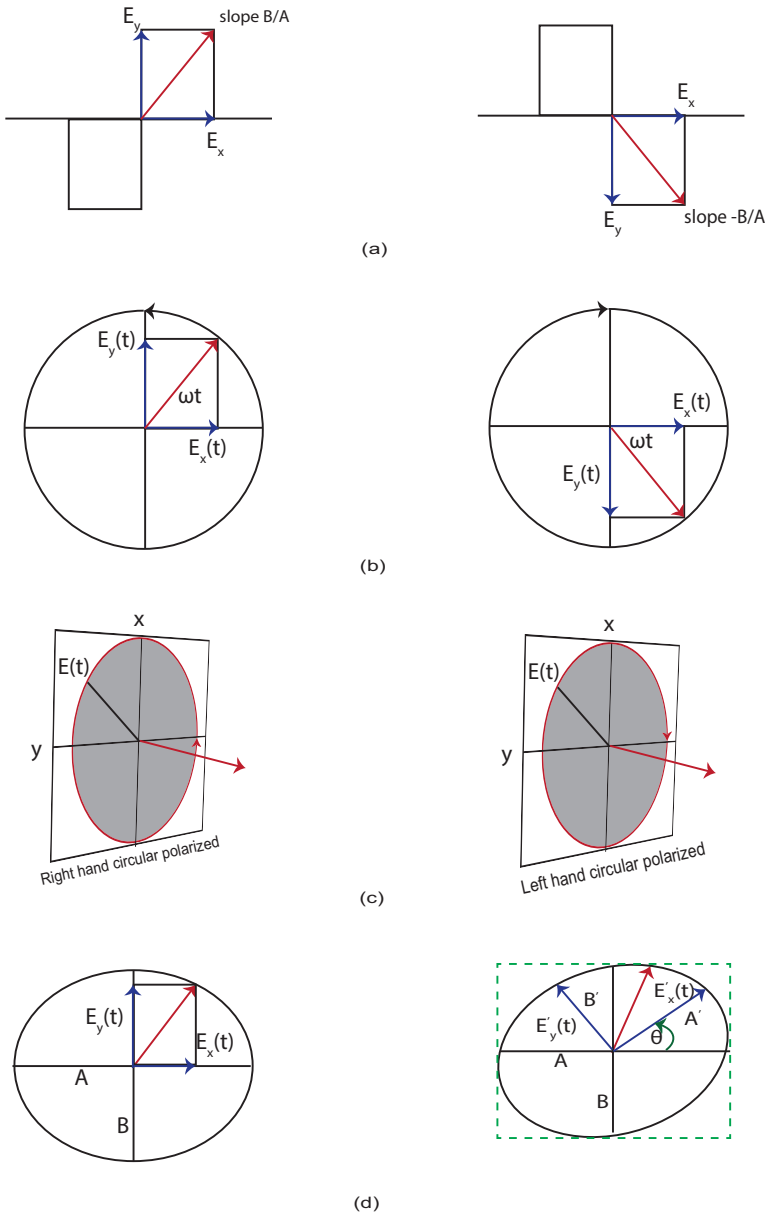

Figure 1-3: (a) Linear polarization. (b) Circular polarization. (c) Right hand circular polarization (RHCP) and Left hand circular polarization (LHCP). (d) Elliptical polarization.

Linear Polarization

Linear polarization can be defined as the case when the vector that describes the electric field at a point in space as a function of time is always directed along the same line, which is normal to the direction of wave propagation. Therefore, from Eq. 1.17, this can be easily written as

$$\left(\frac{E_x}{A} \mp \frac{E_y}{B}\right)^2 = 0, \tag{1.18}$$

which is shown in Fig. 1-3(a).

Circular Polarization

When the x and y components of the electric field are equal in magnitude and maintain a constant 90° phase shift as shown in Fig. 1-3 (b), circular polarization is obtained. This is represented as[8]

$$\frac{E_x^2}{A^2} + \frac{E_y^2}{A^2} = 1. \tag{1.19}$$

The sense of rotation, in conjunction with the direction of propagation, defines right hand circular polarization (RHCP) versus left hand circular polarization (LHCP) that has been shown in Fig. 1-3 (c). The electric field of LHCP and RHCP wave can be represented in its phasor form as

$$\mathbf{E}(z) = A(\widehat{\mathbf{x}} + j\widehat{\mathbf{y}})e^{-jkz}, \tag{1.20}$$

$$\mathbf{E}(z) = A(\widehat{\mathbf{x}} - j\widehat{\mathbf{y}})e^{-jkz}. \tag{1.21}$$

Elliptical Polarization

In general, for elliptical polarization, the curve traced by the tip of the electric field vector follows the trajectory of an ellipse which has been shown in Fig. 1-3 (d). If $A \neq B$, however, phase difference, $\phi = 90°$, we get an ellipse with major and minor axis. Therefore, the general equation can be defined as

$$\frac{E_x^2}{A^2} + \frac{E_y^2}{B^2} = 1. \tag{1.22}$$

Besides, if we take the phase difference to be arbitrary instead of 90°, then the major and minor axis will be rotated relative to the x-y plane. The tilt angle θ can be represented as[8]

$$tan2\theta = \frac{2AB}{A^2 - B^2} cos\phi. \tag{1.23}$$

A similar form of elliptical polarization can be developed very easily with respect to a semi axis as shown in Fig. 1-3 (d). The corresponding equation is represented as

$$\frac{E_x'^2}{A'^2} + \frac{E_y'^2}{B'^2} = 1. \tag{1.24}$$

Another very important feature of elliptical polarization is the axial ratio as shown in Fig. 1-3 (d), which is the ratio of major to minor axis (including its sign) and defined as[7]

$$AR = \frac{Axis_{major}}{Axis_{minor}} \rightarrow 1 \leq |AR| \leq \infty. \tag{1.25}$$

Recall that if the ellipse has equal major and minor axis, then it transforms into a circle, hence, the field exhibits circular polarization.

1.1.3 General Properties of Plane Waves

Plane waves are not only the simplest solutions of Maxwell's equations, but also they are a very good starting point of many real wave problems. Waves in the far field of a transmitting antenna or diffraction from an object in space are represented by plane waves. Furthermore, complicated waves can be represented as a superposition of plane waves by using the Fourier integral. Therefore, general properties of plane waves are the basic foundation of many real-like problems related to optics and wireless communications.[6]

Maxwell's equations along with linear constitutive relations[6–8] form a linear system of partial differential equations. Considering a sinusoidal time varying field alone, no generality is lost. A monochromatic field vector varying sinusoidally in time with frequency ω and instantaneous vector is shown in Fig. 1-4

A forward propagating time-domain field can be represented as

$$E_x^+ = E_0^+ \cos(\omega t - kz), \tag{1.26}$$

$$H_y^+ = \frac{E_0^+}{\eta} \cos(\omega t - kz). \tag{1.27}$$

The relation between magnetic field and electric field is obtained by solving Maxwell's equations

$$H_y^+ = \frac{1}{\sqrt{\frac{\mu}{\varepsilon}}} E_x^+, \tag{1.28}$$

$$H_y^- = -\frac{1}{\sqrt{\frac{\mu}{\varepsilon}}} E_x^-, \tag{1.29}$$

where in Eq. 1.28 and Eq. 1.29, the intrinsic impedance is obtained from properties of the medium and can be represented as

$$Z_w = \frac{E_x^+}{H_y^+} = -\frac{E_x^-}{H_y^-} = \eta = \sqrt{\frac{\mu}{\varepsilon}}. \tag{1.30}$$

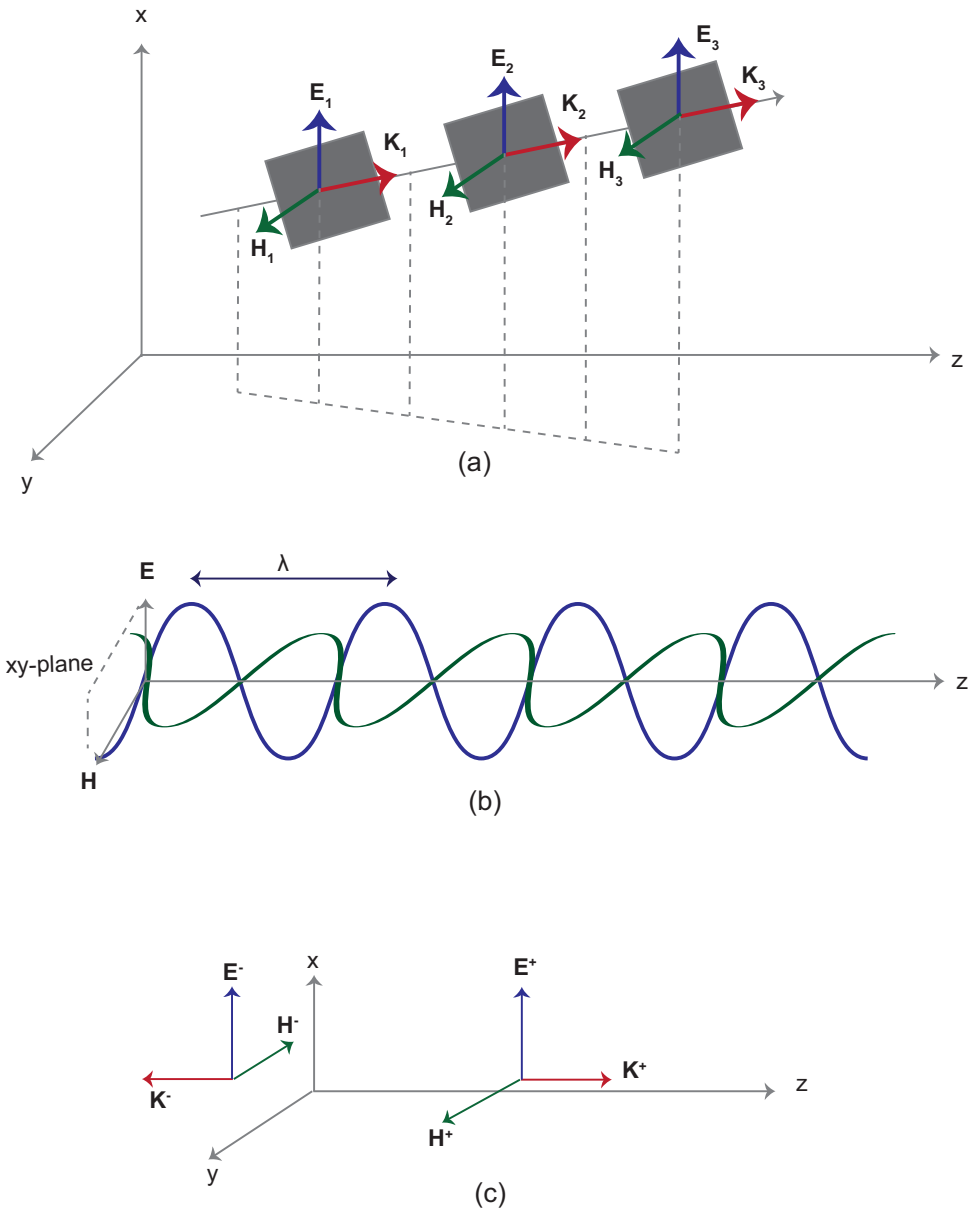

Figure 1-4: (a) Phase fronts of plane waves. (b) Instantaneous fields of a uniform plane wave. (c) Complex fields of a uniform plane wave.

Monochromatic plane wave in a lossless, isotropic medium is a transverse electromagnetic wave where electric and magnetic field lies in the x-y plane normal to the direction of propagation (z), as shown in Fig. 1-4.

1.1.4 Reciprocity and Non-Reciprocity

Reciprocity is one of the fundamental symmetries which state that any exchange of information or experiment is symmetric from both of a source and image point of view.[9] The adjective reciprocal comes from the Latin word "reciprocus" which is the combination of phrase reque and proque with the meaning of "going backward as forward."[4] From microwave or optical power splitter to antenna radiation and every modern communication system, the significance of reciprocity is boundless. In a simple two ports network shown in Fig. 1-5, S parameter of a reciprocal system satisfies a symmetry condition, i.e. $\mathbf{S}^T = \mathbf{S}$ or $\mathbf{S}_{12} = \mathbf{S}_{21}$.[2]

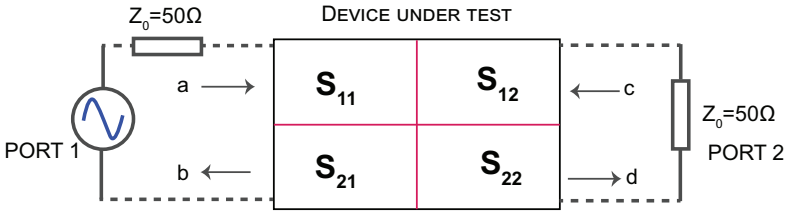

Figure 1-5: Two port network system

The earliest investigation in the field of reciprocity was the theoretical model of light waves developed by Stokes in 1849 and Helmholtz in 1856. In 1860, Kirchhoff reformulated the reciprocity principle of thermal radiation. Later, in 1896, Hendrik Lorentz came up with his famous electromagnetic reciprocity theorem.[10]

Numerous device designs, photonic structures, and microwave circuits are based on the foundation of the Lorentz reciprocity theorem, which require that any linear and time-invariant medium with symmetric permittivity and permeability tensors are reciprocal.[11] On the other hand, non-reciprocal components are very essential in modern communication

systems. Their applications are of use in many areas such as high-power wireless base-station transmitters, simultaneous-transmit-and-receive (STAR) radar, full-duplex wireless radios, quantum computing implementations, signal isolation, cancelling cross talk between transmitter and receiver, and in modern antenna design.[2] In order to obtain non-reciprocal behavior, one needs to break time reversal symmetry. Magnetic biasing provides a well-established means to break reciprocity, but contains innate limitations. For many years, non-reciprocal concepts were exclusively based on ferromagnetic materials biased by permanent magnets, severely limiting their applicability due to size, cost, and complex integration within systems.

The fundamental relationship between the time-reversal invariance on microscopic dynamic equations and reciprocity in dissipative systems was realized by L. Onsager,[12] and developed and extended by H. Casimir[13] to electromagnetic systems in the presence of an external bias field. In addition, with structural complexity, the conventional route of breaking reciprocity experiences severe performance degradation in the microwave and optical regime such as the weak magneto optical effect and noise, which motivates researchers to investigate and develop an artificial non-reciprocity without any static external magnetic field. The ability to implement non-reciprocity artificially and achieve stringent performance requirements has vast potential in modern applications. In recent years, various researchers artificially developed non-reciprocity by using active components such as transistors, temporal modulation of permitivity and conductivity, and hybrid acoustic electronic components.[2,14]

1.2 Research Objectives

As seen above, the idea of non-reciprocity has been around for a long time, mostly implemented based on ferromagnetic materials (ferrites) biased by permanent magnets. As a consequence, there have been very important research developments in the area of creating

magnet-free nonreciprocity, especially in the microwave and optical frequency ranges, which create a vast area of modern applications.

Over the past decade, advances in meta-material and semiconductor research have initiated a real interest for "magnet-free" nonreciprocity, leading novel technologies which neither require any ferromagnetic materials nor any rare earth magnets, however, able to mimic the similar electron spin precession as magnet based ferrite systems.

Concentrating on the idea of easier fabrication, simple system level integration, and magnet free meta-material, there have been several attempts to develop magnet free non-reciprocal components in recent years, specifically 1) active circuits[15–20] and space-time[4] 2) modulated structures,[21–25] and 3) switched structures.[11] However, none of the reported article on this novel idea focused on performance controlling features and multi layer designs which can be very promising from design-purpose and application points of view. In this work, initially, we will discuss detailed design, optimization of magnet free non-reciprocal meta-material, and later we will focus on obtaining tunable Faraday and Kerr rotation of our proposed design for single and multi-layer configuration.

1.3 Thesis Contribution and Organization

The main contribution of this research work is the non-reciprocal device design and optimization framework that will be developed and discussed in Chapters 2 to 4. Due to the rigorous nature of its foundation, which can be derived from Maxwell's equations, this non-reciprocity technique provides a detailed, however, complicated description of meta-material available to date in the literature. Therefore, mathematical modelling of wave propagation in various birefringent media will be described. It yields the non-reciprocal material parameters, given in terms of permeability and permittivity components, as functions of specified electromagnetic transformations. The physics behind split ring resonator

design will be described and practical steps will be discussed from theory to simulation leading to fabrication and measurement in the lab. The combined information available from these three chapters will provide the reader all necessary tools required to design a non-reciprocal device.

In chapter 2, the physics of gyrotropy and non-reciprocity will be studied and its applications in microwave and optics regime will be provided. Besides, time reversal symmetry, time reversal symmetry breaking in electromagnetics along with mathematical modelling, and wave propagation in birefringent media will be discussed in detail.

In chapter 3, necessary idea related to design split ring resonator will be reviewed and for a single-layer transparent magnet free active-passive component based slot line structure will be provided. The detail design procedure along with characterization of all performance indicators will be discussed and analyzed. The non-reciprocal gyrotropic response of the structure will be shown from both simulation and lab measurement and its underlying physics will be explained. Finally, key performance indicators such as Faraday and Kerr rotation along with performance optimization will be examined.

In chapter 4, the multi-layer magnet free non-reciprocal system will be designed and employed. Faraday and Kerr rotation will be explored and challenges with reflection and transmission for multi layer configuration will be introduced. By varying biasing components, the variation of performance will be examined very carefully. A comparative analysis with respect to number of layers will be analyzed.

In chapter 5, the applications and fundamental limitations of the design will be discussed that designers need to consider very carefully. All necessary measurements procedures, electronic setup and test bench will be discussed.

At last, in Chapter 6, conclusive remarks and future works on this concept will be presented.

In summary, magnet-free, non-reciprocal metamaterial has been developed using a variety of methods over this decade, including through the use of active transistors, active amplifiers, passive RLC elements, and nonlinearity. This work extends recent work by others to make the non-reciprocity tunable, and we analyzed the tunable Faraday and Kerr rotation. We envision that the proposed approaches in this work will add a new building block in the research area of magnetic-free non-reciprocal metamaterials.

Chapter 2

Electromagnetic Non-Reciprocity and Polarization Rotation

2.1 Non-Reciprocity Definition and Classification

Non-reciprocity is a foundation of many scientific concepts, and arises in diverse areas of physics such as condensed matter physics, optics, electromagnetism and electronics, and quantum mechanics which host advanced phenomena and applications.[4,10] As described earlier in this thesis, electromagnetic non-reciprocity, essential for one-way communication systems, dictates that the fields created by the source at the observation point are not the same when source and observation points are interchanged, or, in simple words, we can describe that in terms of two ports scattering parameter $S_{21} \neq S_{12}$.

Non-reciprocity is the absence of "reciprocity". In order to achieve non-reciprocity, the most important task in electromagnetics and optical systems is to break time-reversal symmetry. The most conventional method to create non-reciprocity is by applying external magnetic fields to ferromagnetic compounds called ferrites, such as Yttrium Iron Garnet (YIG) and materials composed of iron oxides and other elements (Al,Co,Mn,Ni).[4,26,27] Non-

reciprocal devices play a pivotal role in modern communication systems, from protecting coherent source generators, from reflected signals to cancelling cross talk between transmit and receive signal paths in antenna feeding networks and so on. However, static magnet based technology suffers from severe issues, such as crystallographic incompatibility with semiconductors, bulk size, weight, and cost.

In the presence of an external magnetic field $\mathbf{B}_0$, created by a permanent magnet or a resistive/superconductive coil, ferromagnetic materials exhibit electron spin precession at microwave frequencies can be represented by Eq. 2.1 as

$$\frac{d\mathbf{m}}{dt} = \gamma \mathbf{m} \times (\mathbf{B_0} + \mu_0 \mathbf{H}), \tag{2.1}$$

where $\mathbf{m}$ is the magnetic dipole moment, γ is the gyro-magnetic ratio, $\mathbf{B}_0$ is the magnetic field bias, and $\mathbf{H}$ is the magnetic field intensity. Besides, cyclotron orbiting at optical frequencies can be represented by Eq. 2.2 as[4, 28]

$$\frac{m_e}{e}\frac{d\mathbf{v_e}}{dt} = \mathbf{E} + \mathbf{v_e} \times \mathbf{B_0}, \tag{2.2}$$

where $\mathbf{v}_e$ is the electron velocity, e is the electron charge, and m_e is the electron mass.

During the last decades, there was a significant advancement in the area of semiconductor research underpinning a myriad of phenomena and applications in meta-materials. Therefore, a quest was realized by researchers to create non-reciprocity without any external magnetic bias and ferromagnetic material. Recently, several alternative routes towards realization of nonreciprocal wave propagation in optics and microwave frequencies have been actively investigated resulting in development of a wealth of magnet-free nonreciprocal systems, including meta-materials, space-time varying structures, and nonlinear materials.[4, 10, 29–33]

Non-reciprocal systems may be classified into two fundamentally distinct categories:

linear and nonlinear. For the linear case, a non-reciprocal system is based on breaking time reversal symmetry in the presence of an external bias field, and for the nonlinear case, non-reciprocity is achieved by a combination of self biasing along with structural asymmetry.[4,34]

2.2 Time Reversal Symmetry in Electromagnetics

The concept of electromagnetic reciprocity is closely related to that of the time-reversal symmetry of Maxwell's equations. Mathematically, from Fig. 2-1, time reversal symmetry can be defined as

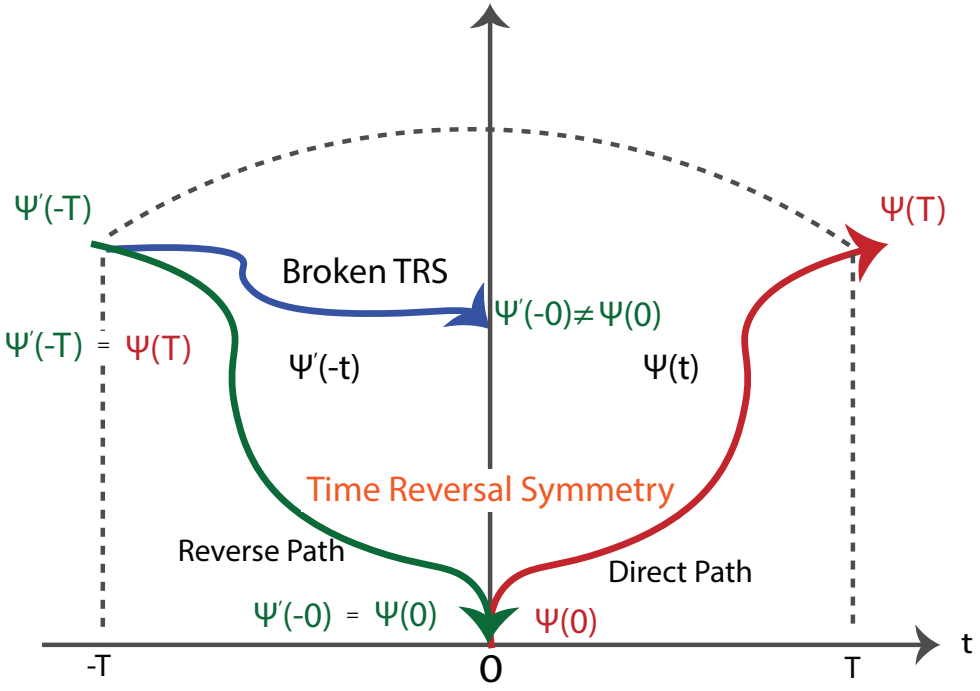

Figure 2-1: Time-reversal symmetry (TRS) (red and green curves) and broken time-reversal symmetry (red and blue curves).

$$T(t) = t^{'} = -t \rightleftharpoons T : t \rightarrow t^{'} = -t, \tag{2.3}$$

where in Eq. 2.3, time reversal is defined by the operator T. A process like Fig. 2-1 can be represented as

$$T(\psi(t)) = \psi^{'}(t^{'}) = \psi^{'}(-t). \tag{2.4}$$

To summarize, if the system remains the same or changes under time reversal, corresponding to the curve pairs described in Fig. 2-1, we can define the system as time reversal symmetric or asymmetric from

$$T\left\{\psi(t)\right\} = \psi^{'}(-t)\left\{\begin{matrix}=\\ \neq\end{matrix}\right\}\psi(t). \tag{2.5}$$

The concept of time reversal symmetry and asymmetry provides a good foundation for reciprocity and nonreciprocity. Besides, the basic laws of physics are classically invariant under time-reversal symmetry and can be intuitively visualized by the Fig. 2-1. Furthermore, the time-reversal symmetry of Maxwell's equations may be easily verified from field parity quantities.[4,10]

2.2.1 Time Reversal Symmetry Breaking

In presence of external or internal bias (in the non-linear case), time-reversal symmetry can be broken. The physical quantities involved in the laws of physics denoted as f(t) may be either time-reversal symmetric or time-reversal antisymmetric can be represented as

$$T\{f(t)\} = f^{'}(t^{'}) = f^{'}(-t^{'}) = \pm f(-t), \tag{2.6}$$

where "+" corresponds to time-reversal symmetry, or even time-reversal parity, and "−" corresponds to time-reversal antisymmetry, or odd time-reversal parity.[4] Equation 2.6 depicts that all physical quantities are either even or odd under time reversal. According to time-reversal parity relations (2-14) described later in this chapter, time-reversal symmetry

breaking requires reversing or maintaining the sign of at least one of the time-reversal even/odd quantities (bias) involved in the system,[4,10] which is the core concept of this thesis work.

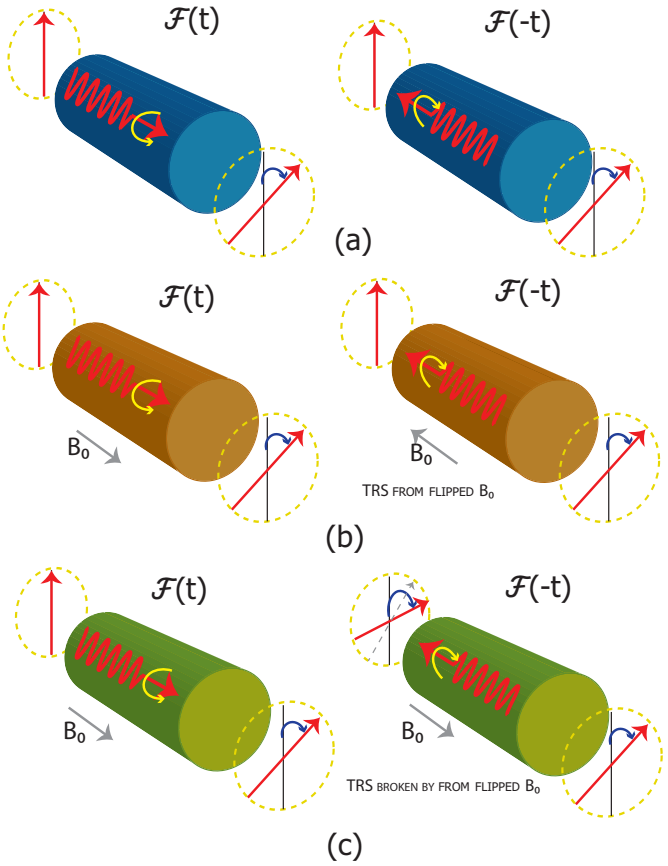

Figure 2-2: Criteria for time reversal symmetry and assymmetry. (a) Chiral system in absence of external bias (TRS). (b) Faraday system altered by flipping external magnetic bias (Forced TRS). (c) Faraday system by unaltered external magnetic bias, hence TRS breaking, non-reciprocal system.

Figure 2-2 illustrates three different systems. Figure 2-2 (a) defines a chiral system. We can see that field polarization of a chiral system symmetrically returns to its original state in absence of bias, thus this is a time reversal symmetric process (reciprocal).

Figure 2-2 (b) defines a condition when forced time reversal symmetry is applied on gyrotropic materials. The direction of polarization rotation has been obtained by applying an external magnetic bias $\mathbf{B}_0$ in forward direction and in the reverse direction the bias field $\mathbf{B}_0$ has been flipped and as a result the polarization rotation has been achieved to its initial

state, because, waves propagating in opposite directions see the same effective medium by symmetry. As per definition, we can not define this experiment as reciprocal or nonreciprocal as the system has been altered upon time reversal, since its spins have been reversed.[4] Although, this experiment does not follow the condition of reciprocity/nonreciprocity, this illustration will give some intuitive ideas for the next scenario.

Figure 2-2 (c) depicts Faraday rotation by keeping the $\mathbf{B}_0$ field unaltered. In order to preserve the nature of this system, and hence, properly decide on its non-reciprocity, one must preserve its spin states by keeping the direction of $\mathbf{B}_0$ unchanged, as shown in Fig. 2-2(c). But this violates a time-reversal symmetry rule, i.e. breaks time-reversal symmetry, or makes the process time-reversal asymmetric.[4,35] Polarization rotation has been shown from source to destination and vice versa, hence, revealing Faraday rotation is nonreciprocal.

2.3 Propagation in Birefringent Media

An electromagnetic wave consists of a coupled oscillating electric field and magnetic field which are always perpendicular to each other and by convention, the "polarization" of electromagnetic waves refers to the direction of the electric field. In linear polarization, the fields oscillate in a single direction. In circular or elliptical polarization, the fields rotate at a constant rate in a plane as the wave travels and can be decomposed into two orthogonal polarization states (right handed and left handed).

In this section, we will discuss wave propagation in anisotropic media that are circularly birefringent. A linear-polarized wave can be decomposed into two circularly-polarized waves, one right-hand circularly polarized (RHCP), and one left-hand circularly-polarized (LHCP). When a circular polarized wave propagates in a birefringent media, right-hand circular polarized and left-hand circular polarized waves propagate with different speeds. After propagating, when viewed as a linearly-polarized wave (recombining the RHCP and

LHCP components), this difference causes the linear-polarized wave to have it's polarization plane rotate as they reflect from the anisotropic media-an effect known as natural optical or Kerr rotation. Optically active or chiral media are circularly birefringent and exhibit these properties. Examples are sugar solutions, proteins, lipids, nucleic acids, amino acids, DNA, vitamins, hormones, and natural substances. On the other hand, linearly birefringent materials can also be used to change one polarization into another, such as changing linear into circular. Examples are the so-called uniaxial crystals, such as calcite, quartz, ice, tourmaline, and sapphire.[8]

Another effect based on the similar physics called Faraday rotation takes place in gyroelectric media (glass, water, conductors, plasmas) and gyromagnetic media (ferrite) when wave propagates through these media in presence of constant external magnetic bias that breaks time reversal symmetry. As discussed in an earlier chapter, these types of media are non-reciprocal.

2.3.1 Uniaxial and Biaxial Media

The lattice structure of uniaxial and biaxial crystals is electrically anisotropic. The constitutive relations for a homogeneous, lossless, and nonmagnetic crystal can be represented as

$$\mathbf{D} = \varepsilon_0 \overrightarrow{\varepsilon} \cdot \mathbf{E}, \tag{2.7}$$

$$\mathbf{B} = \mu_0 \mathbf{H}, \tag{2.8}$$

where $\overline{\varepsilon}$ is a real constant dyadic of tensor of rank 2 and is called the dielectric tensor. By a cartesian tensor of rank 2 of three-dimensional space, under the orthogonal transformation

of the coordinate system, a set of nine quantities in the matrix can be represented as

$$\overrightarrow{\varepsilon} = \left[\varepsilon_{ij}\right] = \begin{bmatrix} \varepsilon_{11} & \varepsilon_{12} & \varepsilon_{13} \\ \varepsilon_{21} & \varepsilon_{22} & \varepsilon_{23} \\ \varepsilon_{31} & \varepsilon_{32} & \varepsilon_{33} \end{bmatrix}. \tag{2.9}$$

The electric property of crystal can be characterized by a real, positive definite, and symmetric dielectric tensor $\overline{\varepsilon}$. Every real symmetric matrix can always be reduced to a diagonal form in an orthogonal coordinate system formed by the eigenvectors and the determinant of $\overline{\varepsilon}$ must always be positive, nonzero, and non-singular.[6]

A media can be characterized as Uniaxial or Biaxial based on the three diagonal elements corresponding to the eigenvalues of $\overline{\varepsilon}$. In uniaxial and biaxial anisotropic dielectrics, the constitutive relationships are given by the diagonal forms shown in Eq. 2.10 and 2.11, respectively. For the uniaxial case, only the x axes is taken to be the extraordinary case with permitivity $\varepsilon_1 = \varepsilon_e$, whereas, y and z axes are ordinary, i.e. $\varepsilon_2 = \varepsilon_2 = \varepsilon_0$. On the other hand, for the biaxial case, diagonal elements of permitivity for all x, y, and z axes are distinct.

$$\begin{bmatrix} D_x \\ D_y \\ D_z \end{bmatrix} = \begin{bmatrix} \varepsilon_e & 0 & 0 \\ 0 & \varepsilon_0 & 0 \\ 0 & 0 & \varepsilon_0 \end{bmatrix} \begin{bmatrix} E_x \\ E_y \\ E_z, \end{bmatrix}, \tag{2.10}$$

$$\begin{bmatrix} D_x \\ D_y \\ D_z \end{bmatrix} = \begin{bmatrix} \varepsilon_1 & 0 & 0 \\ 0 & \varepsilon_2 & 0 \\ 0 & 0 & \varepsilon_3 \end{bmatrix} \begin{bmatrix} E_x \\ E_y \\ E_z \end{bmatrix}. \tag{2.11}$$

Gyrotropy is only established when there are off-diagonal elements in the material response. Furthermore, if the matrial tensor can be diagonalized, that material exhibits reciprocity, if not, the material exhibits non-reciprocity. Therefore, Eq. 2.10 and Eq. 2.11 are applicable for reciprocal systems. The relative phase can be written as[6–8]

$$\phi = (n_1 - n_2)\frac{2\pi l}{\lambda}, \tag{2.12}$$

where n_1 and n_2 are refractive indices defined as $n_1 = \sqrt{\frac{\varepsilon_1}{\varepsilon_0}}$ and $n_2 = \sqrt{\frac{\varepsilon_2}{\varepsilon_0}}$.

Therefore, the nature of the polarization of the field keeps changing as it propagates. The relative phase between x-y plane that is introduced by this propagation is called retardence.

2.3.2 Chiral Media

Chiral materials are characterized by asymmetric microstructures in such a way that those structures and their mirror images are not superimposable. As a consequence, right- and left-hand circularly polarized waves experience different impedances and propagate through the material with different phase velocities. Therefore, a medium made of chiral material shows the remarkable property of rotating the polarization of electromagnetic waves propagating through it. This phenomenon of polarization rotation, also called optical activity, was first observed by Arago with light passing through translucent substance and Biot with light passing thorough quartz in the early 1800s and later, it was explained by Fresnel in terms of circular birefringence in 1821-22.

Electromagnetic chirality is closely related to the three fundamental concepts, i.e. mirror asymmetry, polarization rotation, and magnetoelectric coupling which points out the nontrivial interdependencies existing between them. In summary, the chirality-tirnity can be nicely represented from Fig. 2-3.[36]

For chiral media, the Tellegen form of the constitutive relations can be represented as[8,36,37]

$$\mathbf{D} = \varepsilon\mathbf{E} - j\chi\mathbf{H}, \tag{2.13}$$

$$\mathbf{B} = \mu\mathbf{H} + j\chi\mathbf{E}, \tag{2.14}$$

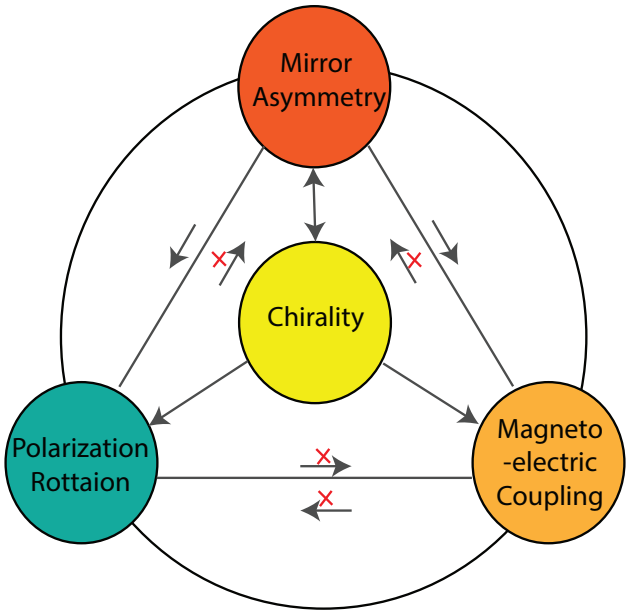

Figure 2-3: The chiral trinity with implication relations between the three fundamentally related concepts of mirror asymmetry, polarization rotation and magneto-electric coupling. The arrows indicate implications and the barred arrows indicate non-implications.

where χ is the parameter describing the chirality of the media. In terms of magneto-electric coupling and vice versa it can be represented as $\xi = +i\chi$ and $\zeta = -i\chi$. As discussed in the beginning of the section, the rotation through chiral media can be represented as

$$\phi = \frac{1}{2}(K_{\circlearrowleft} - K_{\circlearrowright})l, \tag{2.15}$$

where $k_{\circlearrowleft} = n_{\circlearrowleft}K_0 = \omega(\sqrt{\mu\varepsilon} + \chi)$ and $k_{\circlearrowright} = n_{\circlearrowright}K_0 = \omega(\sqrt{\mu\varepsilon} - \chi)$. Here, n defines refractive index of the medium and K_0 represents the free space wave number.

2.3.3 Wire-grid Polarizer

The wire grid polarizer consist of a regular array of parallel metallic wires, placed in a plane perpendicular to the incident beam. The transmitted wave has an electric field purely in the direction perpendicular to the wires, therefore, linearly polarized.

The amount of wave passing through a pair of polarizers can be quantitatively described

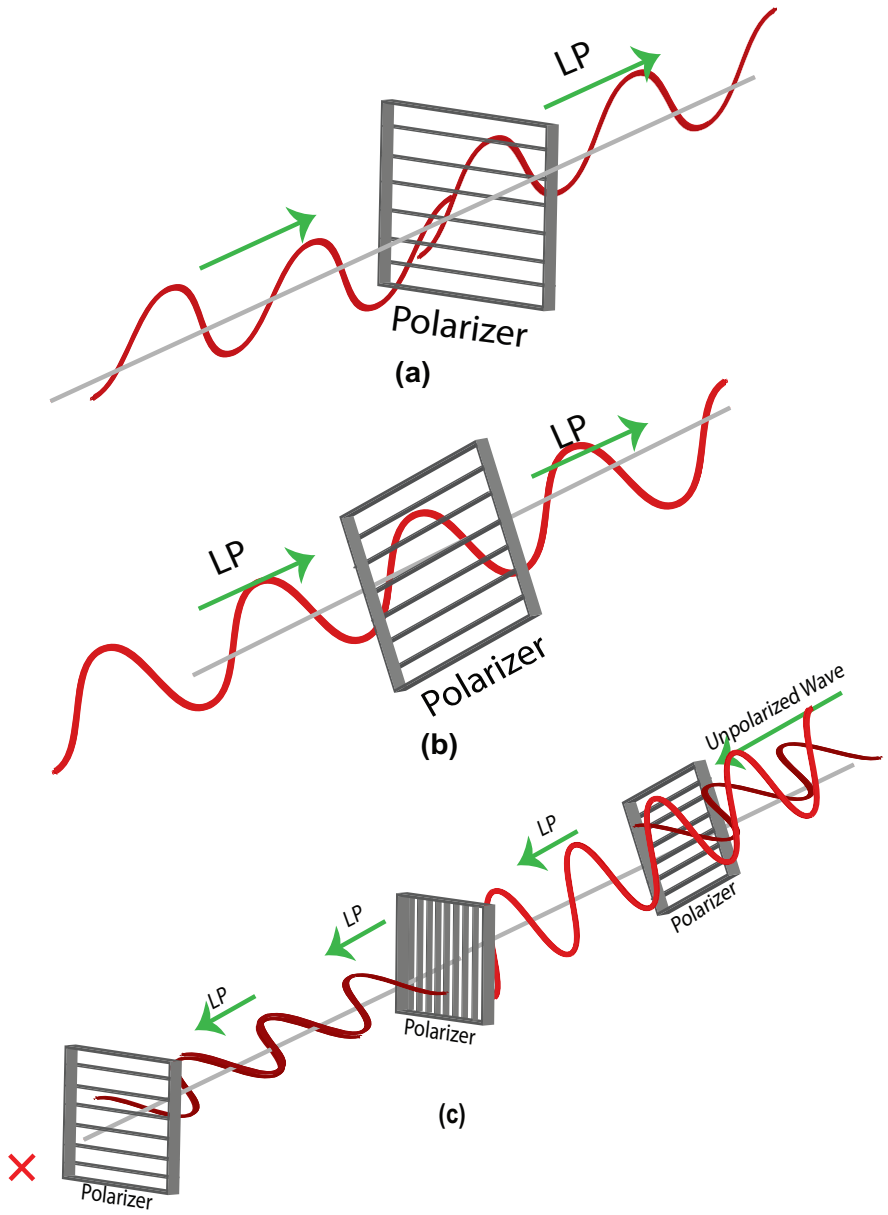

Figure 2-4: (a) and (b) LP Wave propagates when perpendicular to wire-grid. (c) Unpolarized wave passes 1st and 2nd polarizer based on Malus's principle, hence can not propagate past the last wire grid polarizer.

by applying Malus's cosine-squared law, as a function of the angles between the polarizer transmission axes, utilizing the equation $I = I_0\ cos^2\theta$, where, I is the intensity of the wave passing through the analyzer (2nd polarizer), I_0 is the intensity of light that is incident upon the polarizer, and θ is the angle between the transmission axes of the polarizer and analyzer. For example, it can be determined that when the two polarizers are perpendicular to each other, the intensity is zero. In this case, from Fig. 2-4 (c), this is shown that an unpolarized wave passes the 1st and 2nd polarizer (right to left) based on Malus's principle, hence can not propagate past the last wire grid polarizer.

2.3.4 Antenna Polarization

Similar experiments are also applicable in antenna communication. Figure. 2-5 shows that when the polarization of the two pyramidal horn antennas are the same, maximum signal transmission and reception is possible. However, if antenna 1 is y polarized and antenna 2 is x polarized, no communication is established, which can be described similarly by Malus's principle. In antenna communication, this is known as antenna polarization factor. Antenna is a reciprocal device. For both experiments shown in Fig. 2-5, $S_{21} = S_{12}$.

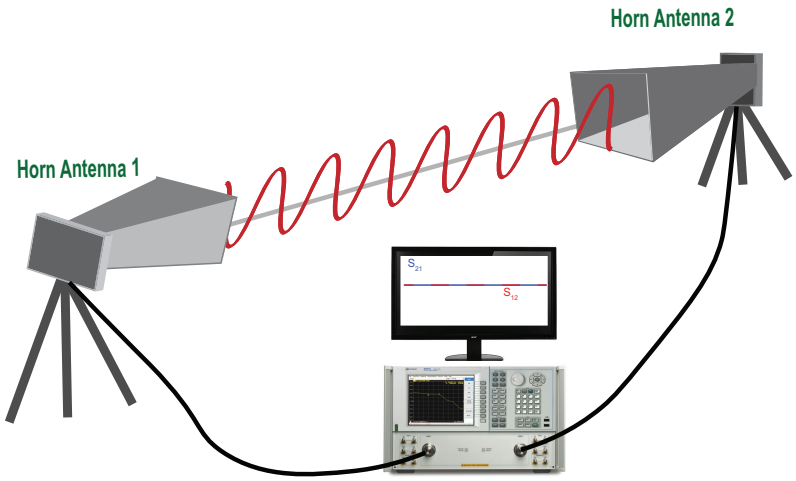

(a)

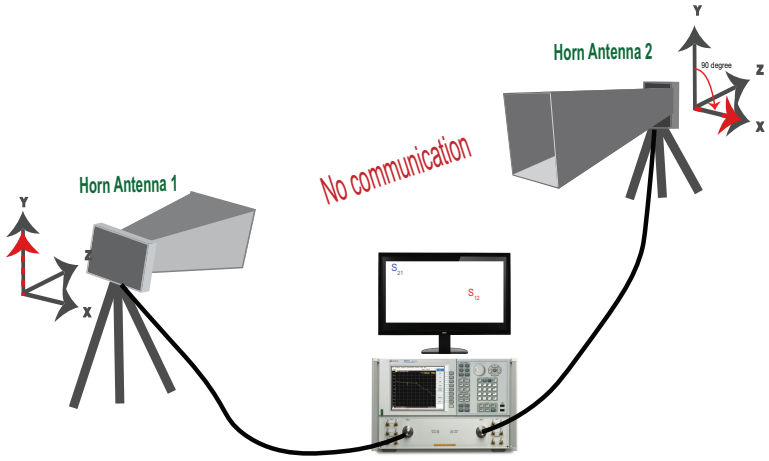

(b)

Figure 2-5: (a) S_{12} and S_{21} are same when two pyramidal horn antenna are same polarized. (b) No communication between antenna 1 and antenna 2 when they are 90° polarized to each other.

2.4 Propagation in Non-Reciprocal Gyrotropic Media

The word gyrotropy comes from the Greek word gyro meaning round, so that the polarization plane of the electromagnetic (EM) waves rotate as it propagates. Specifically, we can write EM waves into the summation of right- and left-handed circularly/elliptically polarized waves. If a media or systems interact differently with right- and left-handed circularly polarized waves (RHCP/LHCP), the polarization plane of the electromagnetic wave is affected. Some material, because of their intrinsic properties, exhibit this feature, i.e. those materials pose different refraction indexes for RHCP and LHCP waves. Therefore, wave propagating through those material experience different impedances, hence, different speeds for different handed waves.[27,38] The reason that the medium behaves differently for right- and left-elliptically polarized wave is the handedness of the structure so that the mirror images of the structure does not overlap with itself. Furthermore, non-reciprocity can be described as a system or a media which cannot return back to its original state when the time is reversed. Thus, non-reciprocal systems do not obey the time-reversal symmetry. Non-reciprocity is a general idea and gyrotropy is one thing that achieves non-reciprocity. Non-reciprocal media can be realized with natural materials such as magnetized ferrites, plasmas or magneto-optic materials. Based on this fundamental concept, many non-reciprocal components such as isolators, circulators, and variable phase shifters for the state-of-the-art telecommunications and radar applications have been developed over decades.

Non-reciprocal gyrotropy is a response of certain materials (e.g. Ferrites, Plasma) such that the medium rotates the polarization plane of an electromagnetic wave in presence of magnetic bias by a different amount other than the negative of the rotation angle when the medium is excited from the receiving port with same transmitted field pattern (time reversed case), as can be seen in Fig. 2-6. The rotation angle in this media is called the

Faraday rotation. Electromagnetic response of gyrotropy can be represented as[39]

$$\Phi = \frac{2(n_{\circlearrowleft} - n_{\circlearrowright})d}{\lambda}. \tag{2.16}$$

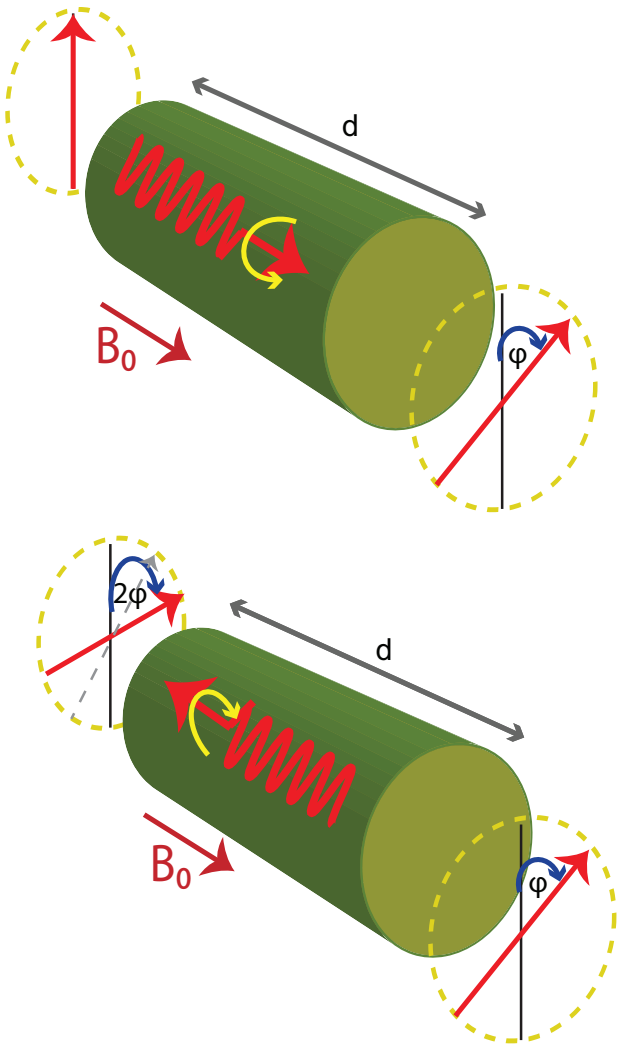

Figure 2-6: Electromagnetic response of gyrotropy.

Gyrotropic or optically active media are non-isotropic media in the presence of constant external magnetic bias. The constitutive relationship at frequency ω can be represented for gyroelectric media such as biased plasma as

$$\begin{bmatrix} D_x \\ D_y \\ D_z \end{bmatrix} = \begin{bmatrix} \varepsilon_1 & j\varepsilon_2 & 0 \\ -j\varepsilon_2 & \varepsilon_1 & 0 \\ 0 & 0 & \varepsilon_3 \end{bmatrix} \begin{bmatrix} E_x \\ E_y \\ E_z. \end{bmatrix}. \tag{2.17}$$

Similarly, the gyromagnetic media like ferrite can be represented as

$$\begin{bmatrix} B_x \\ B_y \\ B_z \end{bmatrix} = \begin{bmatrix} \mu_1 & j\mu_2 & 0 \\ -j\mu_2 & \mu_1 & 0 \\ 0 & 0 & \mu_3 \end{bmatrix} \begin{bmatrix} H_x \\ H_y \\ H_z \end{bmatrix}. \tag{2.18}$$

In summary, permitivity ε follows a tensor form in biased plasma media and μ follows a tensor form in ferrite media. The rotation of the polarization plane in those media is referred to as the Faraday rotation for the case of transmission and Kerr rotation for the case of reflection. A detail mathematical modelling has been developed for reflection and transmission coefficient for a biased ferrite material in normal incidence in the appendix.

2.5 Polarization Rotation, Reciprocity and Non-reciprocity

In earlier sections, we have discussed the various polarization rotation, when the wave propagates in various media. From Fig. 2-2, it is evident that time-reversal symmetry breaking is an operation that destroys, with an external bias, the time symmetry of a process, and hence, makes it time-reversal asymmetric and non-reciprocal.[4] Non-reciprocity has been described as a system which cannot return back to its original state when the time is reversed, thus, does not pose the time reversal symmetry. Ferromagnetic materials exhibit non-reciprocal gyrotropic response when they are biased with a static magnetic field. Besides, we have discussed in an earlier section that the permeability tensor of the ferrite has off-diagonal components, therefore, gyrotropic response of the magnetized ferrite is evident. This can be easily understood by considering the constitutive relation $\mathbf{B} = \overrightarrow{\mu} \cdot \mathbf{H}$, where

the x component of magnetic flux density has contribution both from x and y component of the magnetic field intensity. In addition, from the reciprocity theorem,[40] the reciprocal birefringent media has to satisfy the following conditions

$$\overrightarrow{\varepsilon} = \overrightarrow{\varepsilon}^T, \tag{2.19}$$

$$\overrightarrow{\mu} = \overrightarrow{\mu}^T, \tag{2.20}$$

$$\overrightarrow{\zeta} = -\overrightarrow{\xi}^T, \tag{2.21}$$

where $(.)^T$ is the Hermitian operator, $\overrightarrow{\zeta}$ and $\overrightarrow{\xi}$ are electric-magnetic and magneto-electric coupling tensors, respectively. Therefore, it can be clearly seen that, although, wave propagating through various media such as chiral, wire-grid, uniaxial or biaxial experience polarization rotation, those media do not exhibit non-reciprocal gyrotropic properties, hence, can not be used in non-reciprocal devices. In summary, the key things that necessitate non-reciprocal gyrotropic response for devices are intrinsic properties of material and external bias to break time reversal symmetry.

2.6 Material Classification

The magnetic dipole moment of a system measures the strength and the direction of its magnetism. As per Faraday's law, a bar magnet or a loop of electric current, creates a magnetic dipole moment. Magnetic dipole moment is a vector quantity, with a magnitude and a direction. From an atomic scale point of view of a material, an electron exhibits a magnetic dipole moment, from it's intrinsic clockwise or anticlockwise spin. Magnetic behaviour can be classified into three distinct categories: paramagnetism, diamagnetism, and ferromagnetism.

The spin of a single electron is denoted by the quantum number as $+\frac{1}{2}$ or $-\frac{1}{2}$. Opposite

spins cancel each other in pairs, however, a weak magnetic field is created when the electrons are unpaired. Therefore, the number of unpaired electrons in atomic scale define the magnetic behaviour of a molecule.[27,41]

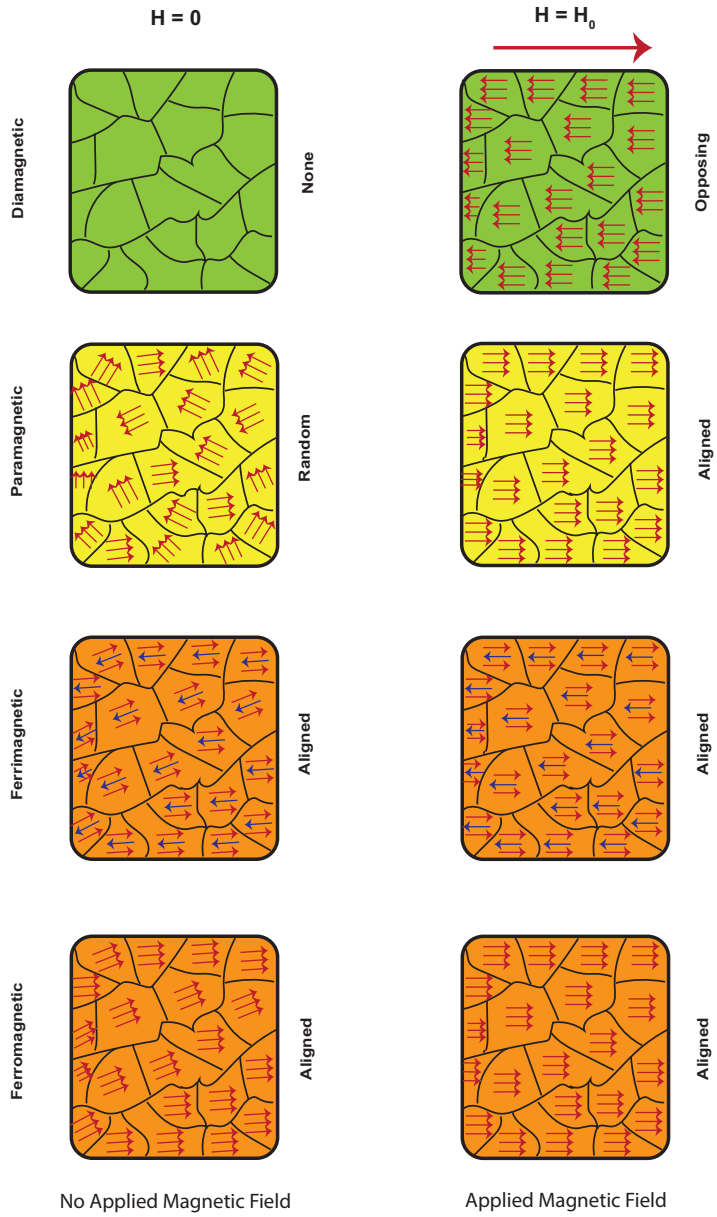

Figure 2-7: Magnetic behavior of materials.

From Fig. 2-7, we can see that the magnetic moment of every atom of diamagnetic substance is zero. In the presence of the applied magnetic field, magnetic moments are introduced that tend to move from stronger part to the weaker part of the field, i.e. applied

magnetic field direction and inherent magnetic moment direction are opposite. Examples are quartz, calcite, and water.

Unlike diamagnetic material, every atom of a paramagnetic substance experiences a weak magnetic moment. They are weakly attracted by the external magnetic field. In the presence of an applied magnetic field, the inherent dipole moments tend to align with the direction of the applied field. Examples are montmorillonite, nontronite, and pyrite.

The most important material for creating non-reciprocity, ferromagnetic and ferrimagnetic materials, exhibit similar properties, although there are some subtle differences. Both ferromagnets and ferrimagnets react towards the direction of an external field. Objects become magnetized when a large number of microscopic magnetic domains align in such a way that their individual tiny magnetic fields add together in the direction of the magnetic field, forming a larger field. In ferrimagnetic material, some fields point in the same direction and some in the opposite direction, although they can not cancel each other due to difference in strength. In ferromagnetism, all point in the same direction. For a ferromagnet and a ferrimagnet of the same size, the ferromagnet will likely have a stronger magnetic field. Examples are the elements Fe, Ni, Co, and many of their alloys are typical ferromagnetic materials. Magnetite is a ferrimagnetic material.

2.6.1 Ferromagnetic Resonance

The idea related to the motion of the magnetic dipole in the presence of the magnetic field and a self-consistent RF magnetic field represents the principle idea of ferromagnetic resonance.[27]

Conceptually, the spinning electron can be considered as a spinning mass which is charged electrically and is similar in many respects to the classical mechanical gyroscope. Therefore, the d-c magnetic forces acting on the magnetic dipole are analogous to gravita-

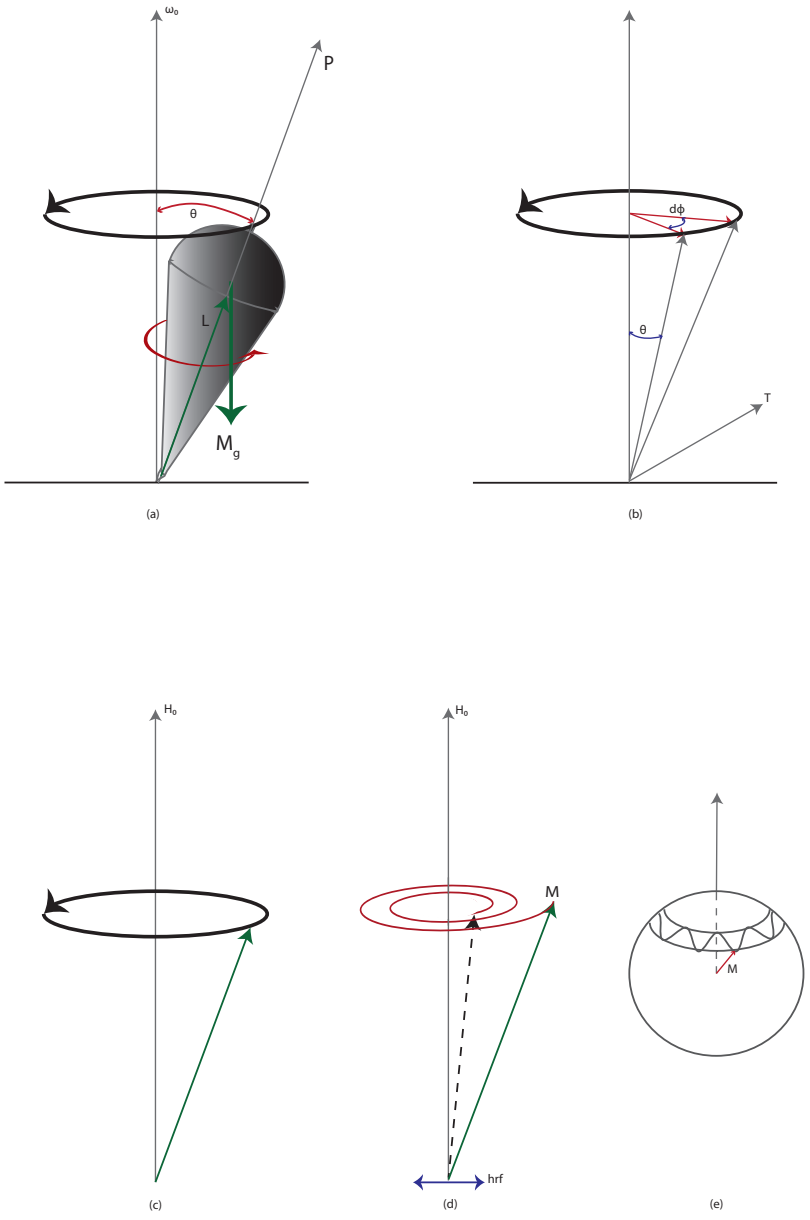

Figure 2-8: (a) Precessional motion of a spinning symmetrical top in a gravitational field (rigid body at frequency ω_0). (b) Angular momentum and torque vectors. (c) Precession of the magnetized vector in a constant magnetic field. (d) Precession of the magnetization vector in an alternating magnetic field when $\omega \neq \omega_0$. (e) The magnitude of a magnetization vector is constant so that oscillation takes place on the surface of the radius $|M|$.

tional force, as depicted in Fig. 2-8(a), and the relation between angular momentum vector **p**, torque **T**, and the constant angle θ can be represented as[27]

$$\frac{d\phi}{dt} = \omega_0 = \frac{T}{\sin\theta}, \tag{2.22}$$

where $\frac{dp}{dt} = T$ and θ is the constant angle between ω_0 and **p**. Therefore the angular momentum vector can be represented as

$$\frac{d\mathbf{p}}{dt} = \omega_0 \times \mathbf{p}. \tag{2.23}$$

Similarly, we can represent the electron spin as a magnetic top. The angular momentum and magnetic moment are parallel vectors having constant absolute values p and μ_e. For the electron, they are oppositely directed.[27] The gyromagnetic ratio is γ = -$\frac{\mu_e}{p}$ and the equation of motion is $\frac{d\mathbf{p}}{dt} = \mathbf{T}$. Therefore magnetization vector can be represented as

$$\frac{d\mathbf{p}}{dt} = -\gamma(\mathbf{p} \times \mathbf{H}) = \gamma(\mathbf{H} \times \mathbf{p}) = \omega_\mathbf{0} \times \mathbf{p}. \tag{2.24}$$

The macroscopic equation of notion of the magnetization vector can be represented as

$$\frac{d\mathbf{M}}{dt} = \gamma(\mathbf{M} \times H), \tag{2.25}$$

where $M = N\mu_e$, N is the number of dipoles per unit volume and $\gamma = \frac{ge}{2mc}$, where g is the Lande' factor (approximately equal to 2), c is the velocity of light, e is the electron charge, and m is the electron mass.

For resonance condition, this is necessary to apply the RF magnetic field (the microwave field) perpendicular to the d-c field. Therefore, microwave magnetism in a ferrite material is based on the precession of the magnetic dipole moments which arise from unpaired electron spins along the axis of an externally applied static magnetic bias[42] as shown in Fig. 2-

8. In this case, $\mathbf{H}_0 \parallel \widehat{\mathbf{z}}$. This quantum mechanical phenomena can be described from Landau-Lifshitz-Gilbert equation as[27,38,43]

$$\frac{d\mathbf{M}}{dt} = \gamma(\mathbf{M} \times \mathbf{H}) - \frac{\alpha}{|M|}\mathbf{M} \times \frac{d\mathbf{M}}{dt}, \tag{2.26}$$

where α is the Gilbert damping term, $\mathbf{M} = \mathbf{i}_z M_0 + \mathbf{m}e^{j\omega t}$, and $\mathbf{H} = \mathbf{i}_z H_i + \mathbf{h}e^{j\omega t}$, where $\mathbf{i}_z$ is the unit vector in the z direction, $\mathbf{m}$, and $\mathbf{h}$ are RF quantities, and H_i is the total internal d-c magnetic field. The nearer the frequency of the microwave field to the natural precession frequency, the greater will be the energy absorbed by the spins.[27]

The Landau-Lifshitz-Gilbert Eq. 2.26 states that the time variation rate of $\mathbf{M}$ due to transverse RF magnetic field signal $\mathbf{H}_t^{RF}$ is equal to the sum of torque exterderd by $\mathbf{H}$ on $\mathbf{M}$ in azimuthal direction $\widehat{\phi}$ and a damping term in elevation direction $\widehat{\theta}$ that reduces the precession angle θ shown in Fig. 2-9 to zero along circular spherical trajectory when the RF signal is relaxed.

Here, one important thing to add is that the longitudinal (z) component does not contribute to precession and therefore, to magnetism. Since, $\mathbf{H}_0 \parallel \widehat{\mathbf{z}}$, the z-component of $\mathbf{M}$ produced by $\mathbf{H}_t^{RF}$ would lead to

$$[M_z^{RF}(\mu_0 H + H^{RF})](\widehat{\mathbf{z}} \times \widehat{\mathbf{z}}) = 0. \tag{2.27}$$

Therefore, the only torque being produced by the transverse component at x-y plane can be stated as

$$(M_t^{RF}\mu_0 H)(\widehat{\mathbf{t}} \times \widehat{\mathbf{z}}) \neq 0. \tag{2.28}$$

To summarize, the magnetization vector described above has a singularity, when $\omega = \omega_0 = \gamma H_0$, which can be defined as the resonance condition. In other words, in order to

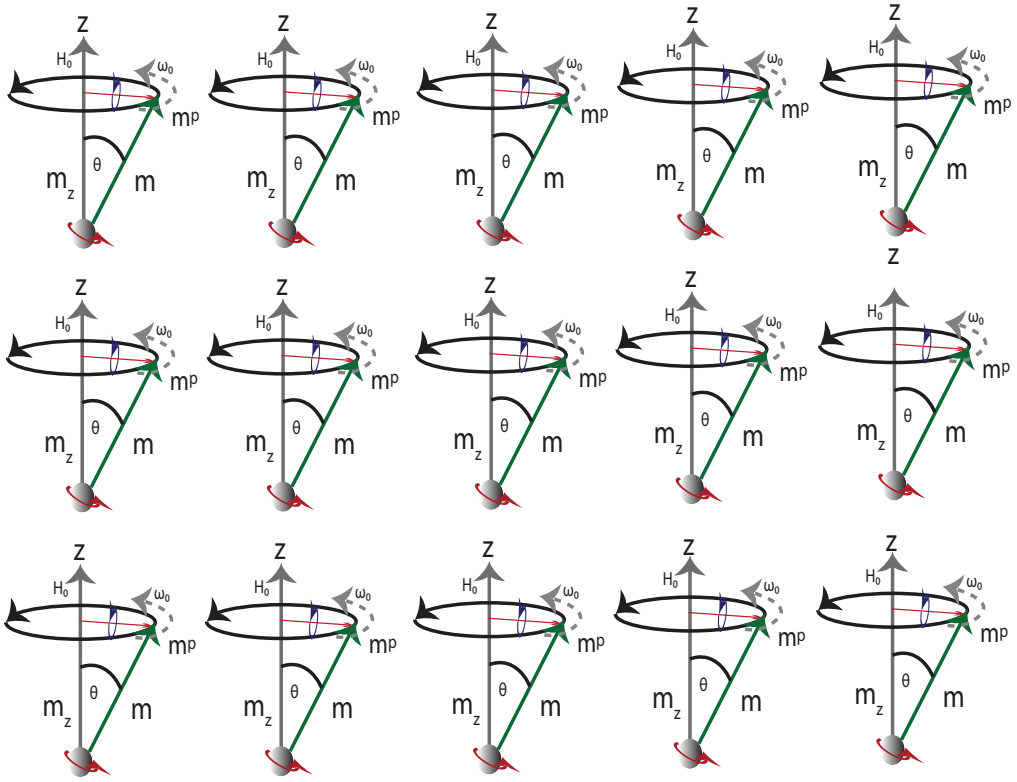

(a)

Figure 2-9: Magnetic dipole precession, arising from electron spinning in a ferrite material around z axis of an externally applied static magnetic bias field, $\mathbf{H}_0$ with effective unidirectional current loops (black arrow and blue arrow) and transverse radial rotating magnetic dipole moment mp associated with unidirectional current loops.

observe resonance, we can either vary the operating frequency or the applied field until the precession frequency equals the microwave frequency. Permeability tensor of ferrite material can be represented as[44,45]

$$\overrightarrow{\mu} = \mu_0 \begin{bmatrix} \mu & -jk & 0 \\ jk & \mu & 0 \\ 0 & 0 & 1 \end{bmatrix}, \tag{2.29}$$

where $\mu = 1 + \frac{\omega_0 \omega_M}{\omega_0^2 - \omega^2}$, $jk = \frac{j\omega\omega_M}{\omega_0^2 - \omega^2}$, and $\omega_M = \gamma 4\pi M_0$.

Physical Description of Spin Waves

Spin waves are very common phenomenon in various branches of physics. The concept of spin waves is based on longitudinal and transverse electric vectors in a tensor medium. For example, in plasma, a restoring force in a ferromagnetic medium tends to align all dipoles. Similarly, in the presence of DC magnetic field, the magnetic dipoles precess about **H**, and all in phase. The internal exchange magnetic field tends to align dipoles, and will act to swing their neighbours in a larger precessional angle, however, with a cost of a small delay in time. In this way, the larger precessional disturbance can travel through the crystal lattice in the form of a wave with both a phase and magnitude change from dipole to dipole. Figure 2-10 illustrates the conceptual understanding of standing spin wave and Fig. 2-11 illustrates the travelling spin wave.[27,46,47]

2.6.2 Faraday and Kerr Rotation

In earlier sections, we have described Faraday and Kerr rotation and necessary conditions to obtain non-reciprocity. Figure 2-12 illustrates Kerr rotation and Fig. 2-13 depicts Faraday rotation. Faraday rotation can be obtained from transmission properties when the medium

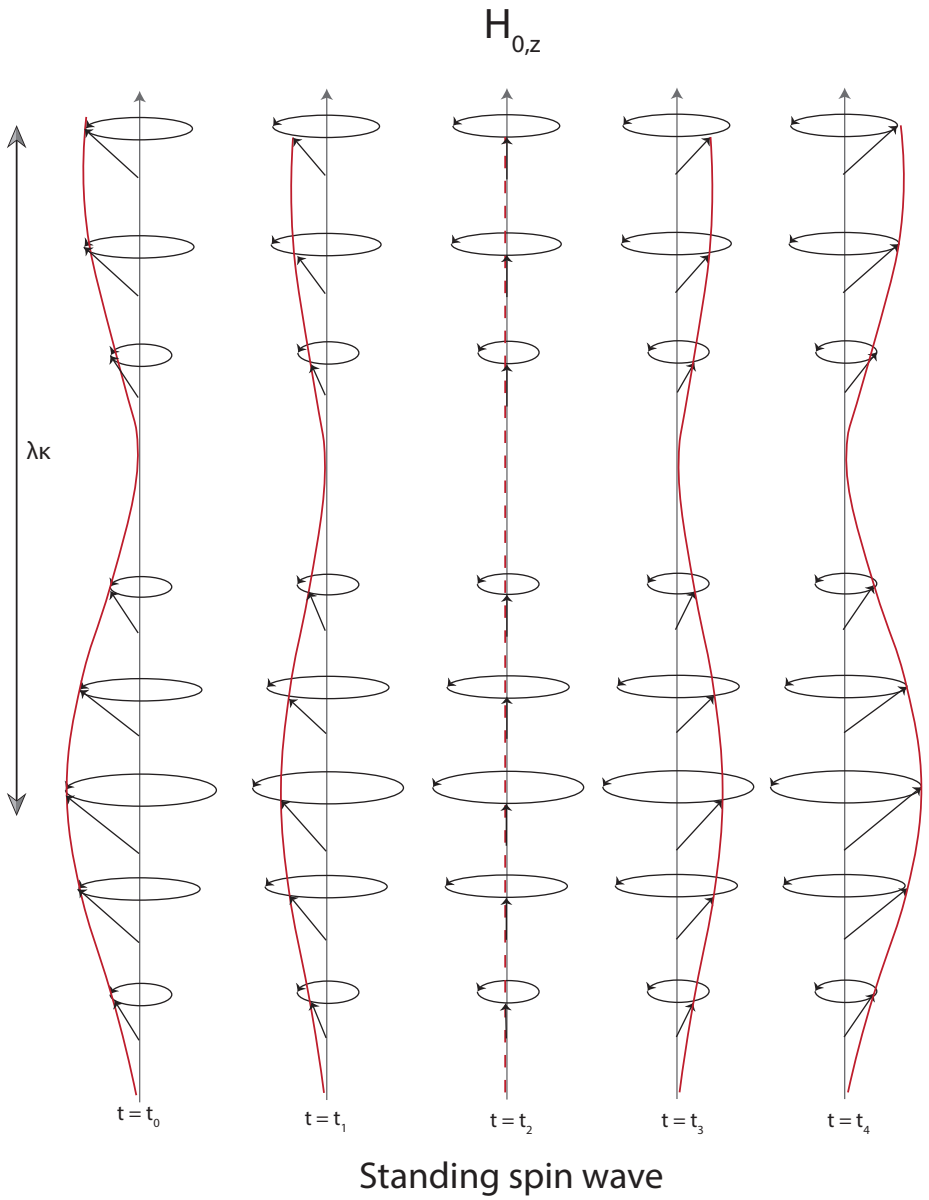

Figure 2-10: Adjacent spin dipoles precessing with different amplitude form a standing spin wave. The diploes precessing counterclockwise are shown at successive times $t_4 > t_3 > t_2 > t_1 > t_0$.

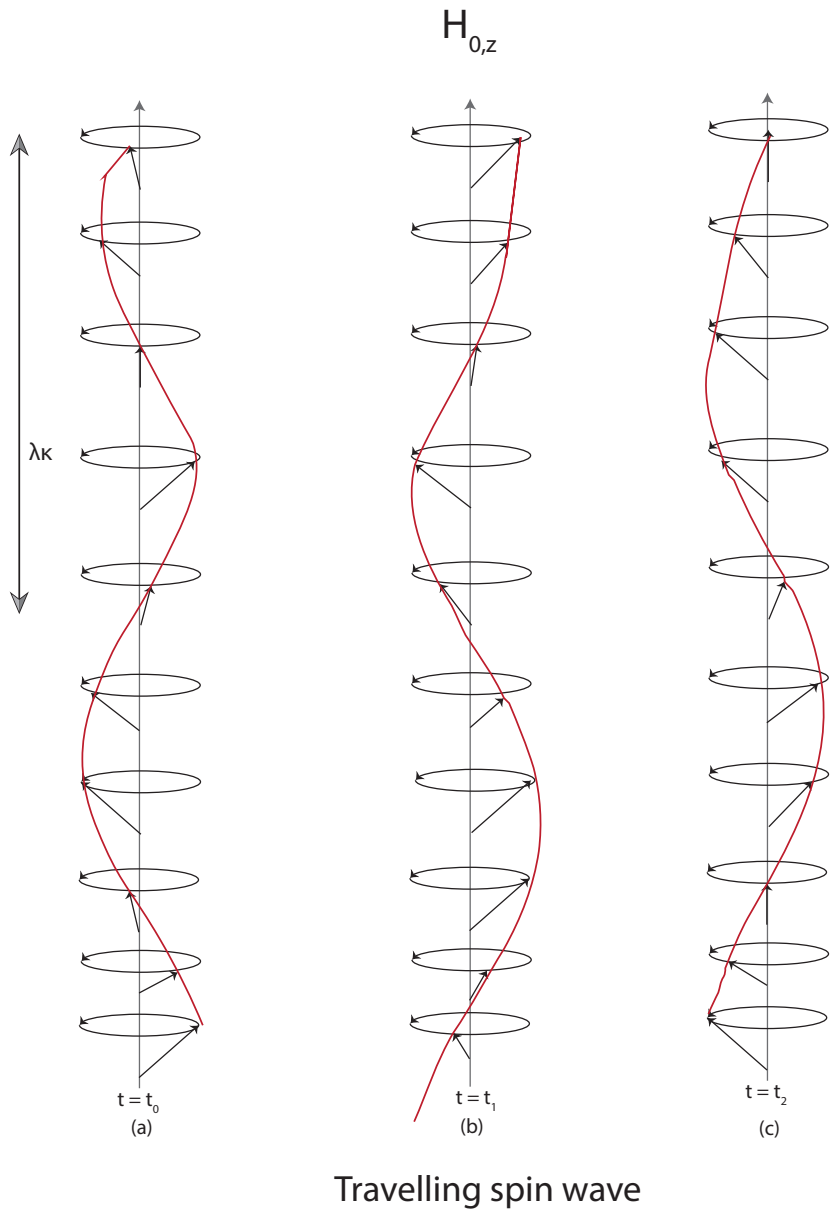

Figure 2-11: Adjacent spin dipoles in the vertical chain are precessing out of phase and forming a travelling spin wave. At a later time $t_1 > t_0$ the node of spin wave has moved upward along the direction of H_0 and therefore called "Z directed spin wave"

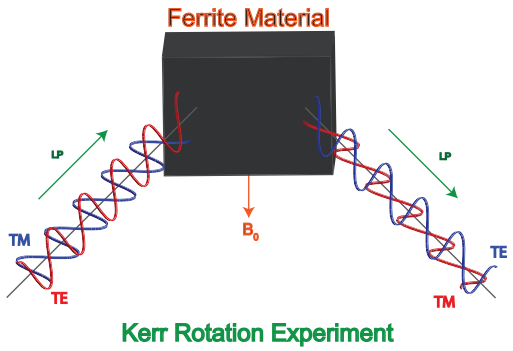

Figure 2-12: Electromagnetic isolation based on Magneto optical Kerr effect, can be achieved in lossless system[10]

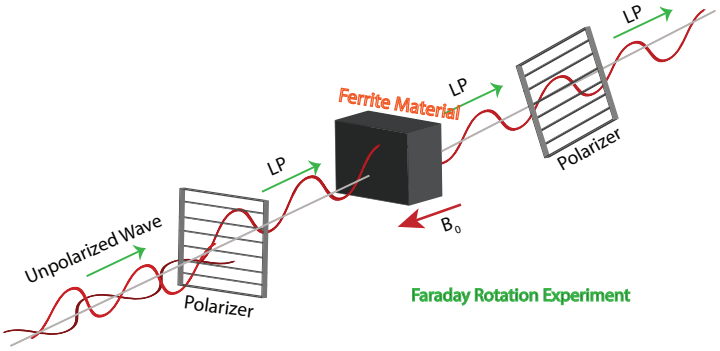

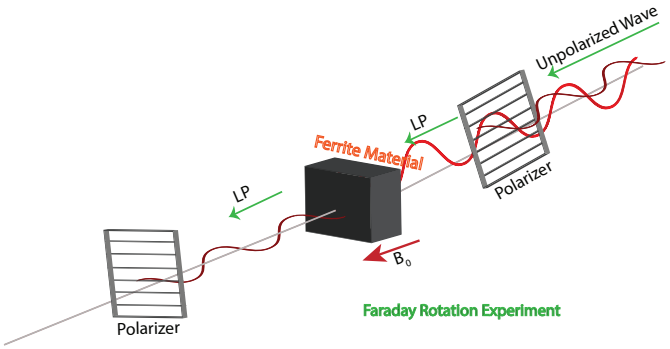

Figure 2-13: Electromagnetic isolation based on Faraday effect, in presence of dissipation losses in the system

is at least partially transparent and the Kerr rotation can be obtained from reflection properties of the medium.

Besides, one-way propagation based on the Faraday effect is achieved, where two linear polarizers are used from both sides of the ferrite material slab. The polarizers are rotated at 45° with respect to each other, and the ferrite slab rotates polarization of the incident wave by the same angle. Therefore, for illumination from the left, half of the un-polarized wave is transmitted through both polarizers and the slab. On the other hand, waves incident from the right side do not pass through the second polarizer based on the polarization property of the wire grid polarizer described in an earlier chapter. This Faraday and Kerr rotation mechanism is a very important concept in isolators and circulators, hence, in most nonreciprocal devices.[10]

At microwave frequencies, the magneto-optical effects are generally stronger than that at higher frequencies because microwaves are "slow enough" to excite resonant precession of electron's magnetic moments (spin) in ferromagnetic materials. Non-reciprocity in biased ferrite materials at microwaves frequencies can be described by the off-diagonal elements of the permeability tensor and due to the duality of permitivity and permeability, the Faraday and Kerr rotation can be observed at microwaves.[10,44,48]

2.7 Artificial Magnetic Metamaterial

Non-reciprocal behaviour can be achieved in ferrite or plasma in presence of external static magnetic bias by breaking time-reversal symmetry of the system. The requirement of the time-reversal asymmetry has been suggested in the scope of Onsager's principle of microscopic reversibility,[12,13,49] where Onsager and later Casmir showed that in the presence of the magnetic field, the current density is an odd vector under time-reversal. The principle of microscopic reversibility suggested by Casimir can also be applied to explain non-reciprocity

of the magnetized ferrite since the magnetic field is also an odd vector under time-reversal. An excellent discussion has been given by Caloz et al. focusing on electromagnetic quantity based on their time reversal odd/even parity[4,10] and is depicted in Fig. 2-14.

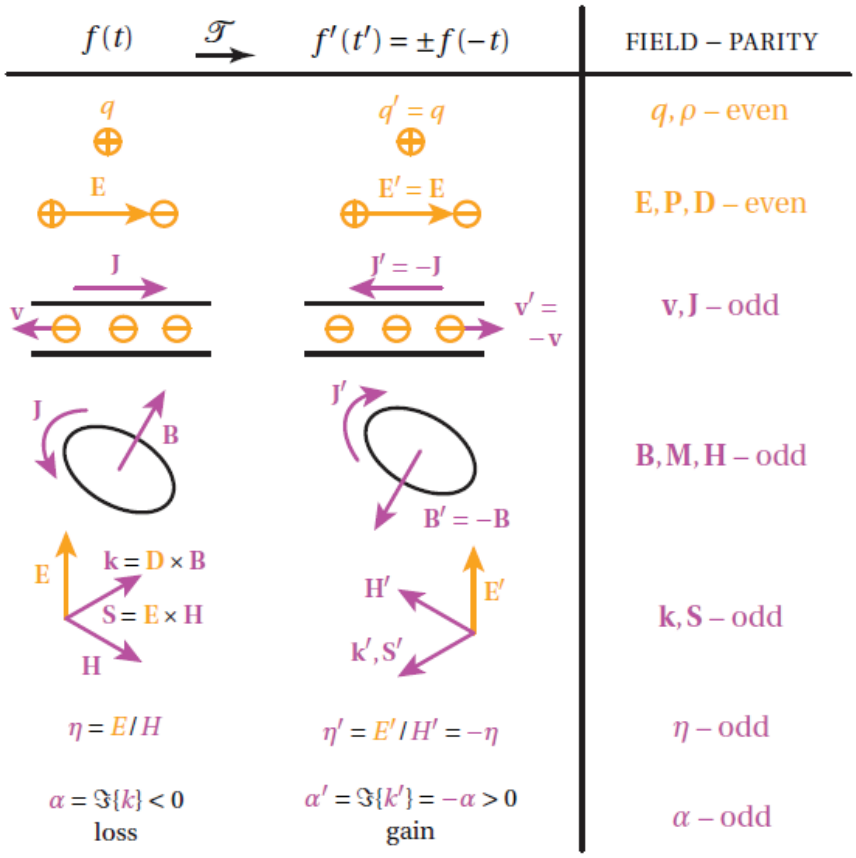

Figure 2-14: Time-reversal parity (even/odd), or symmetry/ anti-symmetry, of the main electromagnetic quantities (time-harmonic dependence $e^{j\omega t}$.)[4]

For many years, in order to overcome the drawbacks of using a rare earth magnet to bias ferrite, scientists showed a great interest to replace ferrites and ferrite based devices (isolators and circulators) with something lightweight, cost-effective, and compatible with semiconductors. Therefore, to implement artificial magnet-free non-reciprocity, major interests have been drawn on those quantities exhibit odd vector under time-reversal conditions, such as magnetic field, current density, linear momentum, and angular momentum.[50] The first magnet-free non-reciprocity was developed by Yu et al.[51] In this work, the isolation and the non-reciprocity was developed and practically verified by exciting indirect photonic

transitions by using the spatio-temporal modulation of the refraction index along a silicon photonic waveguide. For the very first time, this work paved a way of exploring artificial non-reciprocity. However, this work exhibits drawback such as fabrication difficulties and a large footprint. Later, Toshiro et al. for the first time suggested a non-reciprocal gyrotropic metasurface based on odd symmetry of the current under time reversal.[33] Their design exactly mimicks the spinning electron behaviour of magnetized ferrites, i.e. rotating magnetic dipole moment in a plane transverse to biasing direction, by forcing current via the transistor to flow in right- or left-handed along circular conducting ring pair. This results in different interaction mechanisms for right hand circular polarized (RHCP) and left hand circular polarized (LHCP) waves, therefore, the non-reciprocal gyrotropy is achieved. Later, based on this fundamental concept, non-reciprocal gyrotropy metasurfaces have been developed and used in various applications over the years.[2,5,14,52–54]

Industrial applications require a transparent non-reciprocal devices with minimal reflection. Therefore, the importance of the transparent magnet-free non-reciprocal gyrotropic devices are inevitable. None of the reported works till date has investigated tunability with various bias conditions, design optimization approaches, and multi-layer arrangements concentrating completely on Faraday and Kerr rotation. The main idea of this thesis is to design an artificial magnetic meta-surface and incorporate the tunability features. We believe, state of the art design optimization and analysis features in this thesis work will pave a new dimension with this existing novel concepts in device applications. The rest of the thesis is focused on solving these issues. In the following chapters, a detailed design, analysis, and test bench configurations will be developed and key performance indicators will be evaluated.

Chapter 3

Design of Fully Electronic Magnet-free Non-reciprocal Metamaterial

---

3.1 Ring Resonator Design

The field theory for the ring resonator was first introduced by Wolff and Knoppik.[55] In their work, a magnetic wall model was used to describe the curvature effect on the resonant frequency of the ring resonator. Furthermore, Wu and Rosenbaum found the mode chart[56] or frequency modes[57] of the ring resonator obtained from the eigenfunction of Maxwell's equations with the boundary conditions of the ring. The waves in ring resonators do not have beginnings and ends and so have no boundary conditions. Consistent with this requirement, a ring resonator can support two types of waves, standing waves and/or rotating waves. This mix of possibilities is analogous to the possible mix of standing waves and traveling waves in a linear system. When the mean circumference of the ring resonator is equal to an integral multiple of a guided wave-length, resonance is established. Therefore, this

statement follows the condition $2\pi r = n\lambda_g$, with n = 1,2,3..... and r is the mean radius of the ring resonator. Here, n is the mode number and λ_g is the guided-wavelength. For a microstrip ring resonator, guided wavelength λ_g can be related to frequency by

$$\lambda_g = \frac{\lambda_0}{\sqrt{\varepsilon_{eff}}} = \frac{1}{\varepsilon_{eff}} \frac{c}{f}. \tag{3.1}$$

Besides, mean radius of the circular ring can be represented as

$$r = \frac{nc}{2\pi f \sqrt{\varepsilon_{eff}}}, \tag{3.2}$$

where c is the velocity of light and ε_{eff} is the effective permitivity of the substrate used in the design. The mechanism of the circular ring is based on traveling-wave rotating currents along the rings, where the electrical circumference of the ring is a multiple of 2π.

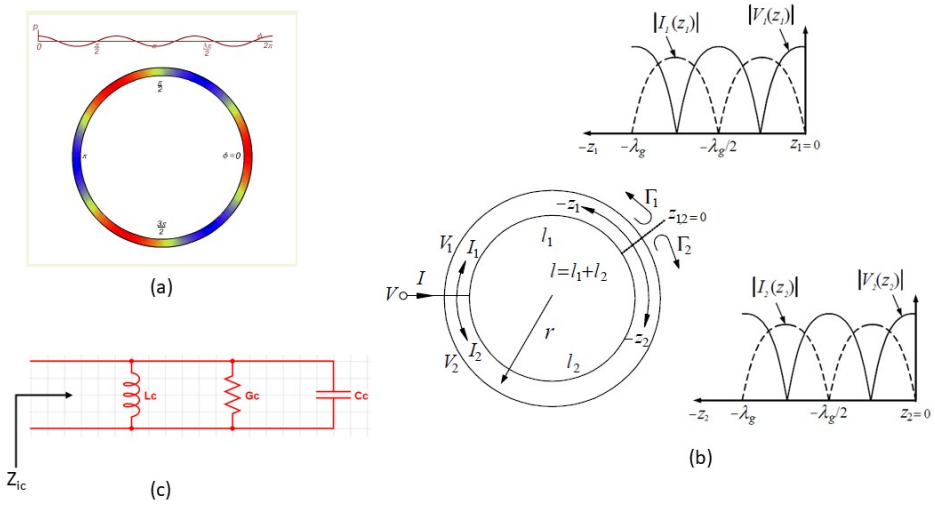

Figure 3-1: (a) Standing wave resonance in a ring resonator. (b) The configurations of one-port annular ring resonators (c) Equivalent circuit of the closed-loop ring resonator.

For a lossless transmission line, from Fig 3-1 (b), the voltages and currents can be

represented as

$$V_{1,2}(z_{1,2}) = V_0^+(e^{-j\beta z_{1,2}} + \Gamma_{1,2}(0)e^{j\beta z_{1,2}}), \tag{3.3}$$

$$I_{1,2}(z_{1,2}) = \frac{V_0^+}{Z_0}(e^{-j\beta z_{1,2}} - \Gamma_{1,2}(0)e^{j\beta z_{1,2}}), \tag{3.4}$$

where $V_0^+ e^{-j\beta z_{1,2}}$ is the incident wave propagating in the $+z_{1,2}$ direction, $V_0^+ e^{j\beta z_{1,2}}$ is the reflected wave propagating in the $-z_{1,2}$ direction, β is the propagation constant, $\Gamma_{1,2}(0)$ is the reflection coefficient at $+z_{1,2} = 0$, and Z_0 is the characteristic impedance of the ring. During resonance, standing waves set up on the ring. The shortest length of the ring resonator can be obtained from the positions of the maximum values of these standing waves. These positions can be calculated from the derivatives of the voltages and currents in Eq. 3.3 as

$$\frac{\partial V_{1,2}(z_{1,2})}{\partial z_{1,2}} = 0, \tag{3.5}$$

and reflection coefficient can be found as $\Gamma_{1,2}(0) = 1$. Therefore, the voltage and current can be obtained from Eq. 3.3 and Eq. 3.4 as

$$V_{1,2}(z_{1,2}) = 2V_0^+ cos(\beta z_{1,2}), \tag{3.6}$$

$$I_{1,2}(z_{1,2}) = \frac{-j2V_0^+}{Z_0} sin(\beta z_{1,2}). \tag{3.7}$$

The absolute values of the maximum voltages ($2V_0^+$) on the ring can be found, when $z_{1,2} = m\frac{\lambda_g}{2}$, where m = 0,1,2...., and, current at this position will be 0. Similarly, the absolute values of the maximum currents ($\frac{2V_0^+}{Z_0}$) can be found at $z_{1,2} = (2m-1)\frac{\lambda_g}{4}$, where m = 0,1,2.... and voltage at this position will be 0. As discussed earlier in this section, the total length of the annular ring resonator with a mean radius r that satisfies the standing wave condition will be $l = n\lambda_g = 2\pi r$.

3.2 Active Device Based Ring Resonator Design

Magnetized ferrites offer strong non-reciprocity, however, can not overcome application oriented problems such as high cost, bulk size, and incompatibility with semiconductor which led to an increasing quest in investigating fundamentally different approaches that non-reciprocity can be achieved without requiring a magnet altogether. In 1947, after the invention of the transistor by Shockley, Bardeen, and Brattain this interest became more realistic. When a transistor based device operates in its gain mode, it becomes intrinsically nonreciprocal. For example, a transistor amplifier can be viewed as an isolator that amplifies the input signal in one direction and blocks it in the reverse direction.[58]

Active devices have been used in the design of metamaterials supporting nonreciprocal scattering of waves in free space[39,52,53] or as magnet-free solutions for planar nonreciprocal devices.[22,23] In a series of publications between 2011 and 2019, Kodera et al.[5,33,39,52,53] explored the unidirectional properties of transistors in the design of non-reciprocal metamaterials. A ring resonator described in previous section normally supports two counter propagating modes with the same resonance frequency, a result of reciprocity. When unidirectional component such as transistor is used in the ring gap, one of the modes is blocked and the ring loaded with transistor resonates only for one type of circularly polarized waves, mimicking the electron spin precession of a magnetic-biased ferrites. As a result, the metamaterial proposed by Kodera et al. exhibits non-reciprocal gyrotropic effects, such as the Faraday rotation, and he also implemented this active device based metamaterial for integrated non-reciprocal devices, such as circulators, isolators, and leaky wave antennas.

Figure. 3-2 shows travelling wave resonance of a slot ring resonator loaded with transistor and passive components mimicking the electron spin precession in a biased ferromagnetic material. This has been shown that the electrical length (λ) of the ring resonator should be 2π. The wave is traveling (as opposed to standing wave) due to the presence of the unilateral (transistor) element. Based on the applied electric bias to the active component,

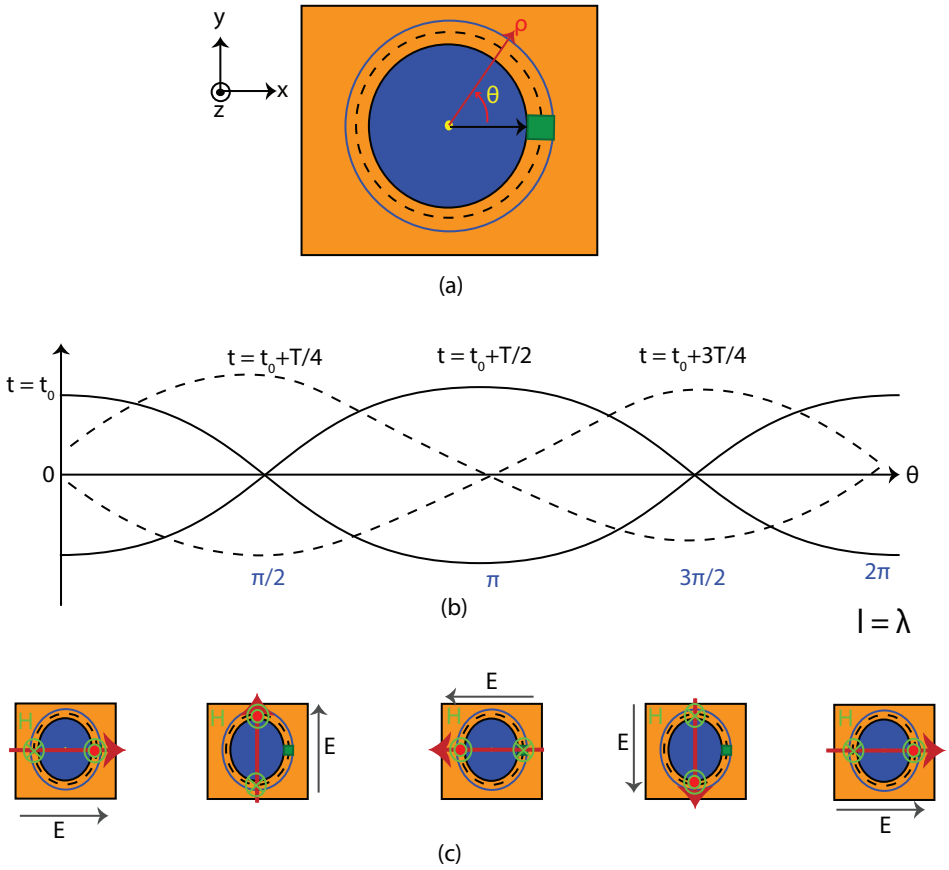

Figure 3-2: Non-reciprocal gyrotropy. Rotating dipole moment in (a) the proposed metamaterial structure consisting of slot-ring resonator loaded with active components (transistor). (b) travelling wave along the ring at four quarter-period spaced time instants. (c) Rotating electric field in the slot-ring and the corresponding electric dipole moment due to vectorial magnetic field pointed outward and inward.

the electric dipole moment (red arrow) rotates along the circular ring at four quarter period spaced time instants. The direction of the electric field follows the direction of the dipole moment. Therefore, non-reciprocal gyrotropy is established in the slot-ring resonator loaded with active and passive components. The circular ring resonates when the electrical length

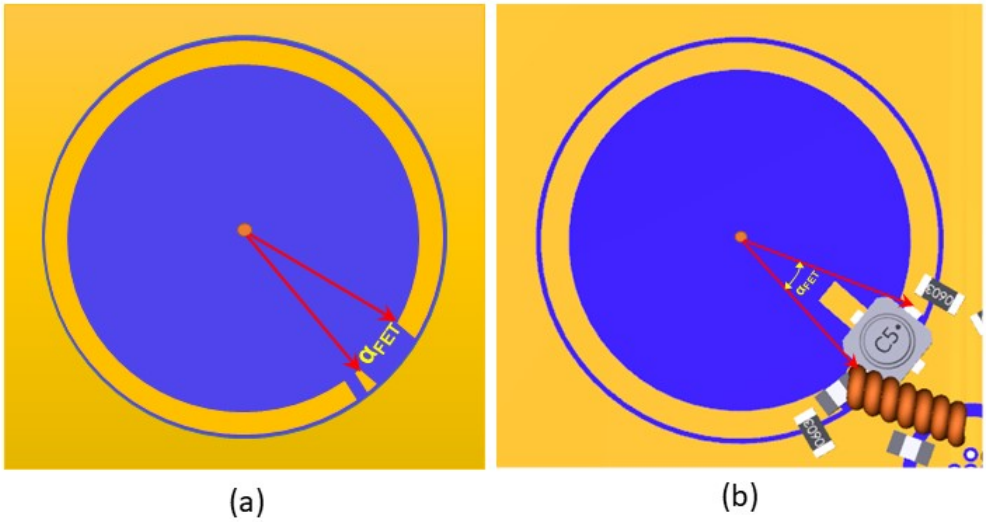

Figure 3-3: (a) Slot ring resonator. (b) Transistor and RLC components loaded slot ring resonator

is equal to an integer multiple of 2π[52]

$$\beta l + \alpha_{FET} = 2m\pi, \tag{3.8}$$

where β is the propagation constant defined by $\frac{2\pi}{\lambda_g}$, α_{FET} is the slot gap as shown in Fig. 3-3 (a), and l is the physical length of the slotted transmission line defined as $l = (2\pi - \alpha_{FET})r_{mean}$. According to Bahl and Trivedi,[59] the effective dielectric constant for a microstrip geometry is

$$\varepsilon_e = \frac{\varepsilon_r + 1}{2} + \frac{\varepsilon_r - 1}{2}\left(1 + 12\left(\frac{H}{W}\right)\right)^{-\frac{1}{2}}, \tag{3.9}$$

where Eq. 3.9 follows the condition i.e. $\frac{W}{H} \geq 1$. Besides, similarly, characteristics

impedance, Z_0 can be calculated as

$$Z_0 = \frac{120\pi}{\sqrt{\varepsilon_e}\left[\frac{W}{H} + 1.393 + \frac{2}{3}\ln\left(\frac{W}{H} + 1.444\right)\right]}. \tag{3.10}$$

In this research work, FR4-TG-140 ($\varepsilon_r = 4.35$) substrate has been used with a thickness of 0.8mm. This is a transparent design meaning that no metal plane has been used at the back of the device for complete reflection. As we are focusing on measuring the Faraday rotation, universal ground plane and circuit components have been designed on geometry of same front side as depicted in Fig. 3-4 (b). Based on the above analysis, initial parameters have been calculated considering a resonance frequency of 7.2 GHz. For simulation and analysis, Ansys Electronics 19.3 has been used. Pattern search algorithm and cost function analysis has been developed for design optimization. Figure 3-5 describes the final dimension and corresponding circuit configuration with slot ring resonator.

The most important concept that mimics the electron spin precession of ferrite media biased by a permanent magnet is the magnetic moment(transverse component), m_ρ depicted in Fig. 3-4 from which the magnetization will arise at the macroscopic level. The magnetic moment may be also produced by a pair of antisymmetric ϕ oriented currents, rotating on the same cylinder, which can be produced by a pair of conducting rings operating in their odd mode,[5,42] as shown in Fig. 3-4 (a). When this ring pair structure is loaded by a transistor, magnetic moment, m_ρ will unidirectionally rotate about z axes when excited by an RF signal. Therefore, artificial gyrotropy will be established in the transistor loaded ring resonator. The longitudinal component m_z does not contribute to electron spin precession, and therefore, magnetism. Since, $\mathbf{H_o}||\widehat{\mathbf{z}}$, the z-component of m produced by $\mathbf{H}_z^{RF}$ would lead to $\mathbf{m}_z^{RF} \times (\mu_0 H + \mu_0 H^{RF})\widehat{\mathbf{z}} = [m_z^{RF}(\mu_0 H + \mu_0 H^{RF})(\widehat{\mathbf{z}} \times \widehat{\mathbf{z}})] = 0$. Therefore, transverse component of the magnetic moment has the only contribution in magnetic precession. $\mathbf{m}_t^{RF} \times (\mu_0 H\widehat{\mathbf{z}} + \mu_0 H^{RF}\widehat{\mathbf{t}}) = [m_t^{RF}\mu_0 H(\widehat{\mathbf{t}} \times \widehat{\mathbf{z}}) + m_t^{RF}\mu_0 H^{RF}(\widehat{\mathbf{t}} \times \widehat{\mathbf{t}}) \neq 0$, where $\mathbf{H}_t^{RF}, \widehat{\mathbf{t}} \in xy$ plane.[5]

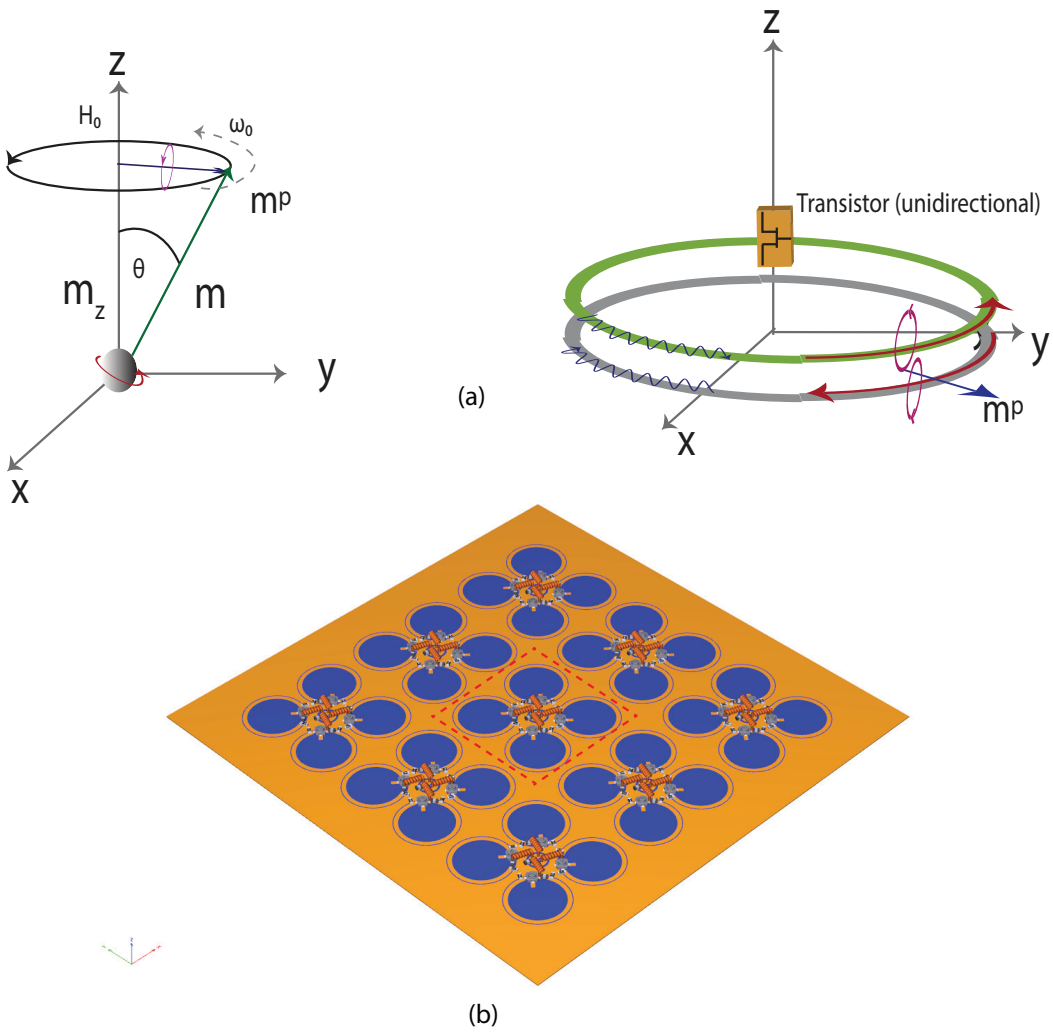

Figure 3-4: (a) Magnetic dipole precession, arising from electron spinning in a ferrite material about the z axis of an externally applied static magnetic bias field, H_0, with effective unidirectional current loops around z axis and magnetic dipole moment m_ρ respectively. (b) slot ring resonator loaded with unidirectional component supporting anti-symmetric current (image theory) and unidirectional current wave resulting radial rotating magnetic dipole moment emulating ferrite magnetic moment precession. (b) Simulated metamaterial board with 3 by 3 super cell array where each super cell consist of 4 slot ring resonator (dotted line) loaded with active-passive components.

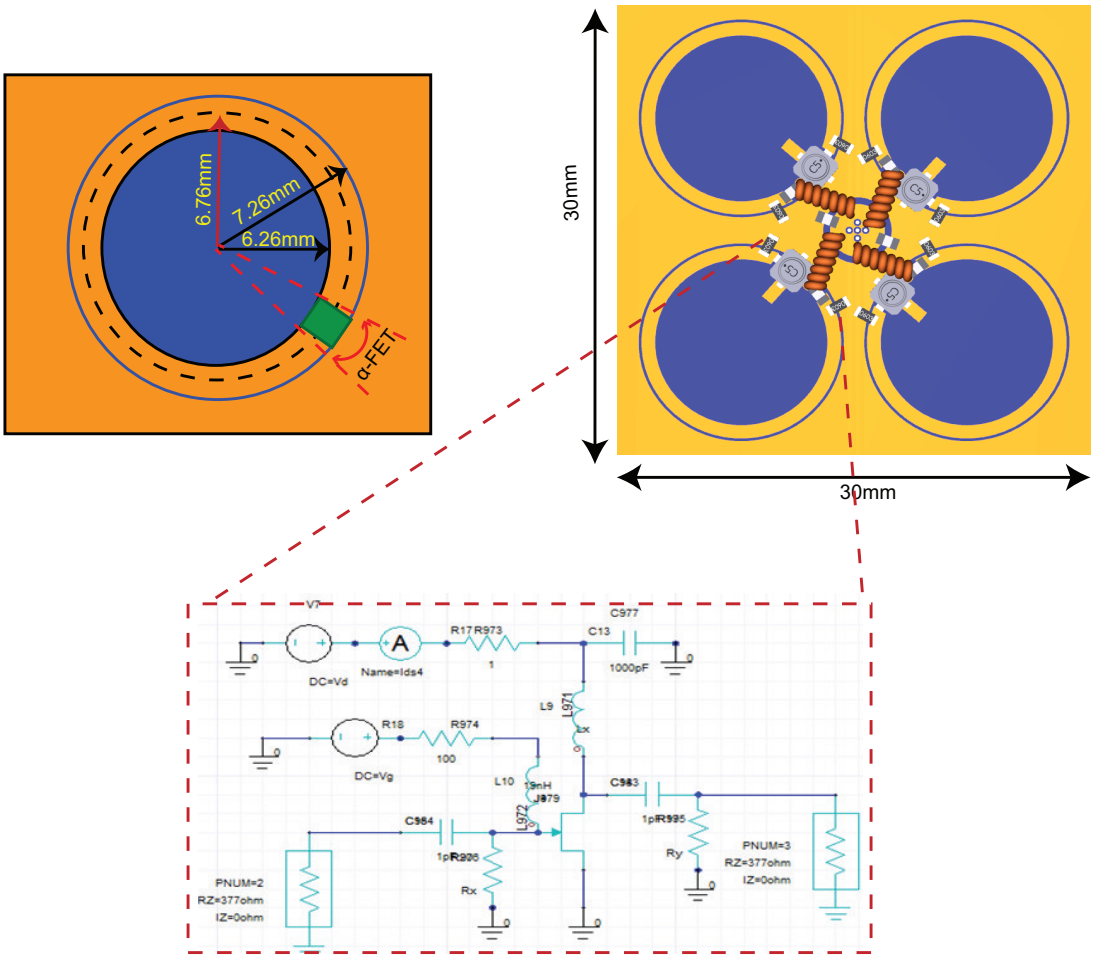

Figure 3-5: Unit super-cell consisting of 4 rings in a 90^0-symmetric configuration. Dimensions of the ring resonator and loaded circuit configuration for each ring slot.

In Ansys, we analyzed the model by doing full wave simulations using the feature called dynamic link which allow to establish a link between the 3D HFSS model and electronic circuit model of the transistor along with RLC components. In general, the full-wave simulations show the desired behavior, however, there exist two types of discrepancies. The first discrepancy is related to the resonance frequency and the second discrepancy is related to the peak values of the reflection coefficient. Both of these discrepancies are attributed to the imperfect matching between the transistor loaded circuit and the circular transmission ring in the full-wave simulations. This is because of the curvature of the ring and the inherent parasitic elements in high frequency structure simulator (HFSS) lumped ports. The presence of parasitic elements associated with the ring gap creates an extra phase shift beyond that the provided phase shift by the transistor loaded circuit. This additional phase shift lowers the resonance frequency. Therefore, the matching between ring and transistor loaded circuit is very important for this design. In the presence of mismatch between the ring and the nonreciprocal circuit components, the excited resonance is accompanied by loss, leading to continuous power reflection and absorption between port 1 and port 2. These events continue until the reflected power at port 2 after successive reflections/absorptions become very negligible. This type of mismatch also results in a nonzero standing wave ratio (SWR). These whole events increase the ellipticity of the rotating magnetic moment and therefore, reduce non-reciprocity. The structure is reciprocal, when, there is an infinite voltage standing wave ratio (VSWR), which leads to no moment rotation.[60]

Figure 3-5 depicts the circuit model used in the ring gap. The 1 pF capacitors are used to prevent dc current leakage to the rings, while, the 1 nF capacitor and the RF choke coils (meander line) are used to block flow of RF signal towards the dc voltage source. The resistors, 65Ω and 100Ω, at the gate and the drain of the high electron mobility transistor (HEMT) are introduced to improve matching. For our work, s parameters/touchstone files of super low noise, Ku band, Galium Arsenide (GaAs) field effect transistor (FET), CE3512K2, has been used for full wave 3D simulation.

3.3 Design, Performance, and Analysis

Since the slot ring resonator loaded with active components shows promising behavior in mimicking non-reciprocal gyrotropic response/ferrite material in the presence of an external magnetic field, it is very important to characterize properties such as Faraday rotation, Kerr rotation, polarization, and ellipticity. The ellipticity, δ_F, is a measure of the polarization state which varies between -1 to +1. The value of ellipticity, δ_F, -1, +1, and 0 define RHCP, LHCP, and LP respectively. The Faraday rotation and ellipticity are defined[27] as

$$\theta_F = \frac{1}{2}\tan^{-1}\left(\frac{T_{\circlearrowleft\circlearrowleft}}{T_{\circlearrowright\circlearrowright}}\right). \tag{3.11}$$

The transmission matrix in a linear basis can be mapped to a transmission matrix in a circular basis as

$$\begin{bmatrix} \mathbf{T}_{\circlearrowright\circlearrowright} & \mathbf{T}_{\circlearrowright\circlearrowleft} \\ \mathbf{T}_{\circlearrowleft\circlearrowright} & \mathbf{T}_{\circlearrowleft\circlearrowleft} \end{bmatrix} = \frac{1}{2}\begin{bmatrix} T_{xx}+T_{yy}+i(T_{xy}-T_{yx}) & T_{xx}-T_{yy}-i(T_{xy}+T_{yx}) \\ T_{xx}-T_{yy}+i(T_{xy}+T_{yx}) & T_{xx}+T_{yy}-i(T_{xy}-T_{yx}) \end{bmatrix}. \tag{3.12}$$

Based on our above discussion and Eq. 3.12, we can describe the $\mathbf{T}$ matrix in the circular basis as

$$\mathbf{T}_{\circlearrowright\circlearrowright} = \text{Incident RHCP to recieved RHCP}, \tag{3.13}$$

$$\mathbf{T}_{\circlearrowleft\circlearrowright} = \text{Incident LHCP to recieved RHCP}, \tag{3.14}$$

$$\mathbf{T}_{\circlearrowright\circlearrowleft} = \text{Incident RHCP to recieved LHCP}, \tag{3.15}$$

$$\mathbf{T}_{\circlearrowleft\circlearrowleft} = \text{Incident LHCP to recieved LHCP}. \tag{3.16}$$

Ellipticity related to transmission can be written as

$$\delta_F = \frac{\mid T_{\circlearrowleft\circlearrowleft} \mid - \mid T_{\circlearrowright\circlearrowright} \mid}{\mid T_{\circlearrowleft\circlearrowleft} \mid + \mid T_{\circlearrowright\circlearrowright} \mid}. \tag{3.17}$$

Similarly, Kerr rotation can be written as

$$\theta_K = \frac{1}{2}\tan^{-1}(\frac{R_{\circlearrowright\circlearrowleft}}{R_{\circlearrowleft\circlearrowleft}}). \tag{3.18}$$

The reflection matrix in a linear basis can be mapped to reflection matrix in a circular basis as

$$\begin{bmatrix} \mathbf{R}_{\circlearrowleft\circlearrowleft} & \mathbf{R}_{\circlearrowright\circlearrowleft} \\ \mathbf{R}_{\circlearrowleft\circlearrowright} & \mathbf{R}_{\circlearrowright\circlearrowright} \end{bmatrix} = \frac{1}{2}\begin{bmatrix} R_{xx}+R_{yy}-i(R_{xy}-R_{yx}) & R_{xx}-R_{yy}-i(R_{xy}+R_{yx}) \\ R_{xx}-R_{yy}+i(R_{xy}+R_{yx}) & R_{xx}+R_{yy}+i(R_{xy}-R_{yx}) \end{bmatrix}. \tag{3.19}$$

Ellipticity related to the reflection matrix can be represented as

$$\delta_K = \frac{\mid R_{\circlearrowleft\circlearrowleft} \mid - \mid R_{\circlearrowright\circlearrowright} \mid}{\mid R_{\circlearrowleft\circlearrowleft} \mid + \mid R_{\circlearrowright\circlearrowright} \mid} \quad . \tag{3.20}$$

R_{xx} is the reflection coefficient of the same polarization (co-polarization) and R_{xy} is the reflection coefficient from one polarization to another (cross-polarization). Similarly, T_{xx} is the transmission coefficient of the same polarization (co-polarization) and T_{xy} is the transmission coefficient from one polarization to the other one (cross-polarization). Furthermore, we have translated this mathematical modelling to Ansys HFSS simulation by using floquet mode analysis, where transverse electric (TE) modes are y polarized and transverse magnetic (TM) modes are x polarized.

In this section, we will discuss various key performance indicators (KPI) of our design. The design has been targeted to achieve transmission type Faraday rotation at 7.2 GHz. Based on the formalism described above, Kerr rotation has also been calculated and analyzed. Conventionally, Kerr rotation is calculated based on complete reflection, however,

the design is different from the conventional approach, where, the design is backed by a perfect conductive plane to achieve complete reflection. Therefore, maximum Kerr rotation has been shifted from the resonance frequency and observed around 5.12GHz. Figure 3-6 depicts the reflection and transmission behaviour when the structure is excited by a normal incidence plane wave from $z > 0$ as depicted in 3-10 (b). In Fig. 3-6, the reflection and transmission components are plotted for TE (y-polarized) and TM (x-polarized) plane wave incidence. It can be clearly seen that at around 7.2 GHz, the travelling wave resonance occurs so that the gyrotropic transmission response is evident form T_{xy} and T_{yx} as expected from an artificial ferrite. Similarly, at around 5.1 GHz, the travelling wave resonance occurs so that the gyrotropic reflection response is evident form R_{xy} and R_{yx}. The resonances as seen from the figures have a large bandwidth which shows that the quality factor (inversely proportional to bandwidth) of the structure is not very high.

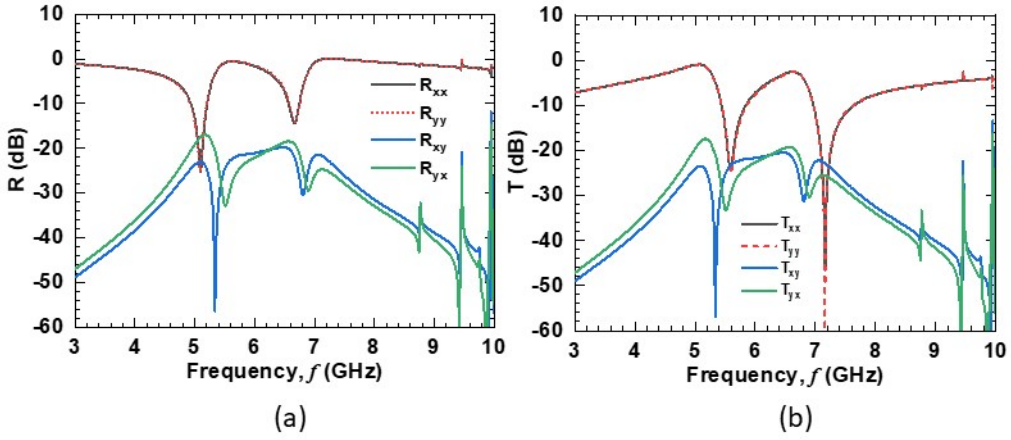

Figure 3-6: x and y polarized plane wave incidence from $z > 0$ (a) Reflection coefficient. (b) Transmission coefficient of the designed structure (Fig. 3-4).

Figure 3-7 depicts the Faraday and Kerr rotation at various bias conditions. The behaviour of the Faraday rotation varies with respect to the applied drain-source voltage, V_{DS}, drain-source current I_{DS}, and gate-source voltage, V_{GS}. We get maximum Faraday and Kerr rotation when $V_{DS} = 3$V and $I_{DS} = 30$mA. Similarly, nonreciprocal behaviour is

absent when the transistor is switched off or $V_{DS} = 0$V. Faraday rotation has been achieved at resonance frequency, 7.20 GHz and at this frequency, the observed Kerr rotation is very low. As discussed earlier, the maximum Kerr rotation has been shifted due to transmission type geometry and observed at 5.12 GHz.

In order to understand the impact of the transistor loaded circuit component in the ring gap, we performed various case-studies. As we discussed earlier in a section that addition of the transistor in ring resonator kills one of the counter propagating modes and allow the ring resonant only for one type of circularly polarized wave. Therefore, in order to proof this statement, we simulated the model in various configurations such as the ring resonator without any unidirectional circuit components, and only the circular ring as depicted in Fig. 3-8 (a-d). In each configuration, we performed floquet mode analysis and corresponding reflection and transmission behavior for different polarization. It is clear from Fig. 3-8 that the unloaded structures do not show any gyrotropic response so that the cross-polarized transmission coefficients T_{xy} and T_{yx} and cross-polarized reflection coefficient R_{xy} and R_{yx} are reciprocal and close to zero in magnitude.

During our analysis, we identified that the cross polarization terms experience a phase difference (approx. 180°) when the ring resonator is loaded with transistors and passive components. However, when there are no unidirectional components such as transistors connected in the ring gap, we don't experience any phase difference between reflection and transmission components. Figure 3-9 depicts the gyrotropic response for various cases, where, R_{xy} and R_{yx} experience significant phase difference when ring resonator is simulated with unidirectional components, however, reciprocal or no phase difference in the absence of a unidirectional component loaded in the gap of ring resonator. Similarly, T_{xy} and T_{yx} follows the same behaviour. Co-pol terms such as R_{xx}, R_{yy}, T_{xx}, and T_{yy} do not exhibit any of the above described phase variation for any configuration.

In order to fulfill the requirement of being an magnet-free non-reciprocal metamaterial,

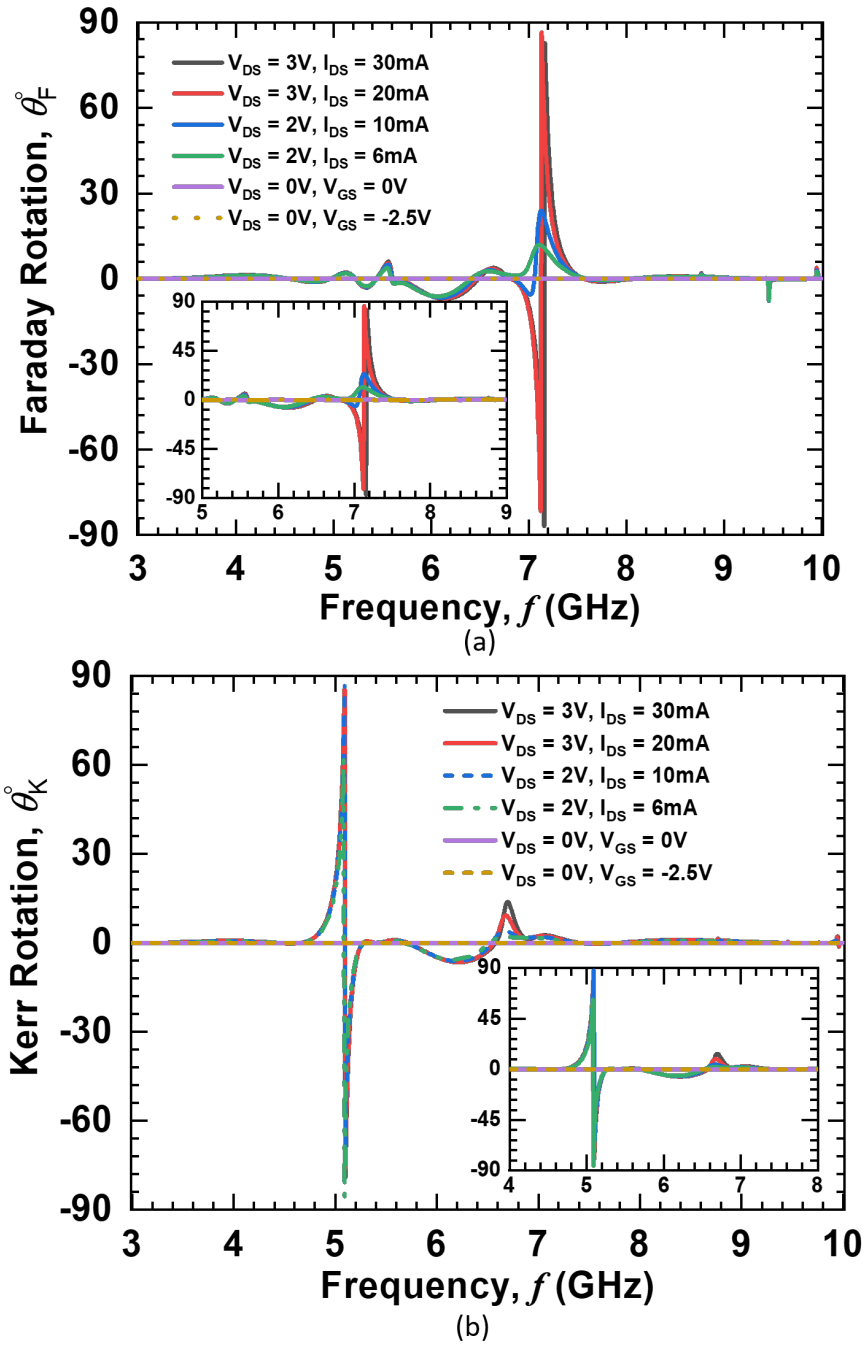

Figure 3-7: (a) Faraday rotation with respect to various bias conditions. (b) Kerr rotation with respect to various bias conditions of the designed structure (Fig. 3-4)

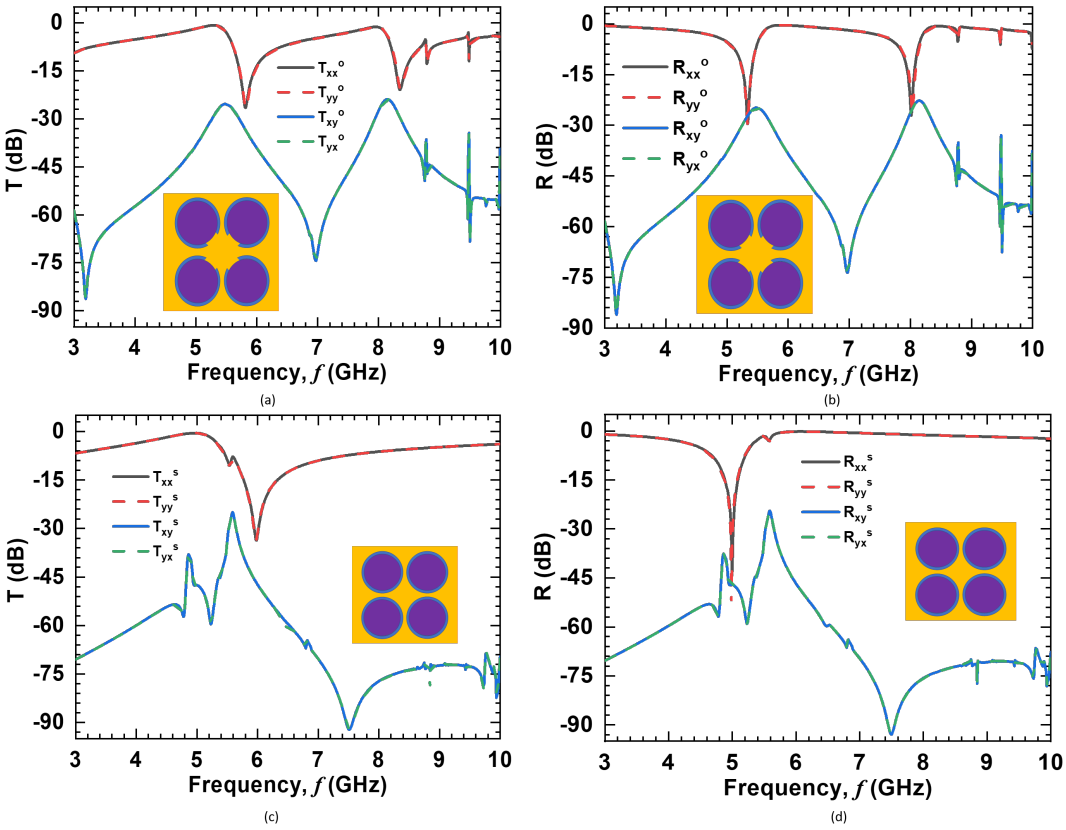

Figure 3-8: Transmission (a) and reflection (b) coefficient for co-pol and cross-pol when the ring resonator is open. Transmission (c) and reflection (d) coefficient for co-pol and cross-pol when the ring resonator is short.

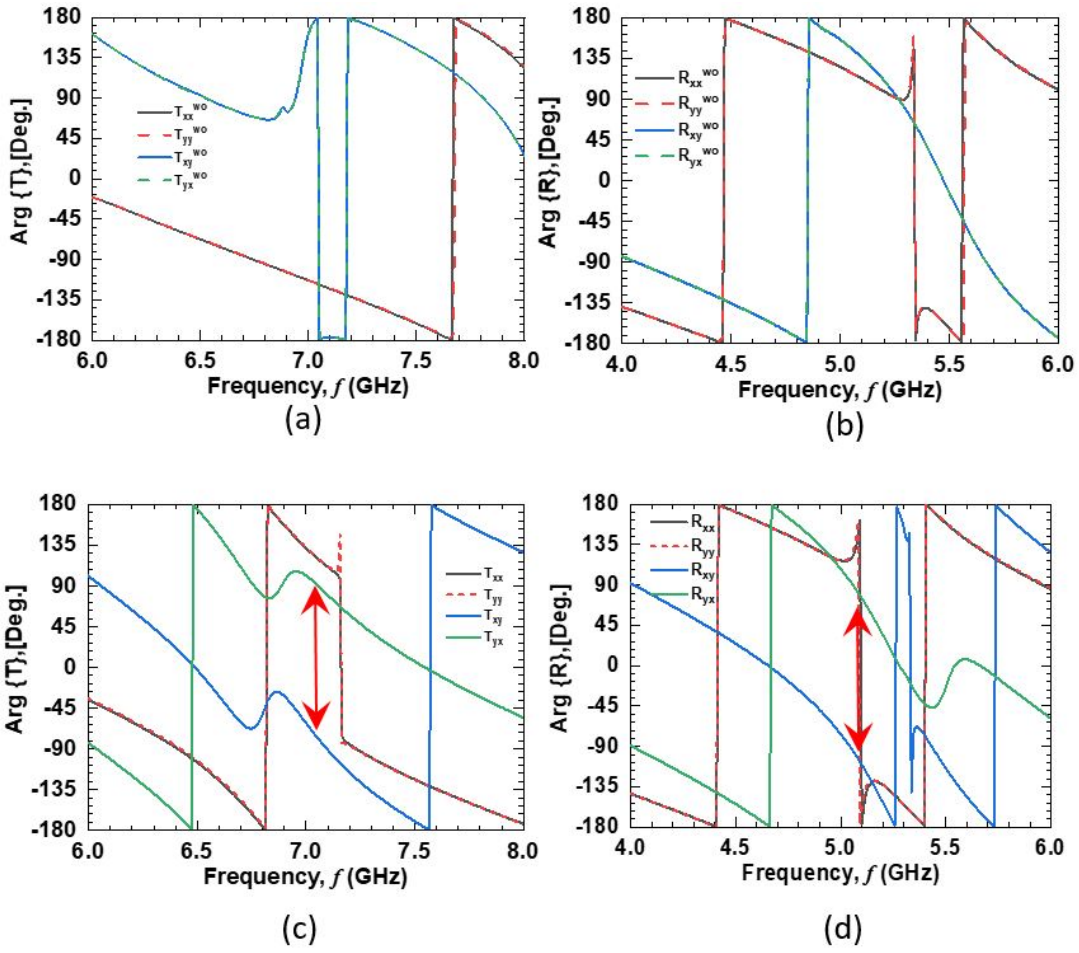

Figure 3-9: Comparison of the phase of the designed structure (Fig. 3-4) (a) Transmission and (b) Reflection coefficient without unidirectional components (transistor). (c) Transmission and (b) Reflection coefficient with unidirectional components (transistor).

the designed structure should have a non-reciprocal response. From Fig. 3-9 (c), the phase of the transmission coefficient and reflection coefficient are plotted in time-reversal schema. From port 1 to port 2, the x-polarized wave is transmitted from region 1 and y-polarized probe (antenna) pick the signal at region 2 and if the time is reversed, from port 2 to port 1, the y-polarized wave is transmitted and x-polarized probe (antenna) pick the signal at region 1. For x-polarized wave and x-polarized probing, phase of the transmission coefficients are same when the time is reversed. Similar description is applicable for Fig 3-9 (d), where, both antenna will be placed at same region. Therefore, as magnetized ferrites, the co-polarized component does not show any change in their phase when the time is reversed, however, the cross-polarized components shows 180° phase difference at the resonance frequency so that the designed structure behaves like a magnetized ferrite where the permeability tensor has cross-components and they are out-of phase such that the non-reciprocal gyrotropic response is evident.

To understand the unit cell analysis, we used the Floquet port approximation in Ansys and analyzed the 1st two mode propagation, i.e. TE and TM. The Floquet port is closely related to a Wave port in that a set of modes ("Floquet modes") represents the fields on the port boundary. Fundamentally, Floquet modes are plane waves with propagation direction set by the frequency, phasing, and geometry of the periodic structures. Figure 3-10 (a) depicts various orientation of unit cell and Fig. 3-10 (c) depicts the corresponding Faraday rotation with respect to the number of unit cells in a super cell. We obtained the highest Faraday rotation for super cell consisting of four ring resonators loaded with unidirectional components.

From Fig. 3-10, we observed that maximum Faraday rotation is obtained for the super cell consisting of four circular rings loaded with unidirectional components where each diagonal ring resonator are facing towards each other. Therefore, we simulated various configurations and obtained Faraday rotation by varying the number of circuit components

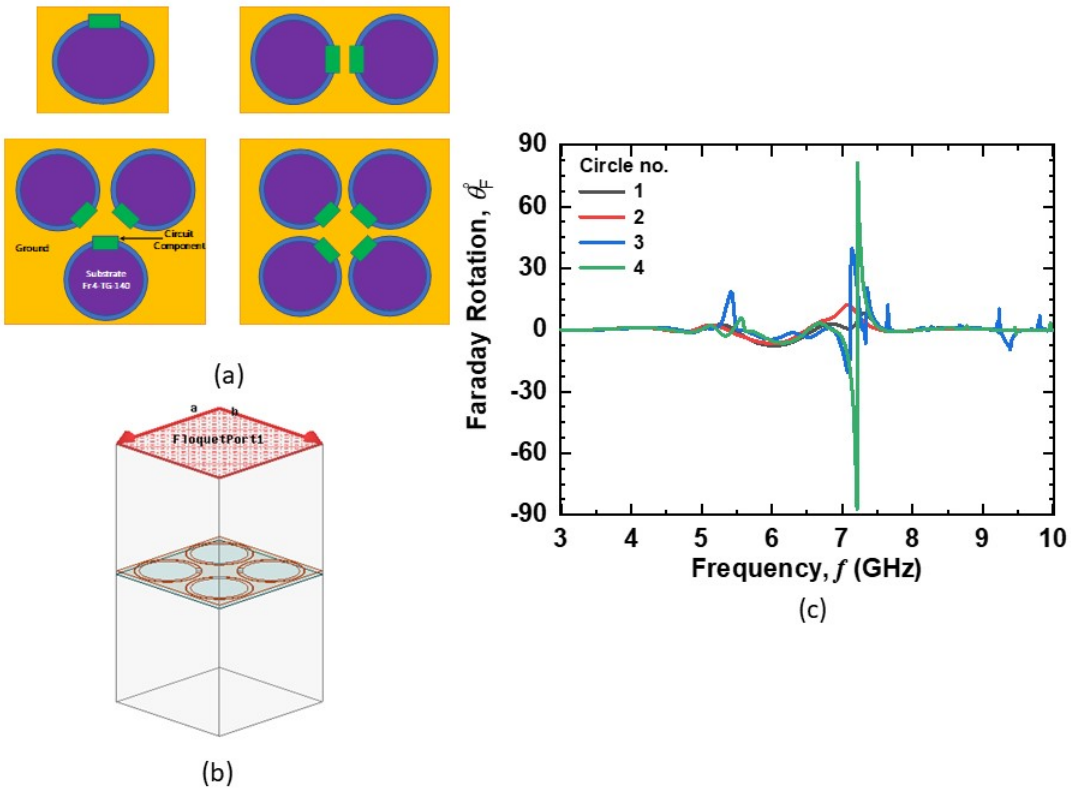

Figure 3-10: (a) Super cell consist of different numbers of ring resonators loaded with active and passive components (b) Floquet modes simulation setup (plane wave with normal incidence) (c) Faraday rotation with respect to the number of ring resonators in the super cell approximation.

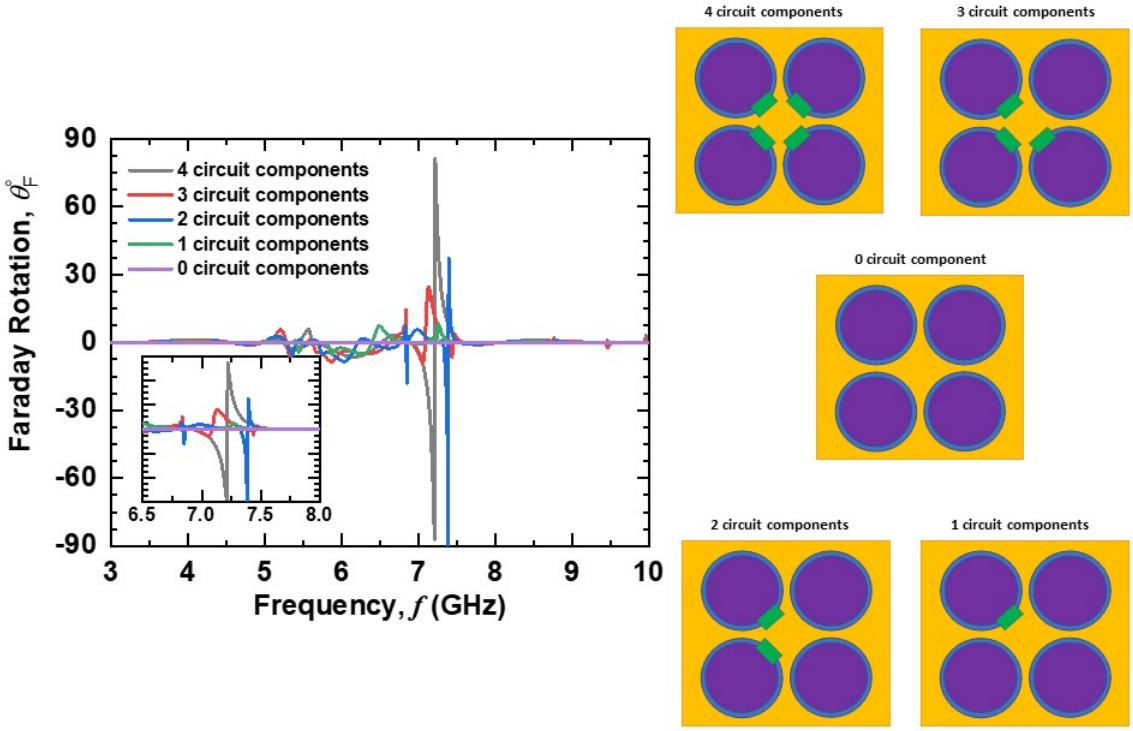

Figure 3-11: Faraday rotation with respect to circuit components used in the resonator gap.

in the ring resonator of the super cell. Figure 3-11 shows that when there are no circuit components, no Faraday rotation is obtained, and the structure represents reciprocal behaviour. Therefore, in order to establish complete gyrotropy, every ring resonator of the super unit cell is required to be connected with a unidirectional component. Perfect transmission line matching will allow aggregated synchronous response, i.e. the structure will exhibit non-reciprocity.

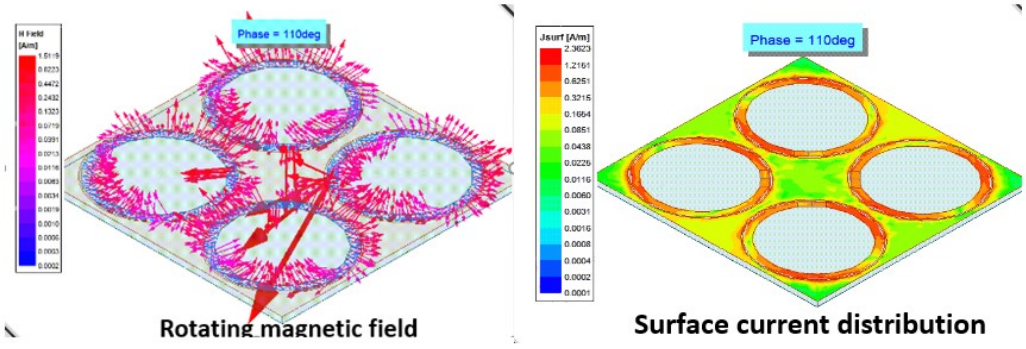

Figure 3-12: Rotating vectorial magnetic field and surface current distribution of the designed structure (Fig. 3-4).

We used the push excitation feature in Ansys in order to understand the artificial gyrotropic response in our design with respect to various phase at resonance frequency. Then, we analyzed the magnetic field rotation, dipole moment, and surface current distribution and observed the rotating vectorial magnetic field. Figure 3-12 depicts that this vectorial magnetic field rotation at the resonance frequency create the gyrotropic response through traveling wave resonance. Besides, surface current distribution on ring resonator is important to understand and optimize the design.

3.3.1 Tunable Faraday and Kerr Rotation Measurements

We investigated various optimization approaches to understand the behaviour of our proposed structure. One of the major focuses of this research work is to obtain tunability in our design. We implemented successfully that different Faraday and Kerr rotation can be achieved by varying biasing conditions electronically in our design. Figure 3-13 and 3-14 represents that by tuning the drain current, Faraday and Kerr rotation can be changed. Besides, by tuning circuit components or adding more electronic components such as varactor diodes, more flexibility in this design can be achieved in the future, such as shifted resonance frequency, multi-band response, and tunable Faraday and Kerr rotation.

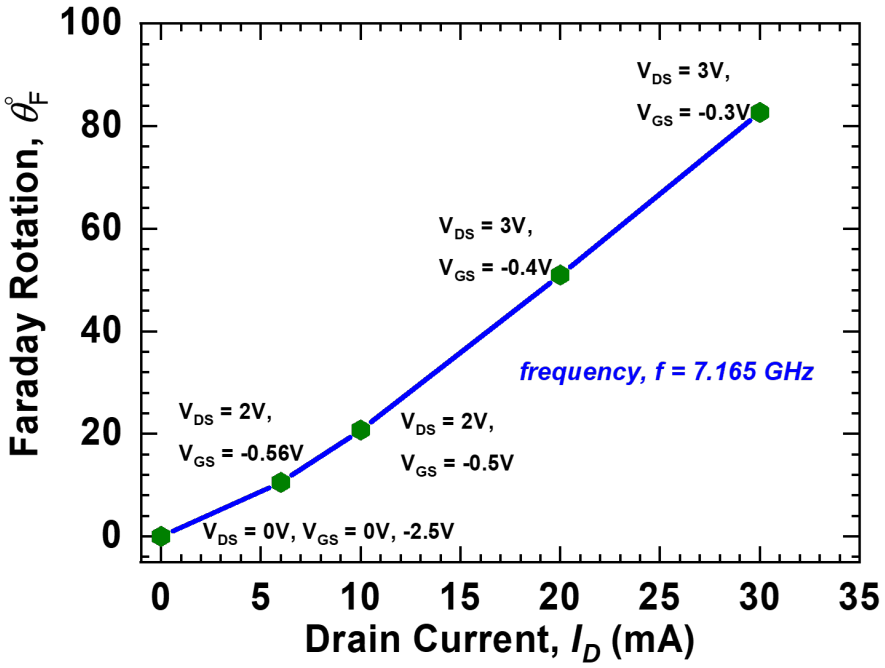

Figure 3-13: Faraday rotation with respect to variable drain current.

Figure 3-13 depicts the Faraday rotation with respect to variable drain current. The Faraday rotation and drain current response follows a linear pattern. Figure 3-14 depicts the Kerr rotation with respect to variable drain current, where, Kerr rotation follows a nonlinear behaviour starting from 6mA drain current to maximum drain current i.e. 30mA. Both of the Faraday and Kerr rotation has been calculated based on the same design configuration.

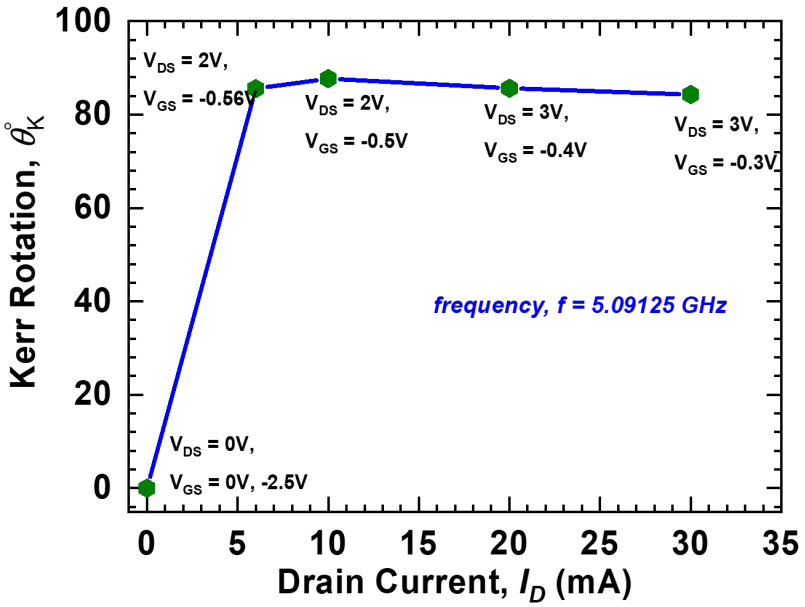

Figure 3-14: Kerr rotation with respect to variable drain current.

As we mentioned in an earlier section that the aim of this design is to analyze transmission components and extract Faraday rotation, therefore, we have obtained shifted Kerr rotation from our resonance frequency because of the partial reflection behaviour of our design. Table 3.1 dictates a comparative analysis of Faraday and kerr rotation at various bias conditions.

Table 3.1: Faraday and Kerr rotation measurement at various bias condition

Bias condition	**Faraday rotation**	**Kerr rotation**
V_{DS} = 0V, V_{GS} = -2.5V	0°	0°
V_{DS} = 0V, V_{GS} = 0V	0°	0°
V_{DS} = 2V, I_{DS} = 6mA	10.06°	59.26°
V_{DS} = 2V, I_{DS} = 10mA	19.39°	78.29°
V_{DS} = 3V, I_{DS} = 20mA	76.09°	83.78°
V_{DS} = 3V, I_{DS} = 30mA	86.96°	86.18°

THIS PAGE INTENTIONALLY LEFT BLANK

Chapter 4

Multi Layer Non-Reciprocal Metamaterial Design

4.1 Design, Optimization and Performance Analysis

The goal of this chapter is to investigate whether it is possible to design a transparent multi-layer magnet-free meta-material with minimal reflection how the key performance indicators vary, and what are the necessary conditions need to take into account from s design point of view.

In microwave engineering, it is always an important task to match circuit elements to ensure that all or most of the incident power is delivered to the load. In general, non-reciprocal gyrotropic materials such as ferrite in presence of a magnet and magneto-optical devices experience high characteristic impedance that causes reflections. In order to achieve ideal isolation and circulation properties, it is very important to design fully transparent, non-reciprocal components especially in high power applications (HPA).

Shul et al.[61] for the first time investigated the response when a normally incident plane wave propagates through a gyromagnetic slab. The simple analysis showed that

reflection and cancellation could be achieved at a certain slab thicknesses where the phase accumulation of the multiple reflections cancel each other. Moreover, to solve the same issues, Moccia et. al[62] suggested a stacked layers of magneto-optic slabs and a dielectric slab to cancel the reflection. Therefore, it is possible to enhance the transmission and Faraday rotation angle of non-reciprocal gyrotropic materials in multi layer configurations.

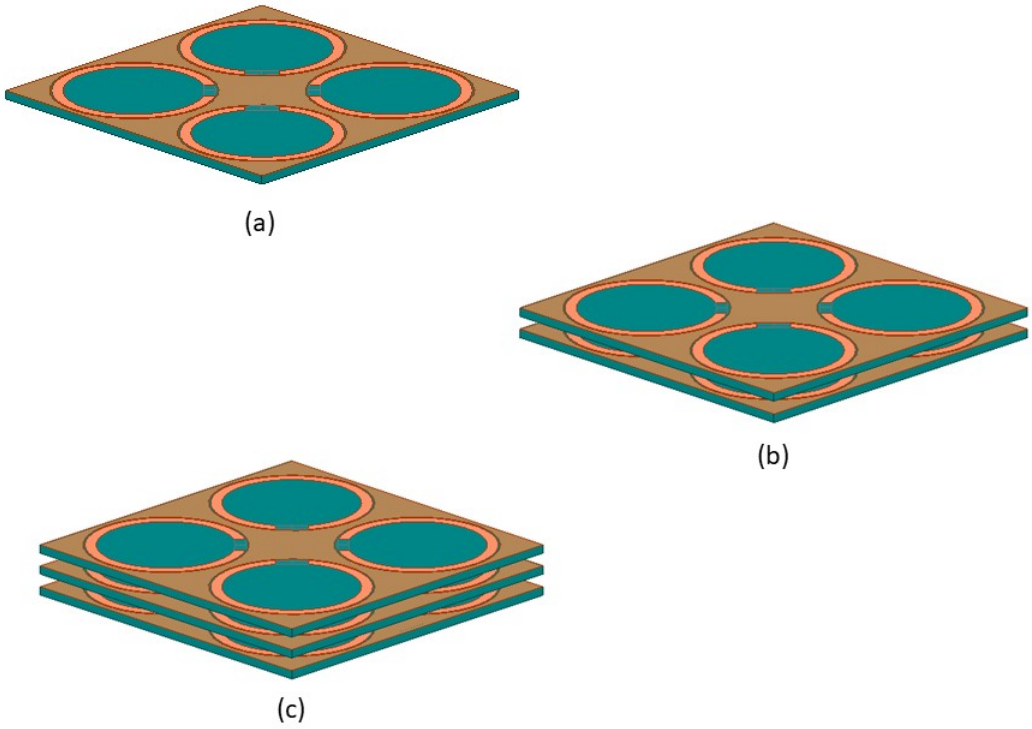

Figure 4-1: (a) Single layer. (b) Double layer. (c) Triple layer design of magnet-free non-reciprocal metamaterial (2mm gap between each consecutive layers).

Figure 4-1 depicts various layer configurations, where, we investigated non-reciprocity on single layer, double layer, and triple layer by keeping the consecutive layer distance as 2mm considering the practical lab environment and meaningful S parameter analysis from vector network analyzer.

4.1.1 Faraday and Kerr Rotation

Based on the layer gap as 2mm, we analyzed the Faraday and Kerr rotation for the double layer configuration. Figure 4-2 and 4-3 represent the response of the double layer configuration. At the resonance frequency, 6.98125 GHz, we obtain maximum Faraday rotation as 89.35°. The resonance frequency of multi-layer metamaterial is shifted from the resonance frequency of the single layer metamaterial because multi-layer configurations consist of permitivity of multiple metamaterial structure and free space between consecutive layers. For the double layer configuration, we obtain Kerr rotation as 17.29° at 5.16125 GHz. As discussed in earlier chapters that our design is not intended to obtain the Kerr rotation, therefore, due to multiple reflection, we did not achieve a very promising Kerr rotation. Figure 4-2 (b) and Fig. 4-3 (b) illustrates Faraday and Kerr rotation with respect to varying drain current. Although, θ_F° increases with applied drain current, however, θ_K° doesn't vary after a certain level. This is due to multiple reflections between layers and partial reflection from the 1st metamaterial structure to measurement antenna. By varying the layer distances, the performance of θ_F° and θ_K° can be improved further.

We followed a similar approach for the triple layer configuration and evaluated θ_F° and θ_K° for various bias conditions. Keeping the same distance, i.e. 2mm, between consecutive layers, we obtained 86.27° as θ_F° at 6.92 GHz and 18.61° as θ_K° at 5.09125 GHz. Similarly, θ_F° increases with applied drain current, however, θ_K° doesn't vary after a certain level of applied drain current. By varying the layer distances, multiple reflection inside fabricated board can be minimized and the performance for both θ_F° and θ_K° can be improved further. Figure 4-4 (b) illustrates the Faraday rotation and Fig. 4-5 (b) illustrates the Kerr rotation when drain current is varied.

Figure 4-6 depicts the comparative analysis between various layer configurations and we can see that the Faraday rotation shifts to lower frequency with respect to higher number of dielectric layers. This is because multiple layers consist of metamaterial structures and

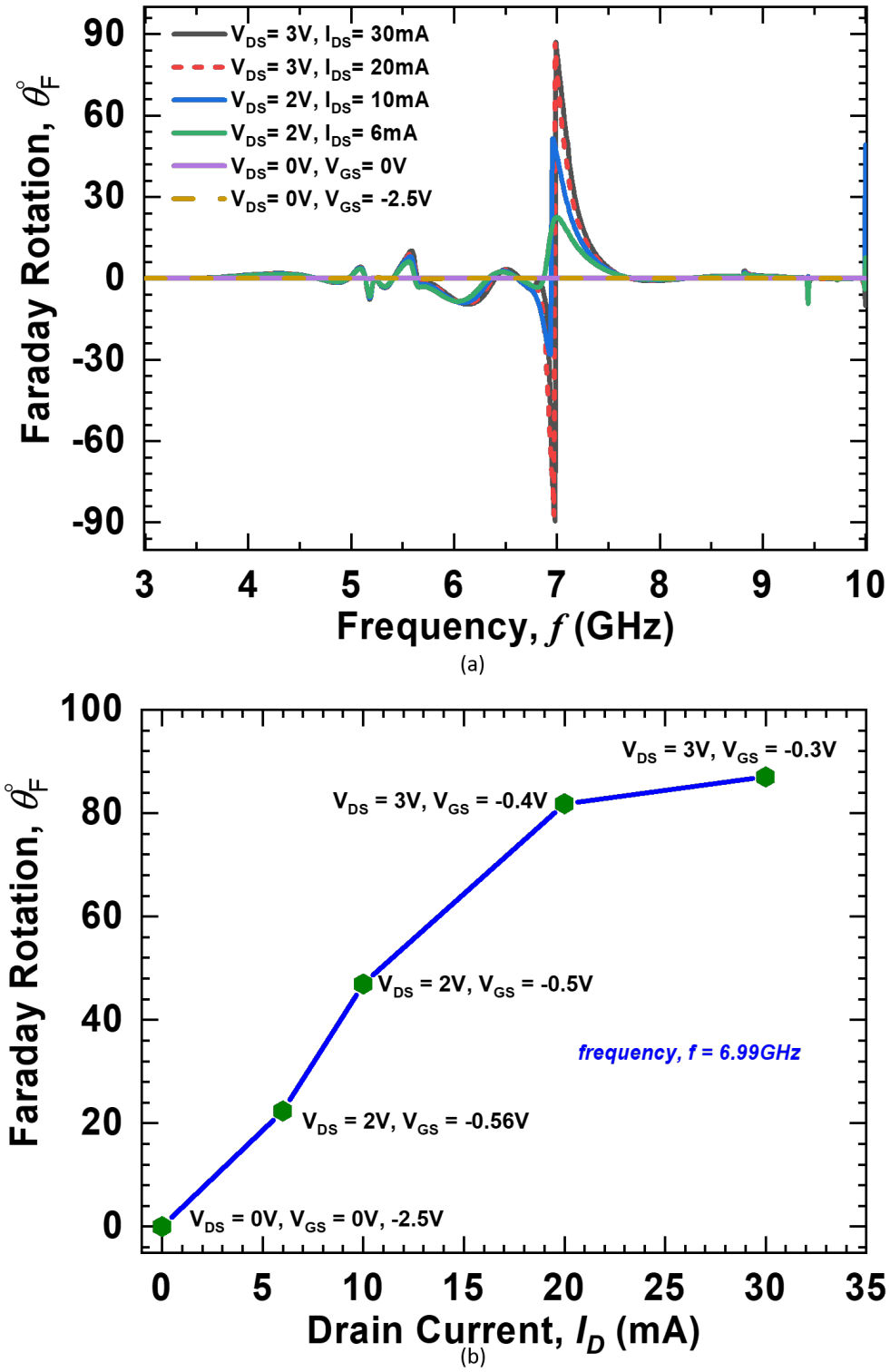

Figure 4-2: Double layer configuration (a) Faraday rotation. (b) Faraday rotation with respect to variable drain current.

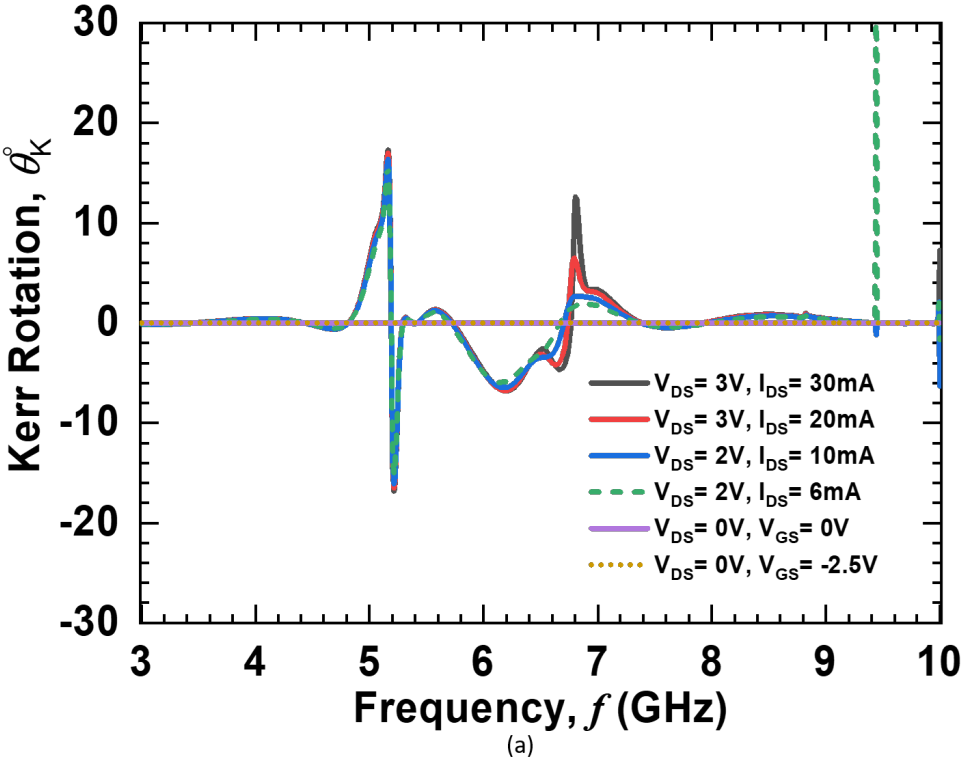

(a)

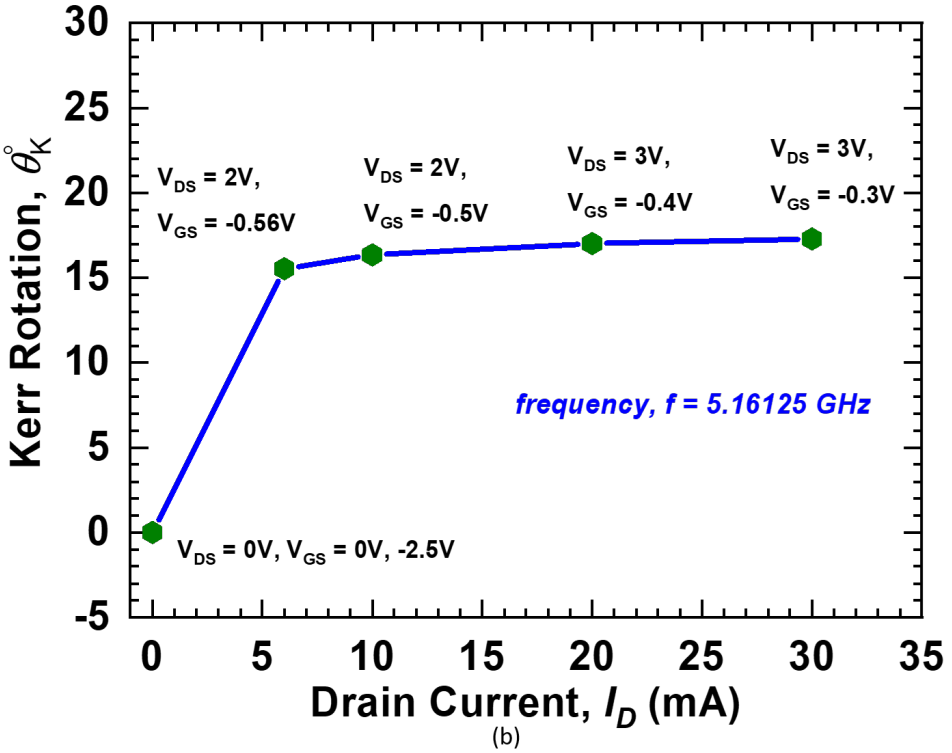

(b)

Figure 4-3: Double layer configuration (a) Kerr rotation. (b) Kerr rotation with respect to variable drain current.

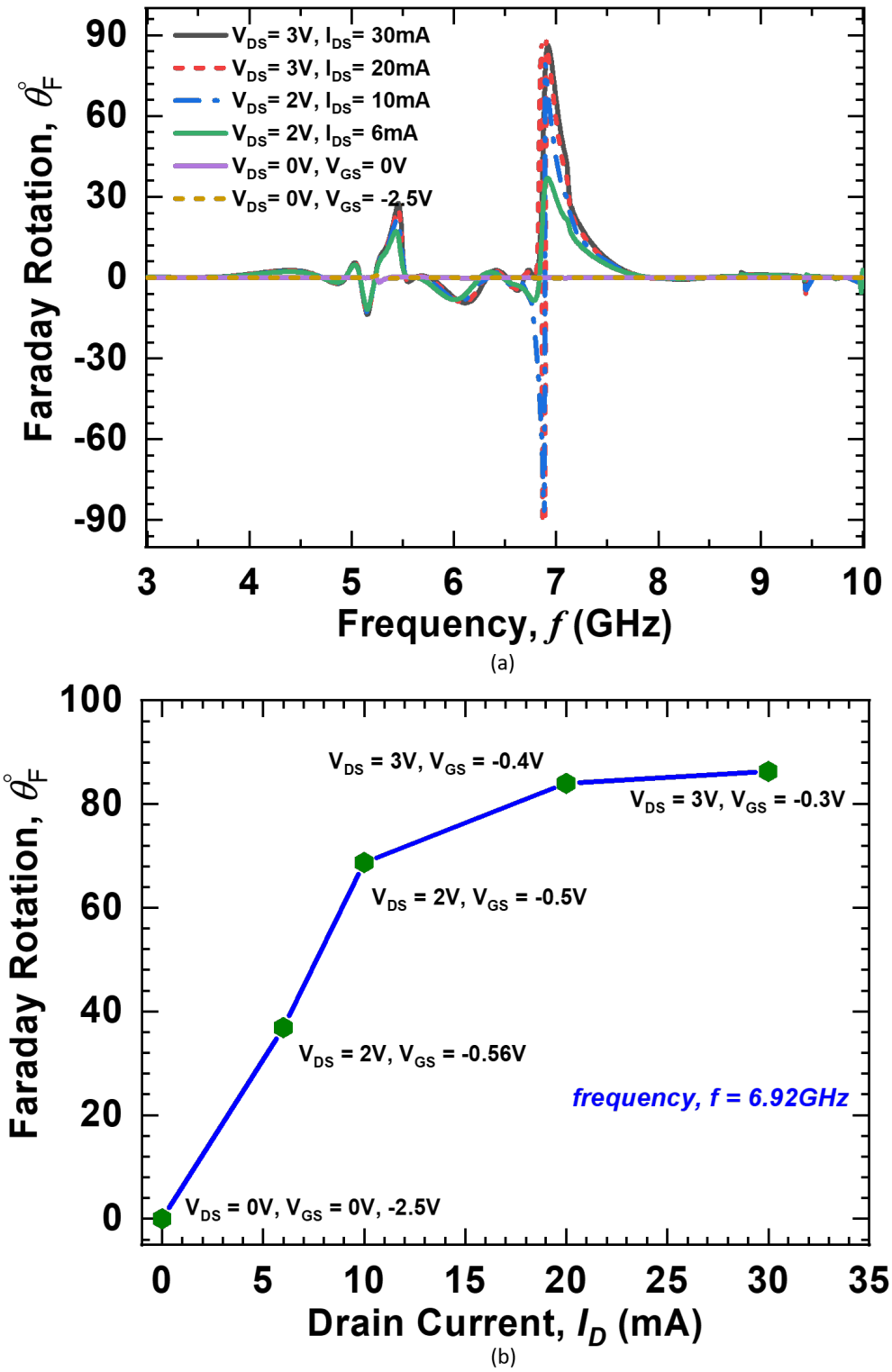

Figure 4-4: Triple layer configuration (a) Faraday rotation. (b) Faraday rotation with respect to variable drain current.

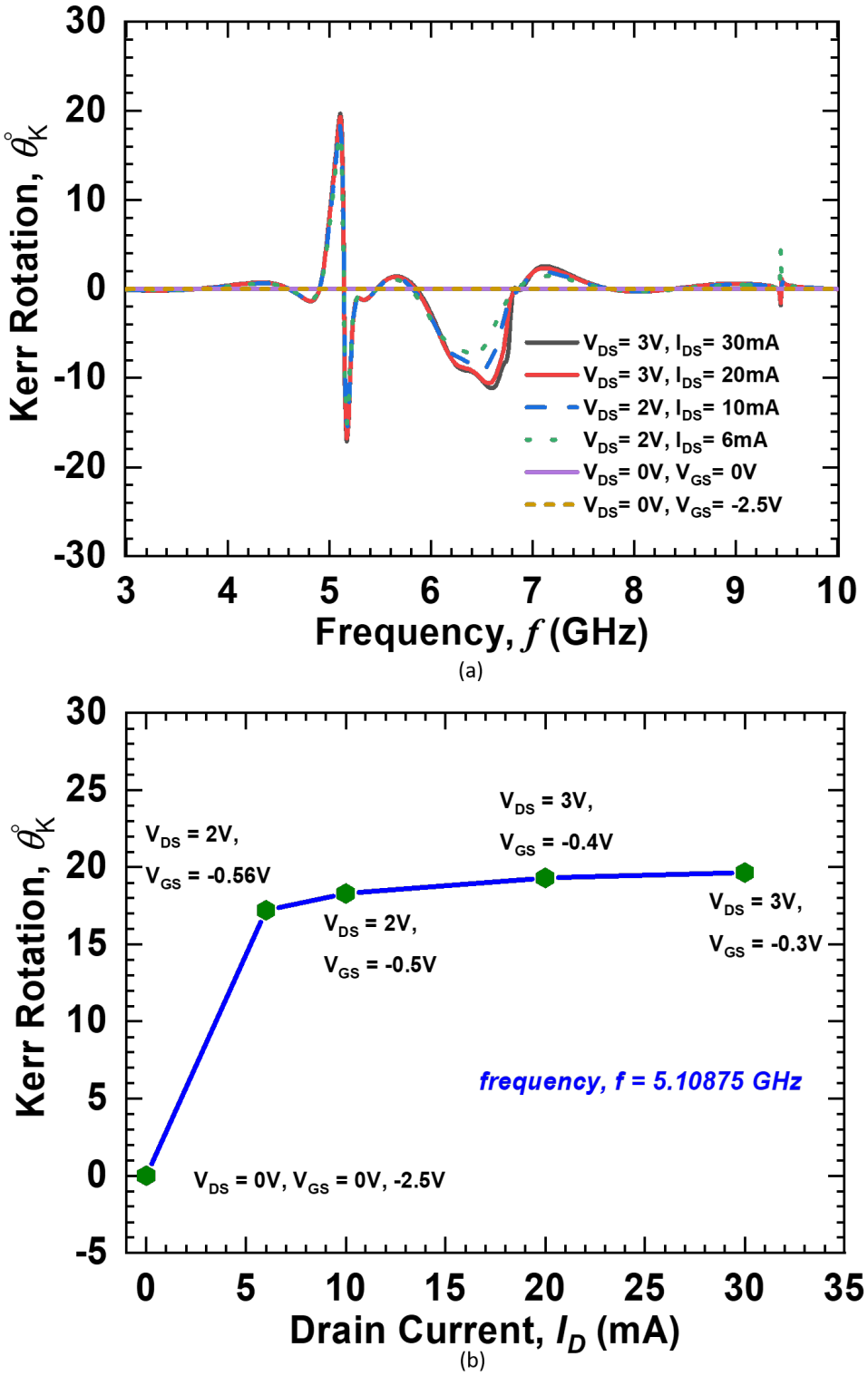

Figure 4-5: Triple layer configuration (a) Kerr rotation. (b) Kerr rotation with respect to variable drain current.

free space change the electric permitivity, therefore, the resonance frequency. We compared the tunability performance at the resonance frequency of single layer board i.e. 7.1125 GHz and analyzed Faraday and Kerr rotation with respect to varying drain current.

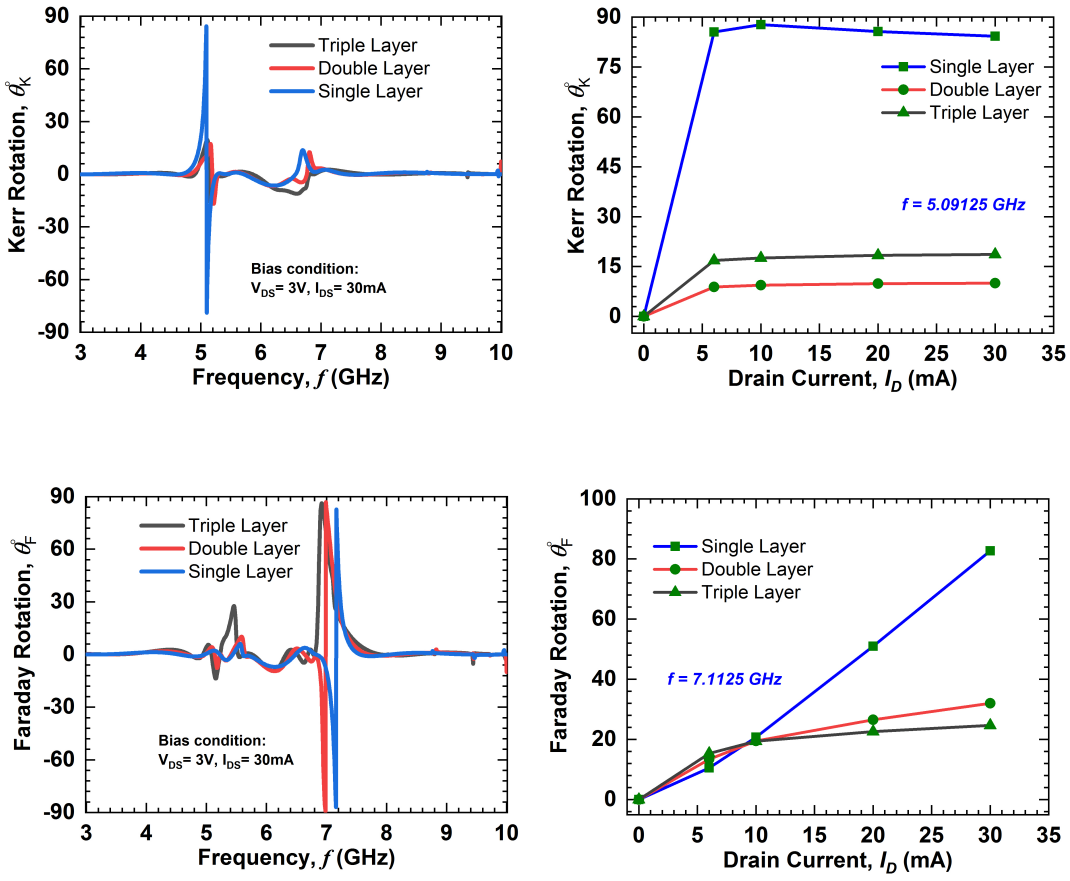

Figure 4-6: (a) Faraday rotation comparison with respect to number of layers. (b) Kerr rotation comparison with respect to number of layers. (c) Faraday rotation comparison with respect to drain current at f = 7.1125 GHz. (d) Kerr rotation comparison with respect to drain current at f = 5.09125 GHz

4.1.2 Test Bench Setup

One very important part of this research is the test bench setup for the measurement. Figure 4-7 depicts the test bench for Faraday rotation measurement. Bottom part of the Fig. 4-7 represents the front view and back view of our fabricated board. The star metalization at

the back of the fabricated board along with the ground plane at the front side will be used to create the necessary bias conditions.

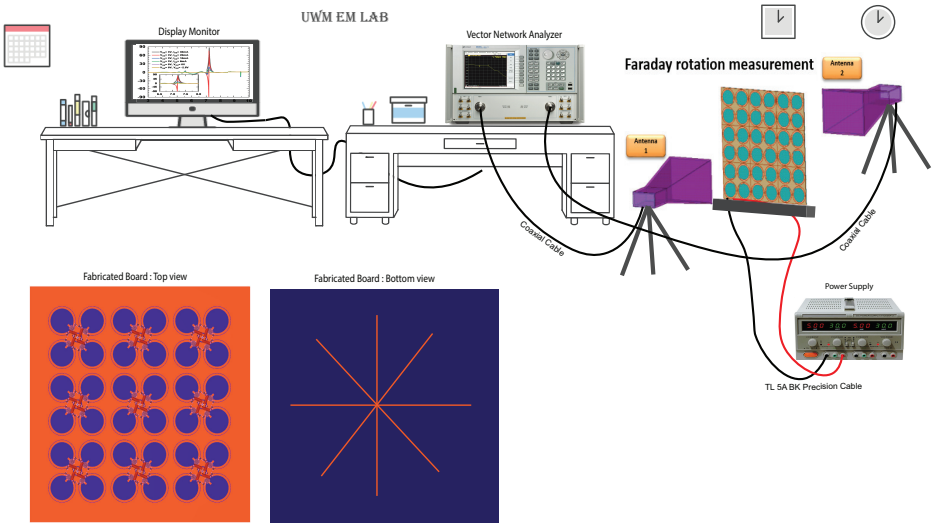

Figure 4-7: Test bench setup for Faraday rotation

As we see from Fig. 4-7, variable biasing states will be controlled by an external power supply and two horn antennas will be placed facing each other. The fabricated board will be placed exactly at the middle of the two horn antennas considering the far field distance from both horn antennas at the resonance frequency. Antenna 1 will be stationary and antenna 2 will be rotated clockwise. This rotation can be done manually or by using stepper motors. During various rotation, S_{21} and S_{12} will be measured and antenna rotation angle for maximum difference between S_{21} and S_{12} will be taken into account as the Faraday rotation on that biasing condition. By tuning the power supply very carefully, we can obtain various biasing conditions, therefore, various θ_F°.

Similarly, Kerr rotation can be measured based on the described setup in Fig.4-8, where, two horn antennas will be positioned at the same side. Based on various biasing conditions, we need to measure S_{21} and S_{12}, where antenna 2 will be rotated and antenna 1 will be static. The maximum difference between S_{21} and S_{12} on a given frequency in this condition is our desired Kerr rotation. For both test bench setup configurations, far field distance from antenna to device under test (fabricated board) and careful antenna rotation based

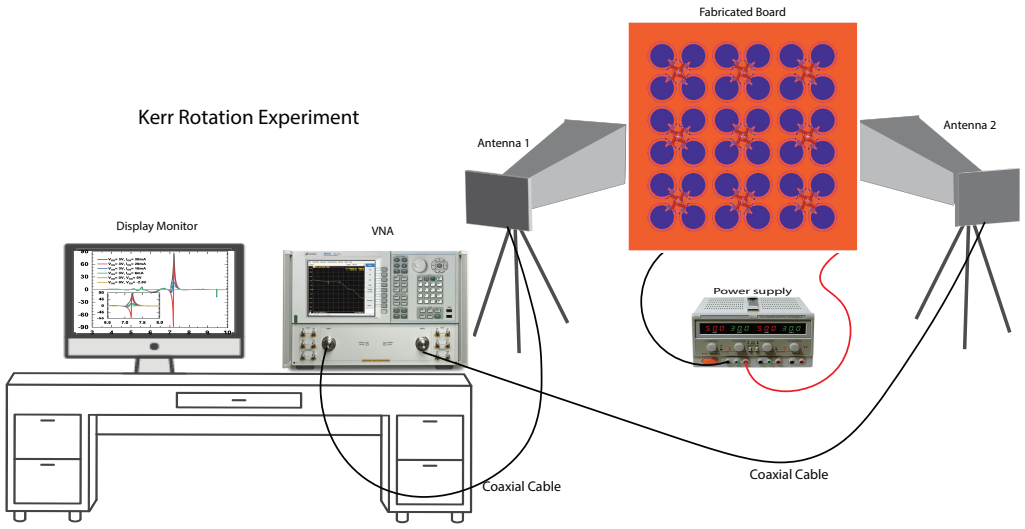

Figure 4-8: Test bench setup for Kerr rotation

on observed S_{21} and S_{12} from vector network analyzer is very important to maintain. Due to Covid-19 lab restrictions, measurements are yet to perform.

4.2 Applications

Directions for non-reciprocal electronics are moving towards advanced semiconductor technologies which help to find new ways to create components capable of one-way transmission. Non-reciprocal devices are a key component of modern communication technology. Non-reciprocal components are commonly used in radars, LiDARs, and defense systems to protect high-power microwave sources from back-reflections due to variations of the load impedance. In biomedical imaging and sensing application such as magnetic resonance imaging (MRI), non-reciprocal devices can be very promising. Besides, in order to protect wireless transmitters from back reflections from the antenna, isolators are used. On the other hand, circulators, a three-port non-reciprocal devices are used to interface a transmitter and a receiver to an antenna, allowing signals to be simultaneously transmitted and received at the same frequency. In the near future, advanced circulator technologies can be deployed in quantum computer. Besides, in recent days, scientists prove that by using two

nonreciprocal devices connected in series, one-way circulation of acoustic waves is possible.[63] Furthermore, nonlinear parity–time symmetric circuits can be used in wireless power transfer, which is very important in a world of mobile devices and electric vehicles.[64]

To recapitulate, with respect to the advancement of the modern applications, concepts of artificial gyrotropy investigated in this research can open many new opportunities in the future. We have presented a detailed analysis on fully electronic non-reciprocal devices. Based on the tunable biasing conditions, we have controlled Faraday and Kerr rotation. It has been pointed out that electronic controllable non-reciprocal devices can be a probable substitute for conventional magnetic biased ferrite material in industrial applications. Besides, our proposed tunability features can add a new dimension on the already ongoing artificial non-reciprocal research.

THIS PAGE INTENTIONALLY LEFT BLANK

Chapter 5

Fundamental Limitations

5.1 Design Consideration

In this research work, we have studied the physics of non-reciprocity and various situations and conditions behind reciprocity and non-reciprocity. Later, we discussed wave matter interaction and how the wave propagates through various media and corresponding rotations in different situations. After that, we focused on establishing artificial gyrotropy by developing transmission line analysis and nonlinear circuit modelling. We performed a detailed analysis via full wave 3D simulation and optimized the design to obtain maximum Faraday and Kerr rotation. These fundamental concepts along with the careful analysis of performance indicators are very important before fabricating any non-reciprocal device. We investigated and optimized the design considering Faraday rotation. However, similar approaches should be useful also for non-reciprocal device design such as isolators, circulators, metamaterials, and leaky wave antennas at various frequencies.

5.1.1 Limitations

The major challenge of this artificial gyrotropy is to match the impedance between circular ring resonator and unidirectional components. Specially, at higher frequencies, phase matching is critical. On the other hand, in the presence of mismatch between the ring and the unidirectional component, the excited resonance is accompanied by loss. Besides, mismatch also results in a nonzero standing wave ratio (SWR). For an infinite standing wave ratio, the device does not exhibit gyrotropy, hence, non-reciprocity. Therefore, full wave 3D simulation along with optimization features were used in this work and highly recommended for any non-reciprocal device design.

One of the major challenge is the multi layer simulation and controlling the optimized parameters. In this research work, we analyzed only double and triple layer configuration by setting the consecutive layer distance as 2 mm. However, multi layer analysis can be investigated by developing network models where exploiting duality theorem, Fabry-perot resonances, and pole, zero analysis of a system can be very useful to approximate the thickness of the dielectric slab and necessary conditions related to layer distance when reflection coefficients become zero. Nevertheless, numerically for a complex design like this, the above described mathematical approach can be a daunting task to solve accurately.

Another possible approach can be developing equivalent circuit models for multiple layers and solving polynomial equations to find out the optimized distance between consecutive layers. Developing an equivalent circuit model for a single layer based on the given unidirectional circuit configuration along with circular ring transmission line might be easy. However, developing the perfect equivalent circuit model for multiple layers is very complex. Therefore, approaches such as parametric tuning of different variables and setting up the cost function can be very useful to reach quickly to the local or global minima and solve the boundary conditions. For example, parametric tuning of internal layer distance and solving of the reflection and transmission scattering parameters can be a more intuitive way

to solve and match the impedances.

Lastly, the number of active/passive components required to implement the artificial gyrotropy can be optimized and reduced. In general, every active/passive component adds some loss and phase difference and nonlinear components like transistor, amplifier has some intrinsic properties related to harmonic balance and 3rd order inter-modulation. Therefore, nonreciprocal devices can exhibit some unintentional radiation which is very important to take into consideration during practical device design.

THIS PAGE INTENTIONALLY LEFT BLANK

Chapter 6

Conclusion and Future Works

6.1 Conclusion

In this thesis, we have presented a very detailed discussion of the mathematical modelling and the realization of electromagnetic non-reciprocity. The major goal of this research work was to provide the reader with a very good understanding from physics and practical design framework and implementation of application oriented non-reciprocal device design, which is as comprehensive as possible.

In chapter 1 and chapter 2, we tried to provide an intuitive and concrete description of the phenomena of electromagnetic nonreciprocity. The definition of time reversal and its relation with reciprocity were discussed. Starting from wave matter interaction in different media, the concept of chirality, non-reciprocity, and gyrotropy were described from the modern applications point of view. Necessary concepts to break time reversal symmetry in order to implement gyrotropy was mainly focused with its importance in device applications. Detailed physical explanations behind electron spin precession, mathematical modelling, disadvantages of conventional approach, and importance of alternative approach along with research progresses in recent years on this sector were briefly highlighted in these chapters.

Chapter 3 put into practice and further detailed conceptual understanding previously developed and discussed in Chapter 2. In this chapter, we focused on designing a split ring resonator loaded with unidirectional circuit components to implement artificial gyrotropy. Two major key performance indicators of non-reciprocity, i.e. Faraday and Kerr rotation, were analyzed and we performed various advanced engineering approach for the optimization. Later, we successfully implemented tunability feature by varying necessary biasing conditions. We did various case studies during optimization of the design and analyzed co-pol and cross-pol terms and mathematically modelled how they are related to Faraday and Kerr rotation.

In Chapter 4, we explored on multi-layer design and analysis and it turned out that reflection between layers and thickness of fabricated boards are very important to take into consideration. Various approaches aiming optimization of the device were discussed and analyzed. Later, we described required test-bench setups for both of Faraday and Kerr rotation.

Chapter 5 mainly focused on fundamental limitations, such as necessary approaches during design, key points, and possible improvements in various practical applications.

6.1.1 Future Research

This research aimed at providing an advanced engineering analysis on electromagnetic non-reciprocity. Ferrimagnetic (dielectric) compounds, called ferrites, such as Yttrium Iron Garnet (YIG) and materials composed of Fe_2O_3 and other elements (Al, Co, Mn, Ni) exhibit electromagnetic gyrotropy in presence of permanent magnetic bias, which is very popular in devices such as isolators, circulators, leaky wave antennas, and metamaterials at microwave and optical regime. However, ferrite based devices are expensive, costly, bulky, and complex to integrate within systems. Therefore, optimized approach to develop artificial gyrotropy along with tunability feature were the centre of our investigation throughout the

research work.

In terms of future work, several questions are still open regarding the perfect design of a single-layer magnet free tunable metamaterial. One major factor is the number of active and passive components required for the design. In addition, the analyzed reflection cancellation procedure can be investigated from a mathematical point of view. Moreover, the design and optimization method given in this thesis is only applicable for normally incident propagating plane waves. Therefore, analysis of non-reciprocal behaviour of single and multi-layer metamaterial under oblique incidence plane wave can be very interesting for mimicking device application in a real world scenario. Lastly, in this research work we investigated tunability features of Faraday and Kerr rotation by varying drain current. Furthermore, tuning of resonance frequency or multi-band operation can be a very smart and cost effective option in this field. In summary, the design and analysis approach of developing artificial non-reciprocity described here can be a very good starting point to design non-reciprocal devices, however, there are still a lots of application-oriented challenges to resolve in the future.

THIS PAGE INTENTIONALLY LEFT BLANK

Bibliography

[1] R.P. Feynman, R.B. Leighton, and M. Sands. *The Feynman Lectures on Physics, Vol. II: The New Millennium Edition: Mainly Electromagnetism and Matter*. Basic Books, 2015.

[2] Aravind Nagulu, Negar Reiskarimian, and Harish Krishnaswamy. Non-reciprocal electronics based on temporal modulation. *Nature Electronics*, 3(5):241–250, May 2020.

[3] C. L. Hogan. The ferromagnetic faraday effect at microwave frequencies and its applications: The microwave gyrator. *The Bell System Technical Journal*, 31(1):1–31, 1952.

[4] Christophe Caloz, Andrea Alù, Sergei Tretyakov, Dimitrios Sounas, Karim Achouri, and Zoé-Lise Deck-Léger. Electromagnetic nonreciprocity. *Physical Review Applied*, 10(4), Oct 2018.

[5] T. Kodera and C. Caloz. Unidirectional loop metamaterials (ulm) as magnetless artificial ferrimagnetic materials: Principles and applications. *IEEE Antennas and Wireless Propagation Letters*, 17(11):1943–1947, 2018.

[6] H.C. Chen. *Theory of Electromagnetic Waves: A Coordinate-free Approach*. Electrical Engineering Series. McGraw-Hill Book Company, 1983.

[7] C.A. Balanis. *Advanced Engineering Electromagnetics*. CourseSmart Series. Wiley, 2012.

[8] Sophocles J Orfanidis. *Electromagnetic waves and antennas*. Rutgers University Press, 2016.

[9] Archana Kamal, John Clarke, and M. H. Devoret. Noiseless non-reciprocity in a parametric active device. *Nature Physics*, 7(4):311–315, Apr 2011.

[10] Viktar S. Asadchy, Mohammad Sajjad Mirmoosa, Ana Díaz-Rubio, Shanhui Fan, and Sergei A. Tretyakov. Tutorial on electromagnetic nonreciprocity and its origins. *arXiv: Applied Physics*, 2020.

[11] Negar Reiskarimian and Harish Krishnaswamy. Magnetic-free non-reciprocity based on staggered commutation. *Nature Communications*, 7(1):11217, Apr 2016.

[12] Lars Onsager. Reciprocal relations in irreversible processes. i. *Phys. Rev.*, 37:405–426, Feb 1931.

[13] H. B. G. Casimir. On onsager's principle of microscopic reversibility. *Rev. Mod. Phys.*, 17:343–350, Apr 1945.

[14] Freek Ruesink, Mohammad-Ali Miri, Andrea Alù, and Ewold Verhagen. Nonreciprocity and magnetic-free isolation based on optomechanical interactions. *Nature Communications*, 7(1), Nov 2016.

[15] S. Tanaka, N. Shimomura, and K. Ohtake. Active circulators—the realization of circulators using transistors. *Proceedings of the IEEE*, 53(3):260–267, 1965.

[16] Y. Ayasli. Field effect transistor circulators. *IEEE Transactions on Magnetics*, 25(5):3242–3247, 1989.

[17] I. J. Bahl. The design of a 6-port active circulator. In *1988., IEEE MTT-S International Microwave Symposium Digest*, pages 1011–1014 vol.2, 1988.

[18] S. Tang, C. Lin, S. Hung, K. Cheng, and Y. Wang. Ultra-wideband quasi-circulator implemented by cascading distributed balun with phase cancelation technique. *IEEE Transactions on Microwave Theory and Techniques*, 64(7):2104–2112, 2016.

[19] S. A. Ayati, D. Mandal, B. Bakkaloglu, and S. Kiaei. Integrated quasi-circulator with rf leakage cancellation for full-duplex wireless transceivers. *IEEE Transactions on Microwave Theory and Techniques*, 66(3):1421–1430, 2018.

[20] K. Fang and J. F. Buckwalter. A tunable 5–7 ghz distributed active quasi-circulator with 18-dbm output power in cmos soi. *IEEE Microwave and Wireless Components Letters*, 27(11):998–1000, 2017.

[21] S. Qin, Q. Xu, and Y. E. Wang. Nonreciprocal components with distributedly modulated capacitors. *IEEE Transactions on Microwave Theory and Techniques*, 62(10):2260–2272, 2014.

[22] N. A. Estep, D. L. Sounas, and A. Alù. Magnetless microwave circulators based on spatiotemporally modulated rings of coupled resonators. *IEEE Transactions on Microwave Theory and Techniques*, 64(2):502–518, 2016.

[23] A. Kord, D. L. Sounas, and A. Alù. Magnet-less circulators based on spatiotemporal modulation of bandstop filters in a delta topology. *IEEE Transactions on Microwave Theory and Techniques*, 66(2):911–926, 2018.

[24] Sajjad Taravati, Nima Chamanara, and Christophe Caloz. Nonreciprocal electromagnetic scattering from a periodically space-time modulated slab and application to a quasisonic isolator. *Phys. Rev. B*, 96:165–144, Oct 2017.

[25] Nicholas A. Estep, Dimitrios L. Sounas, Jason Soric, and Andrea Alù. Magnetic-free non-reciprocity and isolation based on parametrically modulated coupled-resonator loops. *Nature Physics*, 10(12):923–927, Dec 2014.

[26] A.G. Gurevich and G.A. Melkov. *Magnetization Oscillations and Waves*. Taylor & Francis, 1996.

[27] B. Lax, K.J. Button, K. Button, K.J. Button, and Massachusetts Institute of Technology. Lincoln laboratory. *Microwave Ferrites and Ferrimagnetics*. Lincoln Laboratory publications. McGraw-Hill, 1962.

[28] L.D. Landau, J.S. Bell, M.J. Kearsley, L.P. Pitaevskii, E.M. Lifshitz, and J.B. Sykes. *Electrodynamics of Continuous Media*. COURSE OF THEORETICAL PHYSICS. Elsevier Science, 2013.

[29] Michael D. Tocci, Mark J. Bloemer, Michael Scalora, Jonathan P. Dowling, and Charles M. Bowden. Thin-film nonlinear optical diode. *Applied Physics Letters*, 66(18):2324–2326, 1995.

[30] Benoy Anand, Ramakrishna Podila, Kiran Lingam, S. R. Krishnan, S. Siva Sankara Sai, Reji Philip, and Apparao M. Rao. Optical diode action from axially asymmetric nonlinearity in an all-carbon solid-state device. *Nano Letters*, 13(12):5771–5776, Dec 2013.

[31] Ahmed M. Mahmoud, Arthur R. Davoyan, and Nader Engheta. All-passive nonreciprocal metastructure. *Nature Communications*, 6(1):8359, Sep 2015.

[32] Dimitrios L. Sounas and Andrea Alù. Time-reversal symmetry bounds on the electromagnetic response of asymmetric structures. *Phys. Rev. Lett.*, 118:154302, Apr 2017.

[33] Toshiro Kodera, Dimitrios L. Sounas, and Christophe Caloz. Artificial faraday rotation using a ring metamaterial structure without static magnetic field. *Applied Physics Letters*, 99(3):031114, 2011.

[34] R J Potton. Reciprocity in optics. *Reports on Progress in Physics*, 67(5):717–754, apr 2004.

[35] Christophe Caloz, Andrea Alù, Sergei Tretyakov, Dimitrios Sounas, Karim Achouri, and Zoé-Lise Deck-Léger. What is nonreciprocity? part ii, 2018.

[36] Christophe Caloz and Ari Sihvola. Electromagnetic chirality. *arXiv: Optics*, 2019.

[37] Akhlesh Lakhtakia. First order characterization of electromagnetic fields in isotropic chiral media. *AEU - International Journal of Electronics and Communications*, 45(1):57–59, January 1991.

[38] L. Landau and E. Lifshitz. *On the theory of the dispersion of magnetic permeability in ferromagnetic bodies*, volume 8. Physikalische Zeitschrift der Sowjetunion., 1935.

[39] C. Caloz, T. Kodera, and D. L. Sounas. Semiconductor-based non-reciprocal gyrotropic metamaterials requiring no external magnetic field. In *2013 7th International Congress on Advanced Electromagnetic Materials in Microwaves and Optics*, pages 43–45, 2013.

[40] Jin Au Kong. Theorems of bianisotropic media. *Proceedings of the IEEE*, 60(9):1036–1046, 1972.

[41] David J. Griffiths. *Introduction to Electrodynamics*. Cambridge University Press, 4 edition, 2017.

[42] T. Kodera and C. Caloz. Unidirectional loop metamaterials (ulm) as magnetless artificial ferrimagnetic materials: Principles and applications. *IEEE Antennas and Wireless Propagation Letters*, 17(11):1943–1947, 2018.

[43] Alexander G. Gurevich and Gennadii A. Melkov. *Magnetization Oscillations and Waves*. CRC Press, 1996.

[44] D. Polder. On the theory of ferromagnetic resonance. *Physica*, 15(1):253 – 255, 1949.

[45] D.M. Pozar. *Microwave Engineering, 4th Edition*. Wiley, 2011.

[46] F. Bloch. Zur theorie des ferromagnetismus. *Zeitschrift für Physik*, 61(3):206–219, Mar 1930.

[47] Conyers Herring and Charles Kittel. On the theory of spin waves in ferromagnetic media. *Phys. Rev.*, 81:869–880, Mar 1951.

[48] C. L. Hogan. The ferromagnetic faraday effect at microwave frequencies and its applications: The microwave gyrator. *The Bell System Technical Journal*, 31(1):1–31, 1952.

[49] Lars Onsager. Reciprocal relations in irreversible processes. ii. *Phys. Rev.*, 38:2265–2279, Dec 1931.

[50] John David Jackson. *Classical electrodynamics; 2nd ed.* Wiley, New York, NY, 1975.

[51] Zongfu Yu and Shanhui Fan. Optical isolation based on nonreciprocal phase shift induced by interband photonic transitions. *Applied Physics Letters*, 94(17):171116, 2009.

[52] T. Kodera, D. L. Sounas, and C. Caloz. Magnetless nonreciprocal metamaterial (mnm) technology: Application to microwave components. *IEEE Transactions on Microwave Theory and Techniques*, 61(3):1030–1042, 2013.

[53] T. Kodera, D. L. Sounas, and C. Caloz. Switchable magnetless nonreciprocal metamaterial (mnm) and its application to a switchable faraday rotation metasurface. *IEEE Antennas and Wireless Propagation Letters*, 11:1454–1457, 2012.

[54] D. L. Sounas, N. A. Estep, A. Kord, and A. Alù. Angular-momentum biased circulators and their power consumption. *IEEE Antennas and Wireless Propagation Letters*, 17(11):1963–1967, 2018.

[55] I. Wolff and N. Knoppik. Microstrip ring resonator and dispersion measurement on microstrip lines. *Electronics Letters*, 7(26):779–781, 1971.

[56] Y. S. Wu and F. J. Rosenbaum. Mode chart for microstrip ring resonators (short papers). *IEEE Transactions on Microwave Theory and Techniques*, 21(7):487–489, 1973.

[57] Kai Chang, S. Martin, Fuchen Wang, and J. L. Klein. On the study of microstrip ring and varactor-tuned ring circuits. *IEEE Transactions on Microwave Theory and Techniques*, 35(12):1288–1295, 1987.

[58] A. Kord, D. L. Sounas, and A. Alù. Microwave nonreciprocity. *Proceedings of the IEEE*, pages 1–31, 2020.

[59] I.J. Bahl and D.K. Trivedi. A designerŝ guide to microstrip line, leitfaden fuer den entwickler von mikrostreifenleitern, microwaves. *Microwaves*, 16(5):174–182, 1977.

[60] D. L. Sounas, T. Kodera, and C. Caloz. Electromagnetic modeling of a magnetless nonreciprocal gyrotropic metasurface. *IEEE Transactions on Antennas and Propagation*, 61(1):221–231, 2013.

[61] H. Suhl and L. R. Walker. Topics in guided wave propagation through gyromagnetic media. *The Bell System Technical Journal*, 33(5):1133–1194, 1954.

[62] Massimo Moccia, Giuseppe Castaldi, Vincenzo Galdi, Andrea Alù, and Nader Engheta. Enhanced faraday rotation via resonant tunnelling in tri-layers containing magneto-optical metals. *Journal of Physics D: Applied Physics*, 47(2):025002, dec 2013.

[63] Linbo Shao, Wenbo Mao, Smarak Maity, Neil Sinclair, Yaowen Hu, Lan Yang, and Marko Lončar. Non-reciprocal transmission of microwave acoustic waves in nonlinear parity–time symmetric resonators. *Nature Electronics*, 3(5):267–272, May 2020.

[64] Editorial. Directions for non-reciprocal electronics. *Nature Electronics*, 3(5):233–233, May 2020.

THIS PAGE INTENTIONALLY LEFT BLANK

Appendix

CALCULATION OF REFLECTION AND TRANSMISSION COEFFICIENT FOR BIASED FERRITE MATERIAL IN NORMAL INCIDENCE

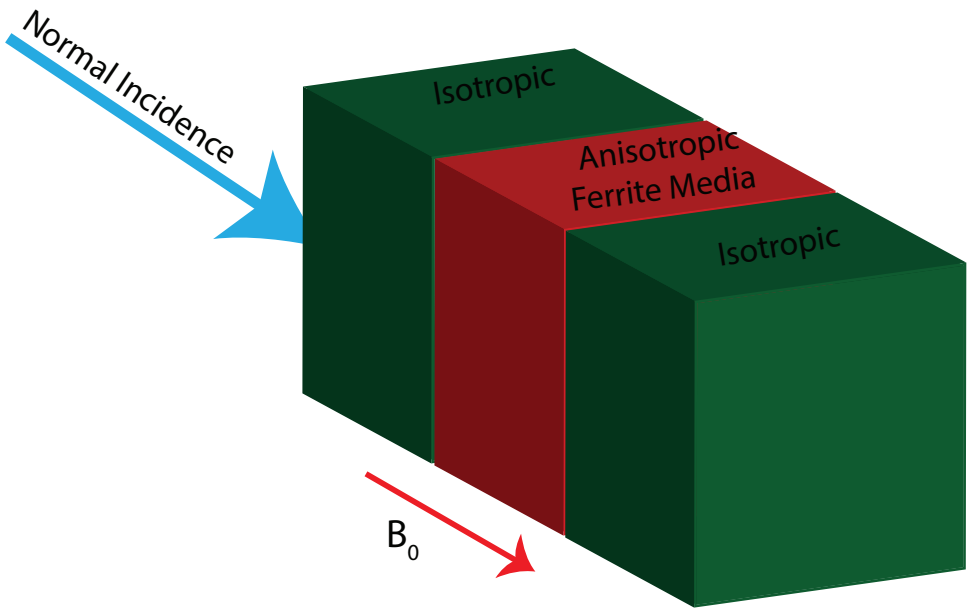

Figure A-1: Biased ferrite material in normal incidence

Figure A-1 depicts the configuration, where, reflection and transmission coefficient will be mathematically derived.

Maxwell's equations in time domain in the p-th medium (p=1,2,3) are as follows

$$\nabla \times \mathbf{E}_p = -\frac{\partial \mathbf{B}_p}{\partial t}, \tag{A.1}$$

$$\nabla \times \mathbf{H}_p = -\frac{\partial \mathbf{D}_p}{\partial t}. \tag{A.2}$$

Similarly, Eq. A.1 and A.2 can be written in frequency domain as

$$i\mathbf{k} \times \mathbf{E}_p = i\omega\mu_0\tilde{\mu}^{(p)} \cdot \mathbf{H}_p, \tag{A.3}$$

$$i\mathbf{k} \times \mathbf{H}_p = -i\omega\varepsilon_0\tilde{\varepsilon}^{(p)} \cdot \mathbf{E}_p. \tag{A.4}$$

The constitutive relations for p-th medium (p=1,2,3) are given as

$$\mathbf{B}_p = \mu_0\tilde{\mu}^{(p)} \cdot \mathbf{H}_p, \tag{A.5}$$

$$\mathbf{D}_p = \varepsilon_0\tilde{\varepsilon}^{(p)} \cdot \mathbf{E}_p, \tag{A.6}$$

where $\tilde{\mu}^{(p)}$ and $\tilde{\varepsilon}^{(p)}$ are tensors. We can define the general form of a tensor as

$$\tilde{\varepsilon}^{(p)} = \varepsilon_0 \begin{bmatrix} \varepsilon_{x,x}^{(p)} & \varepsilon_{x,y}^{(p)} & \varepsilon_{x,z}^{(p)} \\ \varepsilon_{y,x}^{(p)} & \varepsilon_{y,y}^{(p)} & \varepsilon_{y,z}^{(p)} \\ \varepsilon_{z,x}^{(p)} & \varepsilon_{z,y}^{(p)} & \varepsilon_{z,z}^{(p)} \end{bmatrix}, \tag{A.7}$$

$$\tilde{\mu}^{(p)} = \mu_0 \begin{bmatrix} \mu_{x,x}^{(p)} & \mu_{x,y}^{(p)} & \mu_{x,z}^{(p)} \\ \mu_{y,x}^{(p)} & \mu_{y,y}^{(p)} & \mu_{y,z}^{(p)} \\ \mu_{z,x}^{(p)} & \mu_{z,y}^{(p)} & \mu_{z,z}^{(p)} \end{bmatrix}. \tag{A.8}$$

We introduce $\vec{K}$ as the tensor that satisfies the below relation

$$\mathbf{k} \times \mathbf{E}_p = \tilde{\mathbf{K}} \cdot \mathbf{E}_p, \tag{A.9}$$

$$\mathbf{k} \times \mathbf{H}_p = \tilde{\mathbf{K}} \cdot \mathbf{H}_p. \tag{A.10}$$

So matrix form of tensor $\vec{K}$ for pth medium can be represented as

$$\tilde{\mathbf{K}}_p = \begin{bmatrix} 0 & -k_z^{(p)} & k_y^{(p)} \\ k_z^{(p)} & 0 & -k_x^{(p)} \\ -k_y^{(p)} & k_x^{(p)} & 0 \end{bmatrix}. \tag{A.11}$$

From above Eq. A.1 - A.11, this can be written as

$$\tilde{\mathbf{K}}_p \cdot \mathbf{E}_p = -\frac{\omega^2}{c^2}(\tilde{\mu}^{(p)} \cdot \tilde{\mathbf{K}}_p^{-1} \cdot \tilde{\varepsilon}^{(p)} \cdot \mathbf{E}_p), \tag{A.12}$$

$$\left\{ \frac{\omega^2}{c^2}(\tilde{\mathbf{K}}_p^{-1} \cdot \tilde{\mu}^{(p)} \cdot \tilde{\mathbf{K}}_p^{-1} \cdot \tilde{\varepsilon}^{(p)}) + \mathbf{I} \right\} \cdot \mathbf{E}_p = 0. \tag{A.13}$$

For normal incidence, $k_x^{(p)} = k_y^{(p)} = 0$, therefore, the Eq. A.13 will be in the matrix form

$$\left\{ n^{(p)} \right\}^{-2} \begin{bmatrix} 0 & 1 \\ -1 & 0 \end{bmatrix} \begin{bmatrix} \mu_{x,x}^{(p)} & \mu_{x,y}^{(p)} \\ \mu_{y,x}^{(p)} & \mu_{y,y}^{(p)} \end{bmatrix} \begin{bmatrix} 0 & 1 \\ -1 & 0 \end{bmatrix} \begin{bmatrix} \varepsilon_{x,x}^{(p)} & \varepsilon_{x,y}^{(p)} \\ \varepsilon_{y,x}^{(p)} & \varepsilon_{y,y}^{(p)} \end{bmatrix} + \begin{bmatrix} 1 & 0 \\ 0 & 1 \end{bmatrix}, \tag{A.14}$$

Where $n^{(p)}$ is defined as

$$n^{(p)} \equiv \frac{ck_z^{(p)}}{\omega}, \tag{A.15}$$

$$\left\{ n^{(p)} \right\}^{-2} \begin{bmatrix} \mu_{y,x}^p \varepsilon_{y,x}^p - \varepsilon_{x,x}^p \mu_{y,y}^p & \mu_{y,x}^p \varepsilon_{y,y}^p - \mu_{y,y}^p \varepsilon_{x,y}^p \\ \mu_{x,y}^p \varepsilon_{x,x}^p - \mu_{x,x}^p \varepsilon_{y,x}^p & \mu_{x,y}^p \varepsilon_{x,y}^p - \mu_{x,x}^p \varepsilon_{y,y}^p \end{bmatrix} + \begin{bmatrix} 1 & 0 \\ 0 & 1 \end{bmatrix}, \tag{A.16}$$

Let,

$$M_{x,x}^{(p)} = \mu_{y,x}^p \varepsilon_{y,x}^p - \varepsilon_{x,x}^p \mu_{y,y}^p, \tag{A.17}$$

$$M_{x,y}^{(p)} = \mu_{y,x}^p \varepsilon_{y,y}^p - \mu_{y,y}^p \varepsilon_{x,y}^p, \tag{A.18}$$

$$M_{y,x}^{(p)} = \mu_{y,x}^p \varepsilon_{y,y}^p - \mu_{y,y}^p \varepsilon_{x,y}^p, \tag{A.19}$$

$$M_{y,y}^{(p)} = \mu_{x,y}^p \varepsilon_{x,y}^p - \mu_{x,x}^p \varepsilon_{y,y}^p. \tag{A.20}$$

Therefore, Eq. A.16 can be written as

$$\left(\left\{ n^{(p)} \right\}^{-2} \begin{bmatrix} M_{x,x}^{(p)} & M_{x,y}^{(p)} \\ M_{y,x}^{(p)} & M_{y,y}^{(p)} \end{bmatrix} + \begin{bmatrix} 1 & 0 \\ 0 & 1 \end{bmatrix} \right) \cdot \begin{bmatrix} E_{p,x} \\ E_{p,y} \end{bmatrix} = \begin{bmatrix} 0 \\ 0 \end{bmatrix}, \tag{A.21}$$

which can be written in eigen value form as

$$\begin{bmatrix} M_{x,x}^{(p)} & M_{x,y}^{(p)} \\ M_{y,x}^{(p)} & M_{y,y}^{(p)} \end{bmatrix} \cdot \begin{bmatrix} E_{p,x} \\ E_{p,y} \end{bmatrix} = - \left\{ n^{(p)} \right\}^{-2} \begin{bmatrix} E_{p,x} \\ E_{p,y} \end{bmatrix}, \tag{A.22}$$

The following requirement is required to be satisfied

$$Det \left(\left\{ n^{(p)} \right\}^{-2} \begin{bmatrix} M_{x,x}^{(p)} & M_{x,y}^{(p)} \\ M_{y,x}^{(p)} & M_{y,y}^{(p)} \end{bmatrix} + \begin{bmatrix} 1 & 0 \\ 0 & 1 \end{bmatrix} \right) = 0, \tag{A.23}$$

yields the following two eigen-values

$$\left\{ n_j^{(p)} \right\}^2 = \zeta_j^{(p)} = -\frac{1}{2} \left(M_{x,x}^{(p)} + M_{y,y}^{(p)} + s_j \sqrt{(M_{x,x}^{(p)} - M_{y,y}^{(p)})^2 + 4 M_{x,y}^{(p)} M_{y,x}^{(p)}} \right), \tag{A.24}$$

which correspond to the following eigen-vectors

$$\mathbf{V}_{p,j} = \frac{1}{\sqrt{1 + \left| \frac{\zeta_j^{(p)} - M_{x,x}^{(p)}}{M_{x,y}^{(p)}} \right|^2}} \begin{bmatrix} 1 \\ \frac{\zeta_j^{(p)} - M_{x,x}^{(p)}}{M_{x,y}^{(p)}} \end{bmatrix} ; \; j = 1, 2, \tag{A.25}$$

with the coefficient s_j being given as

$$s_1 = 1, s_2 = -1$$

We, hereafter, assume medium 1 and 3 are isotropic (no off-diagonal element) i.e.

$$\varepsilon_{x,x}^{(p)} = \varepsilon_{y,y}^{(p)} \; , \; \varepsilon_{x,y}^{(p)} = -\varepsilon_{y,x}^{(p)} = 0 \; ; \; p = 1, 3 \tag{A.26}$$

$$\mu_{x,x}^{(p)} = \mu_{y,y}^{(p)} \ , \ \mu_{x,y}^{(p)} = -\mu_{y,x}^{(p)} = 0 \ ; \ p = 1, 3, \tag{A.27}$$

and we also assume that medium 2 is gyrotropic

$$\varepsilon_{x,x}^{(2)} = \varepsilon_{y,y}^{(2)}, \ \varepsilon_{x,y}^{(2)} = -\varepsilon_{y,x}^{(2)} = -i\varepsilon_g \neq 0, \tag{A.28}$$

$$\mu_{x,x}^{(2)} = \mu_{y,y}^{(2)}, \ \mu_{x,y}^{(2)} = -\mu_{y,x}^{(2)} = -i\mu_g \neq 0. \tag{A.29}$$

Therefore,

$$M_{x,x}^{(p)} = M_{y,y}^{(p)}, \ M_{x,y}^{(p)} = -M_{y,x}^{(p)}, \tag{A.30}$$

and so the eigen values reduce to

$$\left\{ n_j^{(p)} \right\}^2 = \zeta_j^{(p)} = -(M_{x,x}^{(p)} + is_j M_{x,y}^{(p)}). \tag{A.31}$$

The refractive index of each medium is given as

$$n^{(1)} = \sqrt{\mu_{x,x}^{(1)} \varepsilon_{x,x}^{(1)}}, \tag{A.32}$$

$$n_j^{(2)} = \sqrt{-(M_{x,x}^{(2)} + is_j M_{x,y}^{(2)})} = \sqrt{\mu_{x,x}^{(p)} \varepsilon_{x,x}^{(p)} - \mu_{x,y}^{(p)} \varepsilon_{x,y}^{(p)} + is_j (\mu_{x,y}^{(p)} \varepsilon_{x,x}^{(p)} + \mu_{x,x}^{(p)} \varepsilon_{x,y}^{(p)})} \tag{A.33}$$

$$= \sqrt{\left(\varepsilon_{x,x}^{(p)} + is_j \varepsilon_{x,y}^{(p)} \right) \left(\mu_{x,x}^{(p)} + is_j \mu_{x,y}^{(p)} \right)}, \tag{A.34}$$

$$n^{(3)} = \sqrt{\mu_{x,x}^{(3)} \varepsilon_{x,x}^{(3)}}, \tag{A.35}$$

Furthermore, the eigen-vector corresponding to gyrotropic medium take the following simplified form

$$\mathbf{V}_{p,j} = \frac{\hat{\mathbf{e}}_x + is_j \hat{\mathbf{e}}_y}{\sqrt{2}} = \frac{1}{\sqrt{2}} \begin{bmatrix} 1 \\ is_j \end{bmatrix}, \ j = \circlearrowleft, \circlearrowright \tag{A.36}$$

The eigen-vectors for gyrotropic medium correspond to left handed circularly polarized (LHCP) wave and right handed circularly polarized (RHCP) wave. Here, we adopt, $j = \circlearrowleft, \circlearrowright$ labels instead of $j = 1, 2$.

Since the eigen-vectors given by Eq. A.36 from a complete set in two dimensional space, the electromagnetic field in all three media can be expressed as a linear combination of these eigen-vectors. In medium 1 (isotropic), i.e., $-\infty < z < 0$, the forward and backward propagating waves are described by

$$\mathbf{E}_1^{\pm} = (E_{1,\circlearrowleft}^{\pm}\hat{\mathbf{E}}_{\circlearrowleft} + E_{1,\circlearrowright}^{\pm}\hat{\mathbf{E}}_{\circlearrowright}) \exp\left(\mp\frac{i\omega z n^{(1)}}{c}\right), \tag{A.37}$$

and in medium 2 (anisotropic), i.e., $0 < z < d$, the forward and backward propagating waves are described by

$$\mathbf{E}_2^{\pm} = E_{2,\circlearrowleft}^{\pm}\hat{\mathbf{E}}_{\circlearrowleft} \exp\left(\mp\frac{i\omega z n_{\circlearrowleft}}{c}\right) + E_{2,\circlearrowright}^{\pm}\hat{\mathbf{E}}_{\circlearrowright} \exp\left(\mp\frac{i\omega z n_{\circlearrowright}}{c}\right), \tag{A.38}$$

and in medium 3 (isotropic), i.e., $d < z < \infty$ the forward propagating waves are described by

$$\mathbf{E}_3^{+} = (E_{3,\circlearrowleft}^{+}\hat{\mathbf{E}}_{\circlearrowleft} + E_{3,\circlearrowright}^{+}\hat{\mathbf{E}}_{\circlearrowright}) \exp\left(-\frac{i\omega(z-d) n^{(3)}}{c}\right). \tag{A.39}$$

For medium 2, there will be no reflecting wave from medium 3. At medium 2, propagated wave will be left and right hand circularly polarized wave and experience different phase velocity due to different refractive index, hence, different impedances.

Magnetic Field:

Maxwell's equation (Faraday's law) can be written again as

$$\nabla \times \mathbf{E}_p^{\pm} = -\frac{\partial \mathbf{B}_p}{\partial t} \tag{A.40}$$

Based on our above derivation, electric and magnetic field can be written as

$$\mathbf{E}_p^{\pm} = \sum_{j=\circlearrowleft,\circlearrowright} E_{p,j}^{\pm} \hat{\mathbf{E}}_j \exp\left(\mp \frac{iz\omega}{c} n_j\right), \tag{A.41}$$

$$\mathbf{H}_p^{\pm} = \sum_{j=\circlearrowleft,\circlearrowright} H_{p,j}^{\pm} \hat{\mathbf{E}}_j \exp\left(\mp \frac{iz\omega}{c} n_j\right). \tag{A.42}$$

So from above Eq. A.40 - A.42, we get

$$-i\omega\mu_0\tilde{\mu}^{(p)} \cdot \sum_{j=\circlearrowleft,\circlearrowright} H_{p,j}^{\pm} \hat{\mathbf{E}}_j \exp\left(\mp \frac{iz\omega}{c} n_j^{(p)}\right) = \sum_{j=\circlearrowleft,\circlearrowright} (\mp\frac{i\omega}{c}) E_{p,j}^{\pm} n_j^{(p)} [\hat{\mathbf{e}}_z \times \hat{\mathbf{E}}_j] \exp\left(\mp \frac{iz\omega}{c} n_j^{(p)}\right), \tag{A.43}$$

We used the following identities in Eq. A.43:

$$\hat{\mathbf{E}}_{\circlearrowleft} = \frac{\hat{\mathbf{e}}_x - i\hat{\mathbf{e}}_y}{\sqrt{2}}, \tag{A.44}$$

$$\hat{\mathbf{E}}_{\circlearrowright} = \frac{\hat{\mathbf{e}}_x + i\hat{\mathbf{e}}_y}{\sqrt{2}}, \tag{A.45}$$

$$\hat{\mathbf{e}}_z \times \hat{\mathbf{E}}_j = -is_j \hat{\mathbf{E}}_j, \tag{A.46}$$

where $s_{\circlearrowleft} = 1$ and $s_{\circlearrowright} = -1$ Left side of Eq. A.43 can be written as

$$\begin{aligned} \tilde{\mu}^{(p)} \cdot \hat{\mathbf{E}}_j &= \frac{1}{\sqrt{2}} \begin{bmatrix} \mu_{x,x}^{(p)} & \mu_{x,y}^{(p)} \\ -\mu_{x,y}^{(p)} & \mu_{x,x}^{(p)} \end{bmatrix} \begin{bmatrix} 1 \\ is_j \end{bmatrix} \\ &= \frac{1}{\sqrt{2}} \begin{bmatrix} is_j\mu_{x,y}^{p} + \mu_{x,x}^{p} \\ is_j\mu_{x,x}^{p} - \mu_{x,y}^{p} \end{bmatrix} = (\mu_{x,x}^{(p)} + is_j\mu_{x,y}^{(p)})\hat{\mathbf{E}}_j. \end{aligned} \tag{A.47}$$

So Eq. A.42 can be reduced to

$$H_{p,j}^{\pm} = \mp is_j \frac{E_{p,j}^{\pm}}{Z_{p,j}}, \tag{A.48}$$

where $Z_{p,j}^{(p)}$ is the impedance of the p-th medium experienced by the j-th plane wave ($j = \circlearrowleft$

, ↻)

$$Z_j^{(p)} = Z_0 \sqrt{\frac{\mu_{x,x}^{(p)} + is_j\mu_{x,y}^{(p)}}{\varepsilon_{x,x}^{(p)} + is_j\varepsilon_{x,y}^{(p)}}}. \tag{A.49}$$

with, $Z_0 = \sqrt{\frac{\mu_0}{\varepsilon_0}} = \mu_0 c = 377\Omega$, impedance of the free space.

Reflection and Transmission Coefficient

Medium 1 (Isotropic) to medium 2 (Gyrotropic)

$$\mathbf{E}_1^+ = (E_{1,\circlearrowleft}^+ \hat{\mathbf{E}}_{\circlearrowleft} + E_{1,\circlearrowright}^+ \hat{\mathbf{E}}_{\circlearrowright}) \exp\left(-\frac{i\omega z n^{(1)}}{c}\right). \tag{A.50}$$

Reflected Wave

$$\mathbf{E}_1^- = (E_{1,\circlearrowleft}^- \hat{\mathbf{E}}_{\circlearrowleft} + E_{1,\circlearrowright}^- \hat{\mathbf{E}}_{\circlearrowright}) \exp\left(+\frac{i\omega z n^{(1)}}{c}\right). \tag{A.51}$$

Transmitted Wave

$$E_2^+ = E_{2,\circlearrowleft}^+ \exp\left(-\frac{i\omega z n_{\circlearrowleft}^{(2)}}{c}\right) + E_{2,\circlearrowright}^+ \exp\left(-\frac{i\omega z n_{\circlearrowleft}^{(2)}}{c}\right). \tag{A.52}$$

The continuity of the tangential component of the total electric field at $z = 0$ requires that

$$\mathbf{E}_1^+(z=0) + \mathbf{E}_1^-(z=0) = \mathbf{E}_2^+(z=0) + \mathbf{E}_2^-(z=0), \tag{A.53}$$

$$\mathbf{H}_1^+(z=0) + \mathbf{H}_1^-(z=0) = \mathbf{H}_2^+(z=0) + \mathbf{H}_2^-(z=0). \tag{A.54}$$

Besides, the tangential component of the total electrical field at $z = d$ requires that

$$\mathbf{E}_2^+(z=d) + \mathbf{E}_2^-(z=d) = \mathbf{E}_3^+(z=d), \tag{A.55}$$

$$\mathbf{H}_2^+(z=d) + \mathbf{H}_2^-(z=d) = \mathbf{H}_3^+(z=d). \tag{A.56}$$

The magnetic field corresponding to the incident, reflected, and transmitted fields are given as

$$H_p^{\pm} = \sum_{j=\circlearrowleft,\circlearrowleft} H_{p,j}^{\pm} \hat{\mathbf{E}}_j \exp\left(\mp \frac{iz\omega}{c} n_j^{(2)}\right), \tag{A.57}$$

Medium 1 and 3

$$H_{p,j}^{\pm} = \mp i s_j \frac{E_{p,j}^{\pm}}{Z_r^{(p)}}; p = 1, 3, \tag{A.58}$$

where $Z_r^{(p)}$ denotes the relatative impedance of the p-th isotropic medium (p=1,3) and is defined as follows

$$Z_r^{(p)} = Z_0 \sqrt{\frac{\mu_{x,x}^{(p)}}{\varepsilon_{x,x}^{(p)}}} \tag{A.59}$$

Medium 1

$$\mathbf{H}_1^{+} = -i s_{\circlearrowleft} \frac{E_{1,\circlearrowleft}^{+}}{Z_r^{(1)}} \hat{\mathbf{E}}_{\circlearrowleft} \exp\left(-\frac{iz\omega}{c} n_{\circlearrowleft}^{(2)}\right), \tag{A.60}$$

$$\mathbf{H}_1^{+} = -i s_{\circlearrowleft} \frac{E_{1,\circlearrowleft}^{+}}{Z_r^{(1)}} \hat{\mathbf{E}}_{\circlearrowleft} \exp\left(-\frac{iz\omega}{c} n_{\circlearrowleft}^{(2)}\right), \tag{A.61}$$

$$\mathbf{H}_1^{-} = i s_{\circlearrowleft} \frac{E_{1,\circlearrowleft}^{-}}{Z_r^{(1)}} \hat{\mathbf{E}}_{\circlearrowleft} \exp\left(+\frac{iz\omega}{c} n_{\circlearrowleft}^{(2)}\right), \tag{A.62}$$

$$\mathbf{H}_1^{-} = i s_{\circlearrowleft} \frac{E_{1,\circlearrowleft}^{-}}{Z_r^{(1)}} \hat{\mathbf{E}}_{\circlearrowleft} \exp\left(+\frac{iz\omega}{c} n_{\circlearrowleft}^{(2)}\right). \tag{A.63}$$

Medium 2

$$\mathbf{H}_2^{+} = -i s_{\circlearrowleft} \frac{E_{2,\circlearrowleft}^{+}}{Z_j^{(2)}} \hat{\mathbf{E}}_{\circlearrowleft} \exp\left(-\frac{iz\omega}{c} n_{\circlearrowleft}^{(2)}\right), \tag{A.64}$$

$$\mathbf{H}_2^{+} = -i s_{\circlearrowleft} \frac{E_{2,\circlearrowleft}^{+}}{Z_j^{(2)}} \hat{\mathbf{E}}_{\circlearrowleft} \exp\left(-\frac{iz\omega}{c} n_{\circlearrowleft}^{(2)}\right), \tag{A.65}$$

$$\mathbf{H}_2^{-} = i s_{\circlearrowleft} \frac{E_{2,\circlearrowleft}^{-}}{Z_j^{(2)}} \hat{\mathbf{E}}_{\circlearrowleft} \exp\left(+\frac{iz\omega}{c} n_{\circlearrowleft}^{(2)}\right), \tag{A.66}$$

$$\mathbf{H}_2^{-} = i s_{\circlearrowleft} \frac{E_{2,\circlearrowleft}^{-}}{Z_j^{(2)}} \hat{\mathbf{E}}_{\circlearrowleft} \exp\left(+\frac{iz\omega}{c} n_{\circlearrowleft}^{(2)}\right). \tag{A.67}$$

Medium 3

$$\mathbf{H}_3^+ = -is_{\circlearrowleft}\frac{E_{3,\circlearrowleft}^+}{Z_r^{(3)}}\hat{\mathbf{E}}_{\circlearrowleft}\exp\left(-\frac{iz\omega}{c}n_{\circlearrowleft}^{(2)}\right), \tag{A.68}$$

$$\mathbf{H}_3^+ = -is_{\circlearrowleft}\frac{E_{3,\circlearrowleft}^+}{Z_r^{(3)}}\hat{\mathbf{E}}_{\circlearrowleft}\exp\left(-\frac{iz\omega}{c}n_{\circlearrowleft}^{(2)}\right). \tag{A.69}$$

Now from the definition of boundary condition, we get at $z = 0$ interface

$$(E_{1,\circlearrowleft}^+\hat{\mathbf{E}}_{\circlearrowleft} + E_{1,\circlearrowleft}^+\hat{\mathbf{E}}_{\circlearrowleft}) + (E_{1,\circlearrowleft}^-\hat{\mathbf{E}}_{\circlearrowleft} + E_{1,\circlearrowleft}^-\hat{\mathbf{E}}_{\circlearrowleft}) = (E_{2,\circlearrowleft}^+\hat{\mathbf{E}}_{\circlearrowleft} + E_{2,\circlearrowleft}^+\hat{\mathbf{E}}_{\circlearrowleft}) + (E_{2,\circlearrowleft}^-\hat{\mathbf{E}}_{\circlearrowleft} + E_{2,\circlearrowleft}^-\hat{\mathbf{E}}_{\circlearrowleft}), \tag{A.70}$$

$$\begin{aligned}
\Rightarrow \quad & -is_{\circlearrowleft}\frac{E_{1,\circlearrowleft}^+}{Z_r^{(1)}}\hat{\mathbf{E}}_{\circlearrowleft} - is_{\circlearrowleft}\frac{E_{1,\circlearrowleft}^+}{Z_r^{(1)}}\hat{\mathbf{E}}_{\circlearrowleft} + is_{\circlearrowleft}\frac{E_{1,\circlearrowleft}^-}{Z_r^{(1)}}\hat{\mathbf{E}}_{\circlearrowleft} + is_{\circlearrowleft}\frac{E_{1,\circlearrowleft}^-}{Z_r^{(1)}}\hat{\mathbf{E}}_{\circlearrowleft} \\
= \quad & -is_{\circlearrowleft}\frac{E_{2,\circlearrowleft}^+}{Z_j^{(2)}}\hat{\mathbf{E}}_{\circlearrowleft} - is_{\circlearrowleft}\frac{E_{2,\circlearrowleft}^+}{Z_j^{(2)}}\hat{\mathbf{E}}_{\circlearrowleft} + is_{\circlearrowleft}\frac{E_{2,\circlearrowleft}^-}{Z_j^{(2)}}\hat{\mathbf{E}}_{\circlearrowleft} + is_{\circlearrowleft}\frac{E_{2,\circlearrowleft}^-}{Z_j^{(2)}}\hat{\mathbf{E}}_{\circlearrowleft}
\end{aligned} \tag{A.71}$$

Similarly, at $z = d$ interface, this can be written as

$$\begin{aligned}
& E_{2,\circlearrowleft}^+\hat{\mathbf{E}}_{\circlearrowleft}\exp\left(-\frac{i\omega dn_{\circlearrowleft}^{(2)}}{c}\right) + E_{2,\circlearrowleft}^+\hat{\mathbf{E}}_{\circlearrowleft}\exp\left(-\frac{i\omega dn_{\circlearrowleft}^{(2)}}{c}\right) \\
& + E_{2,\circlearrowleft}^-\hat{\mathbf{E}}_{\circlearrowleft}\exp\left(+\frac{i\omega dn_{\circlearrowleft}^{(2)}}{c}\right) + E_{2,\circlearrowleft}^-\hat{\mathbf{E}}_{\circlearrowleft}\exp\left(+\frac{i\omega dn_{\circlearrowleft}^{(2)}}{c}\right) \\
= \quad & E_{3,\circlearrowleft}^+\hat{\mathbf{E}}_{\circlearrowleft} + E_{3,\circlearrowleft}^+\hat{\mathbf{E}}_{\circlearrowleft},
\end{aligned} \tag{A.72}$$

$$\begin{aligned}
& -is_{\circlearrowleft}\frac{E_{2,\circlearrowleft}^+}{Z_j^{(2)}}\hat{\mathbf{E}}_{\circlearrowleft}\exp\left(-\frac{i\omega dn_{\circlearrowleft}^{(2)}}{c}\right) - is_{\circlearrowleft}\frac{E_{2,\circlearrowleft}^+}{Z_j^{(2)}}\hat{\mathbf{E}}_{\circlearrowleft}\exp\left(-\frac{i\omega dn_{\circlearrowleft}^{(2)}}{c}\right) + \\
& is_{\circlearrowleft}\frac{E_{2,\circlearrowleft}^-}{Z_j^{(2)}}\hat{\mathbf{E}}_{\circlearrowleft}\exp\left(+\frac{i\omega dn_{\circlearrowleft}^{(2)}}{c}\right) + is_{\circlearrowleft}\frac{E_{2,\circlearrowleft}^-}{Z_j^{(2)}}\hat{\mathbf{E}}_{\circlearrowleft}\exp\left(+\frac{i\omega dn_{\circlearrowleft}^{(2)}}{c}\right) \\
= \quad & -is_{\circlearrowleft}\frac{E_{3,\circlearrowleft}^+}{Z_r^{(3)}}\hat{\mathbf{E}}_{\circlearrowleft} - is_{\circlearrowleft}\frac{E_{3,\circlearrowleft}^+}{Z_r^{(3)}}\hat{\mathbf{E}}_{\circlearrowleft}.
\end{aligned} \tag{A.73}$$

Due to the orthogonality of the left-hand and right hand eigen vector, i.e., $\hat{\mathbf{E}}_n \cdot \hat{\mathbf{E}}_m^* = \delta_{n,m}$ for $n, m =$↻, ↺, the preceding vector equations can be expressed in terms of the following scalar equations.

$Z = 0$ interface

$$E_{1,j}^+ + E_{1,j}^- = E_{2,j}^+ + E_{2,j}^-, \tag{A.74}$$

$$E_{1,j}^+ - E_{1,j}^- = \frac{Z_r^{(1)}}{Z_j^{(2)}}(E_{2,j}^+ - E_{2,j}^-). \tag{A.75}$$

$Z = d$ interface

$$E_{2,j}^+ \exp\left(-\frac{i\omega d n_j^{(2)}}{c}\right) + E_{2,j}^- \exp\left(\frac{i\omega d n_j^{(2)}}{c}\right) = E_{3,j}^+, \tag{A.76}$$

$$s_j \frac{E_{2,j}^+}{Z_j^{(2)}} \exp\left(-\frac{i\omega d n_j^{(2)}}{c}\right) - s_j \frac{E_{2,j}^-}{Z_j^{(2)}} \exp\left(\frac{i\omega d n_j^{(2)}}{c}\right) = s_j \frac{E_{3,j}^+}{Z_r^{(3)}}. \tag{A.77}$$

Multiply both sides of Eq. A.76 by $\frac{s_j}{Z_{p,j}}$ and add with equation Eq. A.77

$$E_{2,j}^+ = \frac{1}{2}(1 + \frac{Z_j^{(2)}}{Z_r^{(3)}}) E_{3,j}^+ \exp\left(\frac{i\omega d n_j^{(2)}}{c}\right) \tag{A.78}$$

Now multiply Eq. A.76 with -$\frac{s_j}{Z_{p,j}^{(2)}}$ and add with equation Eq. A.77

$$E_{2,j}^- = \frac{1}{2}(1 - \frac{Z_j^{(2)}}{Z_r^{(3)}}) E_{3,j}^+ \exp\left(-\frac{i\omega d n_j^{(2)}}{c}\right). \tag{A.79}$$

Now from equation Eq. A.74, we get

$$E_{1,j}^+ + E_{1,j}^- = \frac{1}{2}(1 + \frac{Z_j^{(2)}}{Z_r^{(3)}}) E_{3,j}^+ \exp\left(\frac{i\omega d n_j^{(2)}}{c}\right) + \frac{1}{2}(1 - \frac{Z_j^{(2)}}{Z_r^{(3)}}) E_{3,j}^+ \exp\left(-\frac{i\omega d n_j^{(2)}}{c}\right). \tag{A.80}$$

$$E^{+}_{1,j} - E^{-}_{1,j} = \frac{1}{2}(\frac{Z^{(1)}_r}{Z^{(3)}_r} + \frac{Z^{(1)}_r}{Z^{(2)}_j})E^{+}_{3,j}\exp\left(\frac{i\omega dn^{(2)}_j}{c}\right) + \frac{1}{2}(\frac{Z^{(1)}_r}{Z^{(3)}_r} - \frac{Z^{(1)}_r}{Z^{(2)}_j})E^{+}_{3,j}\exp\left(-\frac{i\omega dn^{(2)}_j}{c}\right) \tag{A.81}$$

Addition or subtraction of the preceding equations leads us to the following expression

$$E^{+}_{3,j} = \frac{4}{(1 + \frac{Z^{(2)}_j}{Z^{(3)}_r} \pm \frac{Z^{(1)}_r}{Z^{(3)}_r} \pm \frac{Z^{(1)}_r}{Z^{(2)}_j})\exp\left(\frac{i\omega dn^{(2)}_j}{c}\right) + (1 - \frac{Z^{(2)}_j}{Z^{(3)}_r} \pm \frac{Z^{(1)}_r}{Z^{3}_r} \mp \frac{Z^{(1)}_r}{Z^{(2)}_j})\exp\left(-\frac{i\omega dn^{(2)}_j}{c}\right)} E^{\pm}_{1,j}. \tag{A.82}$$

Comparing the preceding equation with the definition of transmission tensor

$$\lim_{\delta \longrightarrow 0}[\mathbf{E}^{+}_3(z = d + \delta)] = \tilde{\mathbf{t}} \cdot \lim_{\delta \longrightarrow 0}[\mathbf{E}^{+}_1(z = -\delta)], \tag{A.83}$$

yields,

$$t^{c}_{n,m} = \frac{4\delta_{n,m}}{(1 + \frac{Z^{(2)}_m}{Z^{(3)}_r} + \frac{Z^{(1)}_r}{Z^{(3)}_r} + \frac{Z^{(1)}_r}{Z^{(2)}_m})\exp\left(\frac{i\omega dn^{(2)}_m}{c}\right) + (1 - \frac{Z^{(2)}_m}{Z^{(3)}_r} + \frac{Z^{(1)}_r}{Z^{(3)}_r} - \frac{Z^{(1)}_r}{Z^{(2)}_m})\exp\left(-\frac{i\omega dn^{(2)}_m}{c}\right)} \tag{A.84}$$

with $\delta_{n,m}$ and $t^{c}_{n,m}$ respectively denoting the Kronecker delta function and components of the transmission tensor in LHCP-RHCP basis set, i.e.

$$\tilde{\mathbf{t}} = \sum_{n=\circlearrowleft,\circlearrowleft}\sum_{m=\circlearrowleft,\circlearrowleft} t^{c}_{n,m}\hat{\mathbf{E}}_n\hat{\mathbf{E}}^{*}_m = t^{c}_{\circlearrowleft,\circlearrowleft}\hat{\mathbf{E}}_{\circlearrowleft}\hat{\mathbf{E}}^{*}_{\circlearrowleft} + t^{c}_{\circlearrowleft,\circlearrowright}\hat{\mathbf{E}}_{\circlearrowright}\hat{\mathbf{E}}^{*}_{\circlearrowleft} + t^{c}_{\circlearrowleft,\circlearrowleft}\hat{\mathbf{E}}_{\circlearrowleft}\hat{\mathbf{E}}^{*}_{\circlearrowright} + t^{c}_{\circlearrowleft,\circlearrowright}\hat{\mathbf{E}}_{\circlearrowright}\hat{\mathbf{E}}^{*}_{\circlearrowright} = \begin{bmatrix} t^{c}_{\circlearrowleft,\circlearrowleft} & t^{c}_{\circlearrowleft,\circlearrowright} \\ t^{c}_{\circlearrowleft,\circlearrowleft} & t^{c}_{\circlearrowleft,\circlearrowright} \end{bmatrix}. \tag{A.85}$$

As a result

$$\tilde{\mathbf{t}} = \sum_{m=\circlearrowleft,\circlearrowright} \frac{4}{(1 + \frac{Z^{(2)}_m}{Z^{(3)}_r} + \frac{Z^{(1)}_r}{Z^{(3)}_r} + \frac{Z^{(1)}_r}{Z^{(2)}_m})\exp\left(\frac{i\omega dn^{(2)}_m}{c}\right) + (1 - \frac{Z^{(2)}_m}{Z^{(3)}_r} + \frac{Z^{(1)}_r}{Z^{(3)}_r} - \frac{Z^{(1)}_r}{Z^{(2)}_m})\exp\left(-\frac{i\omega dn^{(2)}_m}{c}\right)} \hat{\mathbf{E}}_m\hat{\mathbf{E}}^{*}_m, \tag{A.86}$$

The components of transmission tensor can be represented in cartesian coordinates as

$$\tilde{\mathbf{t}} = \sum_{n=x,y}\sum_{m=x,y} t_{n,n}\hat{\mathbf{e}}_n\hat{\mathbf{e}}_m = t_{x,x}\hat{\mathbf{e}}_x\hat{\mathbf{e}}_x + t_{x,y}\hat{\mathbf{e}}_x\hat{\mathbf{e}}_y + t_{y,x}\hat{\mathbf{e}}_y\hat{\mathbf{e}}_x + t_{y,y}\hat{\mathbf{e}}_y\hat{\mathbf{e}}_y \equiv \begin{bmatrix} t_{x,x} & t_{x,y} \\ t_{y,x} & t_{y,y} \end{bmatrix}. \quad \text{(A.87)}$$

In order to obtain the components of the transmission tensor in cartesian coordinates, $\hat{\mathbf{E}}_{\circlearrowleft}$ and $\hat{\mathbf{E}}_{\circlearrowleft}$ should be substituted with their cartesian representation

$$\tilde{\mathbf{t}} = t^c_{\circlearrowleft,\circlearrowleft}\left(\frac{\hat{\mathbf{e}}_x - i\hat{\mathbf{e}}_y}{\sqrt{2}}\right)\left(\frac{\hat{\mathbf{e}}_x + i\hat{\mathbf{e}}_y}{\sqrt{2}}\right) + t^c_{\circlearrowleft,\circlearrowleft}\left(\frac{\hat{\mathbf{e}}_x + i\hat{\mathbf{e}}_y}{\sqrt{2}}\right)\left(\frac{\hat{\mathbf{e}}_x - i\hat{\mathbf{e}}_y}{\sqrt{2}}\right). \quad \text{(A.88)}$$

Therefore, the components of the transmission tensor in cartesian coordinates are given as

$$t_{x,x} = t_{y,y} = \sum_{m=\circlearrowleft,\circlearrowleft} \frac{2}{\left(1 + \frac{Z^{(2)}_m}{Z^{(3)}_r} + \frac{Z^{(1)}_r}{Z^{(3)}_r} + \frac{Z^{(1)}_r}{Z^{(2)}_m}\right)\exp\left(\frac{i\omega dn^{(2)}_m}{c}\right) + \left(1 - \frac{Z^{(2)}_m}{Z^{(3)}_r} + \frac{Z^{(1)}_r}{Z^{(3)}_r} - \frac{Z^{(1)}_r}{Z^{(2)}_m}\right)\exp\left(-\frac{i\omega dn^{(2)}_m}{c}\right)}, \quad \text{(A.89)}$$

$$t_{y,x} = -t_{x,y} = i\sum_{m=\circlearrowleft,\circlearrowleft} \frac{2s_m}{\left(1 + \frac{Z^{(2)}_m}{Z^{(3)}_r} + \frac{Z^{(1)}_r}{Z^{(3)}_r} + \frac{Z^{(1)}_r}{Z^{(2)}_m}\right)\exp\left(\frac{i\omega dn^{(2)}_m}{c}\right) + \left(1 - \frac{Z^{(2)}_m}{Z^{(3)}_r} + \frac{Z^{(1)}_r}{Z^{(3)}_r} - \frac{Z^{(1)}_r}{Z^{(2)}_m}\right)\exp\left(-\frac{i\omega dn^{(2)}_m}{c}\right)}. \quad \text{(A.90)}$$

Similarly, reflection tensor can be obtained as

$$E^-_{1,j} = \frac{\left(1 + \frac{Z^{(2)}_j}{Z^{(3)}_r} - \frac{Z^{(1)}_r}{Z^{(3)}_r} - \frac{Z^{(1)}_r}{Z^{(2)}_j}\right)\exp\left(\frac{i\omega dn^{(2)}_j}{c}\right) + \left(1 - \frac{Z^{(2)}_j}{Z^{(3)}_r} - \frac{Z^{(1)}_r}{Z^{(3)}_r} + \frac{Z^{(1)}_r}{Z^{(2)}_j}\right)\exp\left(-\frac{i\omega dn^{(2)}_j}{c}\right)}{\left(1 + \frac{Z^{(2)}_{p,j}}{Z^{(3)}_r} + \frac{Z^{(1)}_r}{Z^{(3)}_r} + \frac{Z^{(1)}_r}{Z^{(2)}_{p,j}}\right)\exp\left(\frac{i\omega dn^{(2)}_j}{c}\right) + \left(1 - \frac{Z^{(2)}_{p,j}}{Z^{(3)}_r} + \frac{Z^{(1)}_r}{Z^{(3)}_r} - \frac{Z^{(1)}_r}{Z^{(2)}_{p,j}}\right)\exp\left(-\frac{i\omega dn^{(2)}_j}{c}\right)} E^+_{1,j}, \quad \text{(A.91)}$$

Comparing the preceding equation with the definition of reflection tensor

$$\lim_{\delta\longrightarrow 0} = [\mathbf{E}^-_1(z = -\delta)] = \tilde{\mathbf{r}}\cdot \lim_{\delta\longrightarrow 0}[\mathbf{E}^+_1(z = -\delta)], \quad \text{(A.92)}$$

yields,

$$r^c_{n,m} = \frac{(1+\frac{Z^{(2)}_m}{Z^{(3)}_r}-\frac{Z^{(1)}_r}{Z^{(3)}_r}-\frac{Z^{(1)}_z}{Z^{(2)}_m})\exp\Big(\frac{i\omega dn^{(2)}_m}{c}\Big)+(1-\frac{Z^{(2)}_m}{Z^{(3)}_r}-\frac{Z^{(1)}_r}{Z^{(3)}_r}+\frac{Z^{(1)}_r}{Z^{(2)}_m})\exp\Big(-\frac{i\omega dn^{(2)}_m}{c}\Big)}{(1+\frac{Z^{(2)}_m}{Z^{(3)}_r}+\frac{Z^{(1)}_r}{Z^{(3)}_r}+\frac{Z^{(1)}_r}{Z^{(2)}_m})\exp\Big(\frac{i\omega dn^{(2)}_m}{c}\Big)+(1-\frac{Z^{(2)}_m}{Z^{(3)}_r}+\frac{Z^{(1)}_r}{Z^{(3)}_r}-\frac{Z^{(1)}_r}{Z^{(2)}_m})\exp\Big(-\frac{i\omega dn^{(2)}_m}{c}\Big)}\delta_{n,m}, \tag{A.93}$$

with $r^c_{n,m}$ denoting the components of the reflection tensor in LHCP-RHCP basis set as

$$\tilde{\mathbf{r}} = \sum_{n=\circlearrowleft,\circlearrowright}\sum_{m=\circlearrowleft,\circlearrowright} r^c_{n,m}\hat{\mathbf{E}}_n\hat{\mathbf{E}}^*_m, \tag{A.94}$$

$$\tilde{\mathbf{r}} = r^c_{\circlearrowleft,\circlearrowleft}\hat{\mathbf{E}}_{\circlearrowleft}\hat{\mathbf{E}}^*_{\circlearrowleft} + r^c_{\circlearrowleft,\circlearrowright}\hat{\mathbf{E}}_{\circlearrowleft}\hat{\mathbf{E}}^*_{\circlearrowright} + r^c_{\circlearrowleft,\circlearrowright}\hat{\mathbf{E}}_{\circlearrowleft}\hat{\mathbf{E}}^*_{\circlearrowright} + r^c_{\circlearrowleft,\circlearrowright}\hat{\mathbf{E}}_{\circlearrowleft}\hat{\mathbf{E}}^*_{\circlearrowright} \equiv \begin{bmatrix} r^c_{\circlearrowleft,\circlearrowleft} & r^c_{\circlearrowleft,\circlearrowright} \\ r^c_{\circlearrowleft,\circlearrowleft} & r^c_{\circlearrowleft,\circlearrowright} \end{bmatrix}. \tag{A.95}$$

As a result

$$\tilde{\mathbf{r}} = \sum_{m=\circlearrowleft,\circlearrowright} \frac{(1+\frac{Z^{(2)}_m}{Z^{(3)}_r}-\frac{Z^{(1)}_r}{Z^{(3)}_r}-\frac{Z^{(1)}_z}{Z^{(2)}_m})\exp\Big(\frac{i\omega dn^{(2)}_m}{c}\Big)+(1-\frac{Z^{(2)}_m}{Z^{(3)}_r}-\frac{Z^{(1)}_r}{Z^{(3)}_r}+\frac{Z^{(1)}_r}{Z^{(2)}_m})\exp\Big(-\frac{i\omega dn^{(2)}_m}{c}\Big)}{(1+\frac{Z^{(2)}_m}{Z^{(3)}_r}+\frac{Z^{(1)}_r}{Z^{(3)}_r}+\frac{Z^{(1)}_r}{Z^{(2)}_m})\exp\Big(\frac{i\omega dn^{(2)}_m}{c}\Big)+(1-\frac{Z^{(2)}_m}{Z^{(3)}_r}+\frac{Z^{(1)}_r}{Z^{(3)}_r}-\frac{Z^{(1)}_r}{Z^{(2)}_m})\exp\Big(-\frac{i\omega dn^{(2)}_m}{c}\Big)}\hat{\mathbf{E}}_m\hat{\mathbf{E}}^*_m \tag{A.96}$$

The components of reflection tensor can be represented in Cartesian coordinates as

$$\vec{r} = \sum_{n=x,y}\sum_{m=x,y} r_{n,m}\hat{\mathbf{e}}_n\hat{\mathbf{e}}_m = r_{x,x}\hat{\mathbf{e}}_{\mathbf{x}}\hat{\mathbf{e}}_x + r_{x,y}\hat{\mathbf{e}}_x\hat{\mathbf{e}}_y + r_{y,x}\hat{\mathbf{e}}_y\hat{\mathbf{e}}_x + r_{y,y}\hat{\mathbf{e}}_y\hat{\mathbf{e}}_y \equiv \begin{bmatrix} r_{x,x} & r_{x,y} \\ r_{y,x} & r_{y,y} \end{bmatrix}. \tag{A.97}$$

The transmission and reflection tensor can be expressed in terms of

$$\theta_m = \frac{\omega dn^{(2)}_m}{c} = 2\pi\frac{n^{(2)}_m d}{\lambda_0} \tag{A.98}$$

as follows

$$t_{x,x} = t_{y,y} = 2 \sum_{m=\circlearrowleft,\circlearrowleft} \frac{1}{(1+\frac{Z_r^{(1)}}{Z_r^{(3)}})\cos\theta_m + i(\frac{Z_m^{(2)}}{Z_r^{(3)}} + \frac{Z_r^{(1)}}{Z_m^{(2)}})\sin\theta_m}, \tag{A.99}$$

$$t_{y,x} = -t_{x,y} = 2i \sum_{m=\circlearrowleft,\circlearrowleft} \frac{s_m}{(1+\frac{Z_r^{(1)}}{Z_r^{(3)}})\cos\theta_m + i(\frac{Z_m^{(2)}}{Z_r^{(3)}} + \frac{Z_r^{(1)}}{Z_m^{(2)}})\sin\theta_m}, \tag{A.100}$$

$$r_{x,x} = r_{y,y} = \frac{1}{2} \sum_{m=\circlearrowleft,\circlearrowleft} \frac{(1-\frac{Z_r^{(1)}}{Z_r^{(3)}})\cos\theta_m + i(\frac{Z_m^{(2)}}{Z_r^{(3)}} - \frac{Z_r^{(1)}}{Z_m^{(2)}})\sin\theta_m}{(1+\frac{Z_r^{(1)}}{Z_r^{(3)}})\cos\theta_m + i(\frac{Z_m^{(2)}}{Z_r^{(3)}} + \frac{Z_r^{(1)}}{Z_m^{(2)}})\sin\theta_m}, \tag{A.101}$$

$$r_{y,x} = -r_{x,y} = \frac{i}{2} \sum_{m=\circlearrowleft,\circlearrowleft} s_m \frac{(1-\frac{Z_r^{(1)}}{Z_r^{(3)}})\cos\theta_m + i(\frac{Z_m^{(2)}}{Z_r^{(3)}} - \frac{Z_r^{(1)}}{Z_m^{(2)}})\sin\theta_m}{(1+\frac{Z_r^{(1)}}{Z_r^{(3)}})\cos\theta_m + i(\frac{Z_m^{(2)}}{Z_r^{(3)}} + \frac{Z_r^{(1)}}{Z_m^{(2)}})\sin\theta_m}. \tag{A.102}$$

Transmission tensor components for a thin slab, i.e., $\theta_{\circlearrowleft\circlearrowleft}$

$$t_{x,x} = t_{y,y} = 2 \sum_{m=\circlearrowleft,\circlearrowleft} (1+\frac{Z_r^{(1)}}{Z_r^{(3)}}) - i(\frac{Z_m^{(2)}}{Z_r^{(3)}} + \frac{Z_r^{(1)}}{Z_m^{(2)}})\theta_m, \tag{A.103}$$

$$t_{y,x} = -t_{x,y} = 2 \sum_{m=\circlearrowleft,\circlearrowleft} (\frac{Z_m^{(2)}}{Z_r^{(3)}} + \frac{Z_r^{(1)}}{Z_m^{(2)}})s_m\theta_m. \tag{A.104}$$

Writing impedance of the media in terms of permitivity and permeability

$$\frac{Z_m^{(2)}}{Z_r^{(3)}} \simeq \sqrt{\frac{\varepsilon_{x,x}^{(3)}}{\mu_{x,x}^{(3)}}}\sqrt{\frac{\mu_{x,x}^{(2)}}{\varepsilon_{x,x}^{(2)}}}\left[1+\frac{is_m}{2}\frac{\mu_{x,y}^{(2)}}{\mu_{x,x}^{(2)}}\right]\left[1-\frac{is_m}{2}\frac{\varepsilon_{x,y}^{(2)}}{\varepsilon_{x,x}^{(2)}}\right] \tag{A.105}$$

$$\simeq \sqrt{\frac{\varepsilon_{x,x}^{(3)}}{\mu_{x,x}^{(3)}}}\sqrt{\frac{\mu_{x,x}^{(2)}}{\varepsilon_{x,x}^{(2)}}}\left[1+\frac{is_m}{2}\left(\frac{\mu_{x,y}^{(2)}}{\mu_{x,x}^{(2)}} - \frac{\varepsilon_{x,y}^{(2)}}{\varepsilon_{x,x}^{(2)}}\right)\right], \tag{A.106}$$

$$\frac{Z_r^{(1)}}{Z_m^{(2)}} \simeq \sqrt{\frac{\varepsilon_{x,x}^{(2)}}{\mu_{x,x}^{(2)}}}\sqrt{\frac{\mu_{x,x}^{(1)}}{\varepsilon_{x,x}^{(1)}}}\left[1-\frac{is_m}{2}\frac{\mu_{x,y}^{(2)}}{\mu_{x,x}^{(2)}}\right]\left[1+\frac{is_m}{2}\frac{\varepsilon_{x,y}^{(2)}}{\varepsilon_{x,x}^{(2)}}\right] \tag{A.107}$$

$$\simeq \sqrt{\frac{\mu_{x,x}^{(1)}}{\varepsilon_{x,x}^{(1)}}}\sqrt{\frac{\varepsilon_{x,x}^{(2)}}{\mu_{x,x}^{(2)}}}\left[1-\frac{is_m}{2}\left(\frac{\mu_{x,y}^{(2)}}{\mu_{x,x}^{(2)}} - \frac{\varepsilon_{x,y}^{(2)}}{\varepsilon_{x,x}^{(2)}}\right)\right], \tag{A.108}$$

$$\theta_m = 2\pi \frac{n_m^{(2)} d}{\lambda_0} = 2\pi \frac{d}{\lambda_0} \sqrt{\varepsilon_{x,x}^{(2)} \mu_{x,x}^{(2)}} \left[1 + \frac{i s_m}{2} \left(\frac{\mu_{x,y}^{(2)}}{\mu_{x,x}^{(2)}} + \frac{\varepsilon_{x,y}^{(2)}}{\varepsilon_{x,x}^{(2)}} \right) \right]. \tag{A.109}$$

$$\begin{aligned} (\frac{Z_m^{(2)}}{Z_r^{(3)}} + \frac{Z_r^{(1)}}{Z_m^{(2)}})\theta_m &\simeq 2\pi \frac{d}{\lambda_0} \sqrt{\varepsilon_{x,x}^{(2)} \mu_{x,x}^{(2)}} \left[\begin{array}{c} \left(\sqrt{\frac{\varepsilon_{x,x}^{(3)}}{\mu_{x,x}^{(3)}}} \sqrt{\frac{\mu_{x,x}^{(2)}}{\varepsilon_{x,x}^{(2)}}} + \sqrt{\frac{\varepsilon_{x,x}^{(2)}}{\mu_{x,x}^{(2)}}} \sqrt{\frac{\mu_{x,x}^{(1)}}{\varepsilon_{x,x}^{(1)}}} \right) \\ + \frac{i s_m}{2} \left(\frac{\mu_{x,y}^{(2)}}{\mu_{x,x}^{(2)}} - \frac{\varepsilon_{x,y}^{(2)}}{\varepsilon_{x,x}^{(2)}} \right) \left(\sqrt{\frac{\varepsilon_{x,x}^{(3)}}{\mu_{x,x}^{(3)}}} \sqrt{\frac{\mu_{x,x}^{(2)}}{\varepsilon_{x,x}^{(2)}}} - \sqrt{\frac{\varepsilon_{x,x}^{(2)}}{\mu_{x,x}^{(2)}}} \sqrt{\frac{\mu_{x,x}^{(1)}}{\varepsilon_{x,x}^{(1)}}} \right) \end{array} \right], \end{aligned} \tag{A.110}$$

$$= 2\pi \frac{d}{\lambda_0} \sqrt{\varepsilon_{x,x}^{(2)} \mu_{x,x}^{(2)}} \left[\begin{array}{c} \left(\sqrt{\frac{\varepsilon_{x,x}^{(3)}}{\mu_{x,x}^{(3)}}} \sqrt{\frac{\mu_{x,x}^{(2)}}{\varepsilon_{x,x}^{(2)}}} + \sqrt{\frac{\varepsilon_{x,x}^{(2)}}{\mu_{x,x}^{(2)}}} \sqrt{\frac{\mu_{x,x}^{(1)}}{\varepsilon_{x,x}^{(1)}}} \right) \\ + i s_m \left(\frac{\mu_{x,y}^{(2)}}{\mu_{x,x}^{(2)}} \sqrt{\frac{\varepsilon_{x,x}^{(3)}}{\mu_{x,x}^{(3)}}} \sqrt{\frac{\mu_{x,x}^{(2)}}{\varepsilon_{x,x}^{(2)}}} + \frac{\varepsilon_{x,y}^{(2)}}{\varepsilon_{x,x}^{(2)}} \sqrt{\frac{\varepsilon_{x,x}^{(2)}}{\mu_{x,x}^{(2)}}} \sqrt{\frac{\mu_{x,x}^{(1)}}{\varepsilon_{x,x}^{(1)}}} \right) \end{array} \right]. \tag{A.111}$$

Therefore,

$$t_{y,x} = -t_{x,y} = 2 \sum_{m=\circlearrowleft,\circlearrowleft} \left(\frac{Z_m^{(2)}}{Z_r^{(3)}} + \frac{Z_r^{(1)}}{Z_m^{(2)}} \right) s_m \theta_m = 8i\pi \frac{d}{\lambda_0} \sqrt{\varepsilon_{x,x}^{(2)} \mu_{x,x}^{(2)}} \left(\frac{\mu_{x,y}^{(2)}}{\mu_{x,x}^{(2)}} \sqrt{\frac{\varepsilon_{x,x}^{(3)}}{\mu_{x,x}^{(3)}}} \sqrt{\frac{\mu_{x,x}^{(2)}}{\varepsilon_{x,x}^{(2)}}} + \frac{\varepsilon_{x,y}^{(2)}}{\varepsilon_{x,x}^{(2)}} \sqrt{\frac{\varepsilon_{x,x}^{(2)}}{\mu_{x,x}^{(2)}}} \sqrt{\frac{\mu_{x,x}^{(1)}}{\varepsilon_{x,x}^{(1)}}} \right), \tag{A.112}$$

$$t_{y,x} = -t_{x,y} = 2 \sum_{m=\circlearrowleft,\circlearrowleft} \left(\frac{Z_m^{(2)}}{Z_r^{(3)}} + \frac{Z_r^{(1)}}{Z_m^{(2)}} \right) s_m \theta_m \simeq 8i\pi \frac{d}{\lambda_0} \left(\mu_{x,y}^{(2)} \sqrt{\frac{\varepsilon_{x,x}^{(3)}}{\mu_{x,x}^{(3)}}} + \varepsilon_{x,y}^{(2)} \sqrt{\frac{\mu_{x,x}^{(1)}}{\varepsilon_{x,x}^{(1)}}} \right). \tag{A.113}$$

$$t_{x,x} = t_{y,y} = 2 \sum_{m=\circlearrowleft,\circlearrowleft} \left(1 + \frac{Z_r^{(1)}}{Z_r^{(3)}} \right) - i \left(\frac{Z_m^{(2)}}{Z_r^{(3)}} + \frac{Z_r^{(1)}}{Z_m^{(2)}} \right) \theta_m \simeq 4 \left(1 + \frac{Z_r^{(1)}}{Z_r^{(3)}} \right) - 8i\pi \frac{d}{\lambda_0} \left(\mu_{x,x}^{(2)} \sqrt{\frac{\varepsilon_{x,x}^{(3)}}{\mu_{x,x}^{(3)}}} + \varepsilon_{x,x}^{(2)} \sqrt{\frac{\mu_{x,x}^{(1)}}{\varepsilon_{x,x}^{(1)}}} \right), \tag{A.114}$$

$$\theta_F \simeq \tan^{-1}(\frac{t_{y,x}}{t_{x,x}}) \simeq \tan^{-1} \left(\frac{8i\pi \frac{d}{\lambda_0} (\mu_{x,y}^{(2)} \sqrt{\frac{\varepsilon_{x,x}^{(3)}}{\mu_{x,x}^{(3)}}} + \varepsilon_{x,y}^{(2)} \sqrt{\frac{\mu_{x,x}^{(1)}}{\varepsilon_{x,x}^{(1)}}})}{4 \left(1 + \sqrt{\frac{\mu_{x,x}^{(1)}}{\varepsilon_{x,x}^{(1)}}} \sqrt{\frac{\varepsilon_{x,x}^{(3)}}{\mu_{x,x}^{(3)}}} \right) - 8i\pi \frac{d}{\lambda_0} \left(\mu_{x,x}^{(2)} \sqrt{\frac{\varepsilon_{x,x}^{(3)}}{\mu_{x,x}^{(3)}}} + \varepsilon_{x,x}^{(2)} \sqrt{\frac{\mu_{x,x}^{(1)}}{\varepsilon_{x,x}^{(1)}}} \right)} \right). \tag{A.115}$$

$$\theta_F \simeq \tan^{-1} \left(\frac{2i\pi \frac{d}{\lambda_0} (\mu_{x,y}^{(2)} \sqrt{\frac{\varepsilon_{x,x}^{(3)}}{\mu_{x,x}^{(3)}}} + \varepsilon_{x,y}^{(2)} \sqrt{\frac{\mu_{x,x}^{(1)}}{\varepsilon_{x,x}^{(1)}}})}{1 + \sqrt{\frac{\mu_{x,x}^{(1)}}{\varepsilon_{x,x}^{(1)}}} \sqrt{\frac{\varepsilon_{x,x}^{(3)}}{\mu_{x,x}^{(3)}}}} \right), \tag{A.116}$$

$$\theta_F \simeq \tan^{-1}\left(\frac{2\pi\frac{d}{\lambda_0}(\mu_g\sqrt{\frac{\varepsilon^{(3)}_{x,x}}{\mu^{(3)}_{x,x}}}+\varepsilon_g\sqrt{\frac{\mu^{(1)}_{x,x}}{\varepsilon^{(1)}_{x,x}}})}{1+\sqrt{\frac{\mu^{(1)}_{x,x}}{\varepsilon^{(1)}_{x,x}}}\sqrt{\frac{\varepsilon^{(3)}_{x,x}}{\mu^{(3)}_{x,x}}}}\right), \tag{A.117}$$

$$\begin{aligned}
\theta_F &\simeq \tan^{-1}\left(\frac{2\pi\frac{d}{\lambda_0}(\mu_g Z_r^{(3)}+\varepsilon_g Z_r^{(1)})}{1+Z_r^{(1)}Z_r^{(3)}}\right) && \text{(A.118)}\\
&\simeq 2\pi\frac{d}{\lambda_0}\frac{(\mu_g Z_r^{(3)}+\varepsilon_g Z_r^{(1)})}{1+Z_r^{(1)}Z_r^{(3)}} && \text{(A.119)}\\
&\simeq 2\pi\frac{n_r^{(2)}d}{\lambda_0}\frac{\frac{\mu_g}{\mu^{(2)}_{xx}}Z_r^{(2)}Z_r^{(3)}+\frac{\varepsilon_g}{\varepsilon^{(2)}_{xx}}\frac{Z_r^{(1)}}{Z_r^{(2)}}}{1+Z_r^{(1)}Z_r^{(3)}}. && \text{(A.120)}
\end{aligned}$$

Sanity check #1:

For $d = 0$ the expressions for reflection and transmission reduces to

$$r_{x,x} = r_{y,y} = \frac{1}{2}\sum_{m=\circlearrowleft,\circlearrowright}\frac{Z_r^{(3)}-Z_r^{(1)}}{Z_r^{(3)}+Z_r^{(1)}} = \frac{1}{2}\frac{Z_r^{(3)}-Z_r^{(1)}}{Z_r^{(3)}+Z_r^{(1)}}\sum_{m=\circlearrowleft,\circlearrowright}2 = \frac{Z_r^{(3)}-Z_r^{(1)}}{Z_r^{(3)}+Z_r^{(1)}}, \tag{A.121}$$

$$r_{y,x} = -r_{x,y} = \frac{i}{2}\sum_{m=\circlearrowleft,\circlearrowright}s_m\frac{Z_r^{(3)}-Z_r^{(1)}}{Z_r^{(3)}+Z_r^{(1)}} = \frac{i}{2}\frac{Z_r^{(3)}-Z_r^{(1)}}{Z_r^{(3)}+Z_r^{(1)}}\sum_{m=\circlearrowleft,\circlearrowright}s_m = 0, \tag{A.122}$$

$$t_{x,x} = t_{y,y} = \sum_{m=\circlearrowleft,\circlearrowright}\frac{Z_r^{(3)}}{Z_r^{(3)}+Z_r^{(1)}} = \frac{Z_r^{(3)}}{Z_r^{(3)}+Z_r^{(1)}}\sum_{m=\circlearrowleft,\circlearrowright}1 = \frac{2Z_r^{(3)}}{Z_r^{(3)}+Z_r^{(1)}}, \tag{A.123}$$

$$t_{y,x} = -t_{x,y} = i\sum_{m=\circlearrowleft,\circlearrowright}s_m\frac{Z_r^{(3)}}{Z_r^{(3)}+Z_r^{(1)}} = \frac{iZ_r^{(3)}}{Z_r^{(3)}+Z_r^{(1)}}\sum_{m=\circlearrowleft,\circlearrowright}s_m = 0. \tag{A.124}$$

Sanity check #2

For $Z_r^{(1)} = Z_r^{(3)} = Z_{\circlearrowleft}^{(2)} = Z_{\circlearrowright}^{(2)}$ and $n_{\circlearrowleft}^{(2)} = n_{\circlearrowright}^{(2)} = n_r^{(2)}$, the expression for reflection and transmission reduces to

$$r_{x,x} = r_{y,y} = \frac{1}{2}\sum_{m=\circlearrowleft,\circlearrowright}\frac{0}{4\exp\left(\frac{i\omega d n_r^{(2)}}{c}\right)} = 0, \tag{A.125}$$

$$r_{x,y} = -r_{y,x} = \frac{i}{2} \sum_{m=\circlearrowleft,\circlearrowright} s_m \frac{0}{4\exp\left(\frac{i\omega d n_r^{(2)}}{c}\right)} = 0, \tag{A.126}$$

$$t_{x,x} = t_{y,y} = \frac{1}{2} \sum_{m=\circlearrowleft,\circlearrowright} \exp\left(-\frac{i\omega d n_m^{(2)}}{c}\right) = \exp\left(-\frac{i\omega d n_r^{(2)}}{c}\right), \tag{A.127}$$

$$t_{y,x} = -t_{x,y} = \frac{i}{2} \sum_{m=\circlearrowleft,\circlearrowright} s_m \exp\left(-\frac{i\omega d n_m^{(2)}}{c}\right) = \frac{i}{2} \exp\left(-\frac{i\omega d n_r^{(2)}}{c}\right) \sum_{m=\circlearrowleft,\circlearrowright} s_m = 0. \tag{A.128}$$

Faraday Rotation:

$$\theta_F = \tan^{-1}\left(\frac{\mathbf{E}_3^+(z=d)\cdot\hat{\mathbf{e}}_y}{\mathbf{E}_3^+(z=d)\cdot\hat{\mathbf{e}}_x}\right) - \theta_{pol} \tag{A.129}$$

$$= \tan^{-1}\left(\frac{t_{y,x}[\mathbf{E}_1^+(z=0)\cdot\hat{\mathbf{e}}_x] + t_{y,y}[\mathbf{E}_1^+(z=0)\cdot\hat{\mathbf{e}}_y]}{t_{x,x}[\mathbf{E}_1^+(z=0)\cdot\hat{\mathbf{e}}_x] + t_{x,y}[\mathbf{E}_1^+(z=0)\cdot\hat{\mathbf{e}}_y]}\right) - \theta_{pol}, \tag{A.130}$$

Since the incident electric field is given by

$$\mathbf{E}_1^+ = E_0 \exp\left(-\frac{i\omega z n^{(1)}}{c}\right)[\cos\theta_{pol}\hat{\mathbf{e}}_x + \sin\theta_{pol}\hat{\mathbf{e}}_y], \tag{A.131}$$

$$\mathbf{E}_1^+ = \frac{E_0}{\sqrt{2}} \exp\left(-\frac{i\omega z n^{(1)}}{c}\right)(e^{i\theta_{pol}}\hat{\mathbf{E}}_{\circlearrowleft} + e^{-i\theta_{pol}}\hat{\mathbf{E}}_{\circlearrowright}). \tag{A.132}$$

We know that

$$E_1^+(z=0)\cdot\hat{\mathbf{e}}_x = E_0\cos\theta_{pol}, \tag{A.133}$$

$$E_1^+(z=0)\cdot\hat{\mathbf{e}}_y = E_0\sin\theta_{pol}. \tag{A.134}$$

which yields

$$\theta_F = \tan^{-1}\left(\frac{t_{y,x}\cos\theta_{pol} + t_{y,y}\sin\theta_{pol}}{t_{x,x}\cos\theta_{pol} + t_{x,y}\sin\theta_{pol}}\right) - \theta_{pol}, \tag{A.135}$$

$$\theta_F = \tan^{-1}\left(\frac{i\cos\theta_{pol}\sum_{m=\circlearrowleft,\circlearrowright} A + \sin\theta_{pol}\sum_{m=\circlearrowleft,\circlearrowright} B}{\cos\theta_{pol}\sum_{m=\circlearrowleft,\circlearrowright} C - i\sin\theta_{pol}\sum_{m=\circlearrowleft,\circlearrowright} D}\right) - \theta_{pol}, \tag{A.136}$$

where

$$A = \frac{s_m}{(1+\frac{Z_r^{(1)}}{Z_r^{(3)}})\cos\theta_m + i(\frac{Z_m^{(1)}}{Z_r^{(3)}} + \frac{Z_r^{(1)}}{Z_m^{(2)}})\sin\theta_m}, \tag{A.137}$$

$$B = \frac{1}{(1+\frac{Z_r^{(1)}}{Z_r^{(3)}})\cos\theta_m + i(\frac{Z_m^{(2)}}{Z_r^{(3)}} + \frac{Z_r^{(1)}}{Z_m^{(2)}})\sin\theta_m}, \tag{A.138}$$

$$C = \frac{1}{(1+\frac{Z_r^{(1)}}{Z_r^{(3)}})\cos\theta_m + i(\frac{Z_m^{(1)}}{Z_r^{(3)}} + \frac{Z_r^{(1)}}{Z_m^{(2)}})\sin\theta_m}, \tag{A.139}$$

$$D = \frac{s_m}{(1+\frac{Z_r^{(1)}}{Z_r^{(3)}})\cos\theta_m + i(\frac{Z_m^{(2)}}{Z_r^{(3)}} + \frac{Z_r^{(1)}}{Z_m^{(2)}})\sin\theta_m}, \tag{A.140}$$

When the bias is perpendicular to the slab, Faraday rotation is not expected to be dependent on the polarization of the incident field. i.e.,

$$\frac{\partial\theta_F}{\partial\theta_{pol}} = 0$$

Therefore, the expression for Faraday rotation can be simplified to

$$\theta_F(\theta_{pol}=0) = \tan^{-1}\left(\frac{i\sum_{m=\circlearrowleft,\circlearrowright}\frac{s_m}{(1+\frac{Z_r^{(1)}}{Z_r^{(3)}})\cos\theta_m + i(\frac{Z_m^{(2)}}{Z_r^{(3)}}+\frac{Z_r^{(1)}}{Z_m^{(2)}})\sin\theta_m}}{\sum_{m=\circlearrowleft,\circlearrowright}\frac{s_m}{(1+\frac{Z_r^{(1)}}{Z_r^{(3)}})\cos\theta_m + i(\frac{Z_m^{(2)}}{Z_r^{(3)}}+\frac{Z_r^{(1)}}{Z_m^{(2)}})\sin\theta_m}}\right). \tag{A.141}$$

Similarly Kerr Rotation can be simplified to

$$\theta_K = \tan^{-1}\left(\frac{E_1^-(z=d)\cdot\hat{\mathbf{e}}_y}{E_1^-(z=d)\cdot\hat{\mathbf{e}}_x}\right) - \theta_{pol}, \tag{A.142}$$

$$\theta_K = \tan^{-1}\left(\frac{r_{y,x}[\mathbf{E}_1^-(z=0)\cdot\hat{\mathbf{e}}_\mathbf{x}] + r_{y,y}[\mathbf{E}_1^-(z=0)\cdot\hat{\mathbf{e}}_y]}{r_{x,x}[\mathbf{E}_1^-(z=0)\cdot\hat{\mathbf{e}}_x] + r_{x,y}[\mathbf{E}_1^-(z=0)\cdot\hat{\mathbf{e}}_y]}\right) - \theta_{pol}, \tag{A.143}$$

which yields

$$\theta_K = \tan^{-1}\left(\frac{r_{y,x}\cos\theta_{pol} + r_{y,y}\sin\theta_{pol}}{r_{x,x}\cos\theta_{pol} + r_{x,y}\sin\theta_{pol}}\right) - \theta_{pol}, \tag{A.144}$$

$$\theta_K = \tan^{-1}\left(\frac{i\cos\theta_{pol}\sum_{m=\circlearrowleft,\circlearrowright} E + \sin\theta_{pol}\sum_{m=\circlearrowleft,\circlearrowright} F}{\cos\theta_{pol}\sum_{m=\circlearrowleft,\circlearrowright} G - i\sin\theta_{pol}\sum_{m=\circlearrowleft,\circlearrowright} H}\right), \tag{A.145}$$

where

$$E = s_m \frac{(1-\frac{Z_r^{(1)}}{Z_r^{(3)}})\cos\theta_m + i(\frac{Z_m^{(2)}}{Z_r^{(3)}} - \frac{Z_r^{(1)}}{Z_m^{(2)}})\sin\theta_m}{(1+\frac{Z_r^{(1)}}{Z_r^{(3)}})\cos\theta_m + i(\frac{Z_m^{(2)}}{Z_r^{(3)}} + \frac{Z_r^{(1)}}{Z_m^{(2)}})\sin\theta_m}, \tag{A.146}$$

$$F = \frac{(1-\frac{Z_r^{(1)}}{Z_r^{(3)}})\cos\theta_m + i(\frac{Z_m^{(2)}}{Z_r^{(3)}} - \frac{Z_r^{(1)}}{Z_m^{(2)}})\sin\theta_m}{(1+\frac{Z_r^{(1)}}{Z_r^{(3)}})\cos\theta_m + i(\frac{Z_m^{(2)}}{Z_r^{(3)}} + \frac{Z_r^{(1)}}{Z_m^{(2)}})\sin\theta_m}, \tag{A.147}$$

$$G = \frac{(1-\frac{Z_r^{(1)}}{Z_r^{(3)}})\cos\theta_m + i(\frac{Z_m^{(2)}}{Z_r^{(3)}} - \frac{Z_r^{(1)}}{Z_m^{(2)}})\sin\theta_m}{(1+\frac{Z_r^{(1)}}{Z_r^{(3)}})\cos\theta_m + i(\frac{Z_m^{(2)}}{Z_r^{(3)}} + \frac{Z_r^{(1)}}{Z_m^{(2)}})\sin\theta_m}, \tag{A.148}$$

$$H = s_m \frac{(1-\frac{Z_r^{(1)}}{Z_r^{(3)}})\cos\theta_m + i(\frac{Z_m^{(2)}}{Z_r^{(3)}} - \frac{Z_r^{(1)}}{Z_m^{(2)}})\sin\theta_m}{(1+\frac{Z_r^{(1)}}{Z_r^{(3)}})\cos\theta_m + i(\frac{Z_m^{(2)}}{Z_r^{(3)}} + \frac{Z_r^{(1)}}{Z_m^{(2)}})\sin\theta_m}. \tag{A.149}$$

When the bias is perpendicular to the slab, Kerr rotation is not expected to be dependent on the polarization of the incident field. i.e.,

$$\frac{\partial\theta_K}{\partial\theta_{pol}} = 0. \tag{A.150}$$

Therefore, the expression for Kerr rotation can be simplified to

$$\theta_K(\theta_{pol}=0) = \tan^{-1}\left(\frac{i\sum_{m=\circlearrowleft,\circlearrowright} s_m \frac{(1-\frac{Z_r^{(1)}}{Z_r^{(3)}})\cos\theta_m + i(\frac{Z_m^{(2)}}{Z_r^{(3)}} - \frac{Z_r^{(1)}}{Z_m^{(2)}})\sin\theta_m}{(1+\frac{Z_r^{(1)}}{Z_r^{(3)}})\cos\theta_m + i(\frac{Z_m^{(2)}}{Z_r^{(3)}} + \frac{Z_r^{(1)}}{Z_m^{(2)}})\sin\theta_m}}{\sum_{m=\circlearrowleft,\circlearrowright} \frac{(1-\frac{Z_r^{(1)}}{Z_r^{(3)}})\cos\theta_m + i(\frac{Z_m^{(2)}}{Z_r^{(3)}} - \frac{Z_r^{(1)}}{Z_m^{(2)}})\sin\theta_m}{(1+\frac{Z_r^{(1)}}{Z_r^{(3)}})\cos\theta_m + i(\frac{Z_m^{(2)}}{Z_r^{(3)}} + \frac{Z_r^{(1)}}{Z_m^{(2)}})\sin\theta_m}}\right). \tag{A.151}$$

Note: If you have any question, query or suggestion about this mathematical modelling, please feel free to reach at **poddarswadesh@gmail.com**.